Human and Robot Arm Control Using the Minimum Variance Principle

Gavin Iain Simmons

Thesis submitted for the degree of Doctor of Philosophy

Department of Electrical and Electronic Engineering

Imperial College London

Imperial College London

Abstract

Many computational models of human upper limb movement successfully capture some features of human movement, but often lack a compelling biological basis. One that provides such a basis is Harris and Wolpert's minimum variance model. In this model, the variance of the hand at the end of a movement is minimised, given that the controlling signal is subject to random noise with zero mean and standard deviation proportional to the signal's amplitude. This criterion offers a consistent explanation for several movement characteristics.

This work formulates the minimum variance model into a form suitable for controlling a robot arm. This implementation allows examination of the model properties, specifically its applicability to producing human-like movement. The model is subsequently tested in areas important to studies of human movement and robotics, including reaching, grasping, and action perception.

For reaching, experiments show this formulation successfully captures the characteristics of movement, supporting previous results. Reaching is initially performed between two points, but complex trajectories are also investigated through the inclusion of via-points.

The addition of a gripper extends the model, allowing production of trajectories for grasping an object. Using the minimum variance principle to derive digit trajectories, a quantitative explanation for the approach of digits to the object surface is provided. These trajectories also exhibit human-like spatial and temporal coordination between hand transport and grip aperture.

The model's predictive ability is further tested in the perception of human demonstrated actions. Through integration with a system that performs perception using its motor system offline, in line with the motor theory of perception, the model is shown to correlate well with data on human perception of movement.

These experiments investigate and extend the explanatory and predictive use of the model for human movement, and demonstrate that it can be suitably formulated to produce human-like movement on robot arms.

Acknowledgements

I would first like to acknowledge the excellent supervision I have received from Dr. Yiannis Demiris. Throughout my PhD work he has provided help, advice and support whenever it was needed. His humour, energy and enthusiasm has helped me to enjoy my work all the more.

I also need to thank my colleagues in the Biologically inspired Autonomous Robots Team (BioART) for all their help, suggestions and assistance over the past few years. Their support has been invaluable. Many thanks to Anthony Dearden, Bassam Khadhouri, Matthew Johnson and Paschalis Veskos. I am happy to have worked for my PhD with them as colleagues, and hope I have contributed in some way to their work, as they have helped with mine.

I would like to thank my Mum, Dad and Sister for everything they have given me, all the opportunities, love and support.

Finally, I would also like to give a special thank you to Eleanor for all the love, support and confidence that she has given me, now and always.

Contents

List of Figures

Chapter 1

Introduction

One path to producing flexible, adaptive movement on a robot is to study how humans produce such movements. Computational neuroscience provides a range of theories and models that attempt to explain the common features that characterise human upper limb movements.[41,119,69,125,52,127,92,68,106,42,128,46,116] The experimental and observational work to identify these common features has been carried out over many years and continues today, leading to a number of qualitative and quantitative laws of movement.[37,91,59,60,57,8,62,70,18]

A major research goal is to identify, through greater understanding of the processes involved in human motor planning and generation, underlying principles of human movement that might be employed to help design new algorithms and strategies for controlling robots.[123,13,107,6,48,4,122,12,27,20,28,23]

There are obviously considerable differences between human and robot arms. Human arms are moved by forces generated by muscles rather than motors. Muscles are often compared to springs, and they exhibit many spring-like properties such as passive compliance; but they act in a way that is considerably more complex than the spring analogy suggests. They also show dynamic properties such as fatigue that are not replicated by motors. One thing human and robot motor systems have in common is noise, which causes inaccuracies in both control and sensory signals, leading to inaccuracies in movement execution.

Understanding these differences is important, as the aim is that the identified principles and algorithms, when applied to the dissimilar mechanical systems and control architectures of robots, capture particular aspects of human movement.

The other side of the generation of motor behaviour by an intelligent agent is its sensory perception of the motor behaviour of others. Once treated as a separate phenomenon to action generation, action perception is increasingly seen as a process that explicitly involves the motor system through the offline simulation of observed movements.[61,103,10,73,53,26,124,74,34,11,99,43,28,29,30] This motor theory of perception is supported by behavioural and imaging experiments in both monkeys and humans.[102,21,118,75,104,39,38,50,71,45]

The ability to recognise the actions of others and understand their goals is a vital component of the ability to learn from demonstration. Providing robots with these abilities becomes an important research goal as robots find increasing use in human orientated environments. Linking together models that capture human-like movement characteristics and systems that provide some level of action recognition through the use of the motor system in perception is a step towards this goal.

Contributions

Within the context given above, the primary contributions of this thesis are in the novel application and synthesis of specific theories of human movement to a platform suitable for robot control. More specifically, the contributions are as follows: implementation of a successful model of human movement, the minimum variance model, for control of a robot arm; extension of this implementation to the problem of prehension, through the combination of two parallel theories of grasp planning and execution; and the integration of this model for reaching and grasping with an existing model for learning from demonstration, the combination of which allows recognition of observed actions.

The first contribution is the novel application of the minimum variance model of human movements to the task of prehension. There have been several previous implementation of the model for reaching[52,117,86,88] using a variety of optimisation methods to produce trajectories for comparison with human movement data. The approach presented here follows the work of Todorov,[117] who used a linear quadratic gaussian (LQG) scheme to iteratively find the optimal state-feedback gains and control law in the presence of signal-dependent noise, and extends his work for reaching movements by adding structures to control the movement of two digits at the end of a two-joint planar arm.

As with any model, it is important to set out the basic assumptions being modelled. This is especially relevant in neuroscience, where studies can be performed at many different levels of detail. For motor control studies, a distinction can be made between the level of detail of the plant and the level of detail of the controller. Both the plant and the controller of the human motor system have evolved together over time. As such, it is important when trying to capture particular aspects of human movement to understand the source of the observed behaviour: is it a consequence of the control strategy, a consequence of the mechanical properties of the arm, or is it due to the interaction of the two? An observed behaviour may also be an emergent property, one that has come about indirectly through evolutionary pressure acting on another part of the system.

Here, this is taken into account by judging movement models not only on the relevant features of human movement that they capture, but also on the degree to which the underlying principles of the model can be applied to controlling a robot arm, and their suitability for implementation. This is the case for the minimum variance model, where valid trajectories have been produced with several different plant models and types of optimisation, yet with the underlying principles unchanged.

The minimum variance model has been shown to predict trajectories for saccadic eye movements and reaching movements, including those that involve obstacle avoidance, but is used here for the first time to predict grasping behaviour. To do this, the model uniquely mixes two grasping paradigms; the separate planning of transport and grip components, and a recent theory that casts grasping as pointing with the digits to targets on an object.[113]

This synthesis of the two paradigms is achieved through the specific principles of the minimum variance model. As has been stated, it has been successfully implemented for the task of reaching to a target with an arm. Its extension to the digits of a gripping mechanism allows the model to grasp by moving the arm and gripper to target positions on the object, following trajectories that obey the minimum variance criterion. However, noise on the control signals of the arm as well as on those of the digits will effect the variance, but by different amounts according to the nature of the task. As such, planning of the transport and grip components must take place separately.

This extension of the reaching model is an important one for robotic control as well, since it raises the model to the level of being able to perform tasks more complex than reaching. Point-to-point reaching movements are the basic units of all upper-limb movements, but the addition of a gripping mechanism and appropriate controller allows for interaction with the environment in a way that pointing alone does not.

The second primary contribution is in the application of the model for reaching and grasping to the problem of learning from demonstration. A scheme that uses the motor theory of perception is adapted to use the optimal control scheme presented here to recognise patterns of reaching movements. The structure of the optimal control scheme is such that predicted movement costs can be calculated and stored without having to perform the movement itself.

When presented with a demonstrated movement, these predicted costs can be used to generate motor commands and produce trajectories using the observed states rather than the system's own state. The predicted trajectories for known movements are compared with the demonstration in progress, in order to calculate the confidence that the prediction matches the observed movement.

If such a system (where the motor generation subsystem is involved in perception) is to confidently recognise a human demonstration, it is a logical step that the system is also able to generate movements corresponding to human movements to some degree. A further test of the minimum variance implementation presented in this work is therefore how successful it is in recognising movements when presented with variations to human-like movement patterns. The third contribution of this work is this investigation, carried out by applying the scheme for action perception described here to the minimum variance model for prehension described above. When the system is presented with normal grasping behaviour and abnormal grasping patterns demonstrated by humans, it correctly assigns a significantly higher confidence to the natural behaviour. This success is further confirmed by the confidence time profiles produced by the system, which are qualitatively similar in form to neural activation patterns of human subjects when presented with the same type of grip patterns.

The contributions of this thesis build on a foundation of neuroscientific theory which is applied to the dissimilar domain of robotic control. Through the increasingly complex applications of reaching, grasping and action perception, the validity and importance of these contributions are demonstrated.

Outline of Thesis

The organisation of the rest of this thesis follows. In Chapter 2, a detailed background is given on the characteristics of human upper limb movement and a range of computational models that have been proposed as explanations. The theoretical backgrounds of several different movement models are described, showing how the trajectories they produce match up with the previously identified features of movement. Models such as the equilibrium point hypothesis are briefly discussed, but the main focus is on the wider class of optimisation models. Among those discussed are the well-studied minimum jerk and minimum torque-change models. From these descriptions several issues are identified that are not covered, leading to the introduction of the minimum variance model in the following chapter.

In Chapter 3, the primary focus is on the details of the minimum variance model and the implementation for robotic reaching movements. As well as describing the theoretical background, a description of an optimal control scheme formulated to capture the relevant principles is given, using a two-link planar effector model suitable for robotic control. This implementation is demonstrated to capture the required features of human movement described in Chapter 2 for point-to-point movements, and is also extended for more complex trajectories involving via-points.

In Chapter 4, the model for human reaching is extended to encompass precision grasping of an object. The basis for this chapter is the competition between two alternative views of human grasping. The first view[59,60] suggests that grasping is performed using two visuomotor channels, one for the reach and one for the grip, which are executed in parallel. The second view[113] predicts that grasping can be thought of as pointing with the digits to target positions on an object. Here, an effector model with separate reach (the arm) and grasp (a gripping mechanism) components is combined with the implementation of the minimum variance model developed in the previous chapter for pointing to a target position.

The resulting digit trajectories are shown to successfully match the well-documented spatial and temporal relationships between peak grip aperture and a number of task-dependent parameters, including object size and degree of perpendicular approach. Unlike other models of grasping, the extension of the minimum variance model to gripping also allows the study of the relative contributions to movement accuracy of the reach and grasp components of the movement, where the results are shown to also match those of previous grasping variability studies performed on human subjects.

Having described the model and its success in replicating features of human-like movement for reaching and grasping, chapter 5 covers experiments that show the model's applicability to the perception of human actions. The model is integrated with a system for action perception based on the motor theory of perception. Structures from the optimal control scheme used to generate movements from the system's own state are instead used to predict the movements of a demonstrator, given the demonstrator's current state. These predictions are given a confidence rating based on how well they match the observed action.

In this chapter, the system is presented with both normal and altered grasping patterns produced by a human demonstrator. The system is shown to successfully recognise the normal grasping behaviour but shows decreased confidence in predictions for other patterns. The confidence profiles are shown to qualitatively take the same form as recordings of neural activation levels of human subjects observing the same type of patterns.[45,31]

The final two chapters discuss the implications and limitations of this work and present some potential directions for further research.

Publications

The primary contributions and results presented in this thesis have also been used by the author in the following articles:

G. Simmons and Y. Demiris. Object grasping using the minimum variance model. *Biological Cybernetics*, 2006 (to appear)[110] : Covers the extension of the minimum variance model from reaching to grasping, including descriptions of the two grasping paradigms used. Results from chapter 4, including the effects of different movement parameters on variability of grasping, also form part of this paper.

Y. Demiris and G. Simmons. Perceiving the unusual: Temporal properties of hierarchical motor representation for action perception. *Neural Networks*, 2006 (to appear)[31] : Paper describing how the minimum variance implementation given in this work can be fitted to the HAMMER architecture[29,30] to recognise the actions of a demonstrator. This is the basis for the action perception work that forms chapter 5.

Additional Information

Supplementary information for some sections is provided in the appendices. Where necessary, this is noted in the text of the appropriate section. Equations and figures are numbered by chapter and the order in which they occur within each chapter. A list of figures is included after the contents list.

Chapter 2

Background

As stated in Chapter 1, computational neuroscience provides a range of theories and models that attempt to explain the common features that characterise human arm movements. Among these features are the straight hand paths and bell-shaped velocity profiles found in point-to-point reaching movements, and the speed-accuracy trade-off formalised by Fitts Law. Many such models generate their trajectories through the optimisation of some aspect of movement, such as hand velocity or joint torque.

This chapter begins with a description of the characteristic features that define "human-like" movement. A number of relevant computational theories of human upper limb movement that attempt to explain these features are then outlined. The focus is primarily on optimisation models, such as the minimum jerk and minimum commanded-torque-change models. For completeness other relevant theories, such as the equilibrium point hypothesis, are also described.

Through this analysis, several areas not covered by these models are identified, leading to the introduction of the minimum variance model in the following chapter.

1 Human Movement

When performing upper limb movements humans show a number of stereotypical patterns, both between individuals and between trials for the same individual. The following section describes these features and some of their implications. The focus is initially on the characteristics of point-to-point reaching movements, since these are among the most basic movements performed by the upper limb. In the next chapter it is shown how these principles still hold for more complex trajectories through the inclusion of via-points.

1.1 Straight, smooth movement

When reaching between two points humans move their arms to make the path of the hand between the two points roughly straight. Slight curvature does occur, depending on the area of the arm's workspace in which the movement occurs.[119] These straight movements are smooth: the acceleration profile of the movement contains no discontinuities (Figure 2.1(c)). This results in a characteristic bell-shaped velocity profile for the movement.[91,40,119], as shown in Figure 2.1(b). However, this bell-shaped profile does not have to be perfectly symmetric, and can be skewed towards either the start or end of the movement depending on the movement parameters of the task.[114]

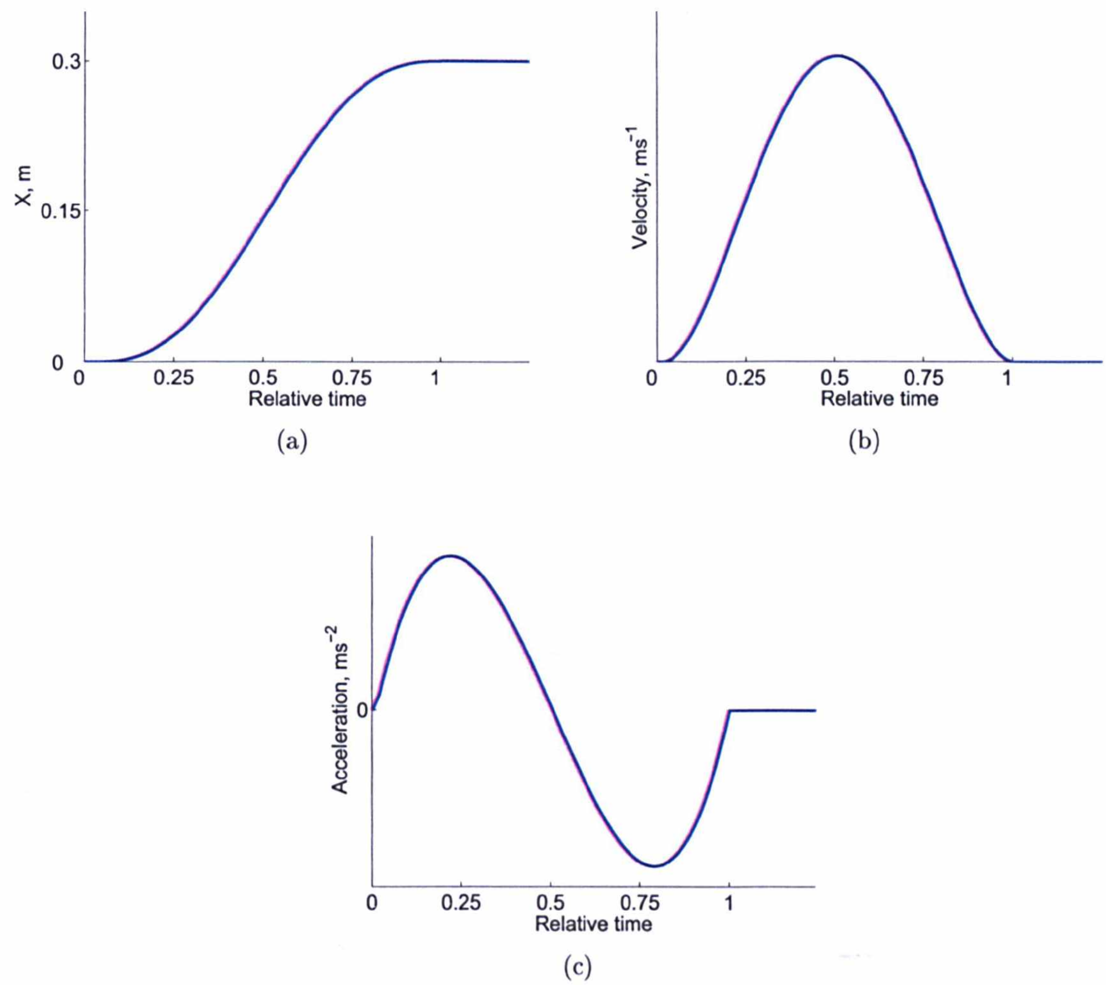

Figure 2.1: Smooth movement between points: (a) Change in x-axis position; (b) Bell-shaped velocity profile; (c) Acceleration profile, showing no discontinuities

1.2 Speed-accuracy trade-off

Point-to-point reaching movements also exhibit an inverse relationship between speed and accuracy, known as Fitts' Law[37] (equation 2.1) which states that the faster the movement, the less accurately it will reach the target.

$$T = a + b\left(\log_2\left(\frac{2A}{W}\right)\right) \tag{2.1}$$

In equation 2.1, T is the movement time, A is the amplitude of the movement, W is the target width, and a and b are coefficients of regression. The term $\frac{2A}{W}$ is known as the index of movement difficulty (ID). Often, a fast inaccurate movement will be followed by short corrective movements to bring the hand back to the target.[32,33] The speed-accuracy trade-off has been extensively studied in human-computer interaction, where various IDs have been proposed and evaluated against human movements.[1] The general form of the trade-off is shown in Figure 2.2.

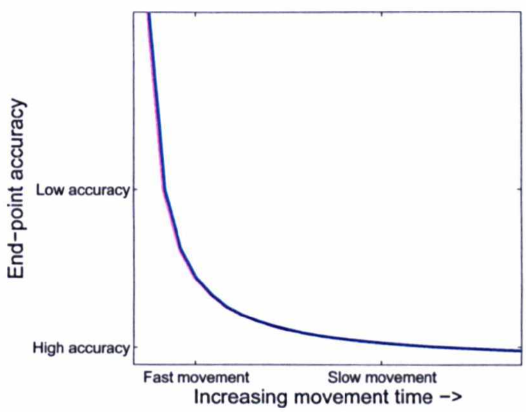

Figure 2.2: General form of the speed-accuracy trade-off observed in human point-to-point reaching movements

1.3 Timing Accuracy

As well as the spatial aspects of a movement many tasks have temporal requirements, including temporal accuracy. In contrast to the speed-accuracy trade-off for spatial goals, variability of timed actions increases almost linearly with the goal movement time,[109] as shown in Figure 2.3. When the movement distance increases but movement time stays constant, timing error doesn't increase despite the increased movement velocity.

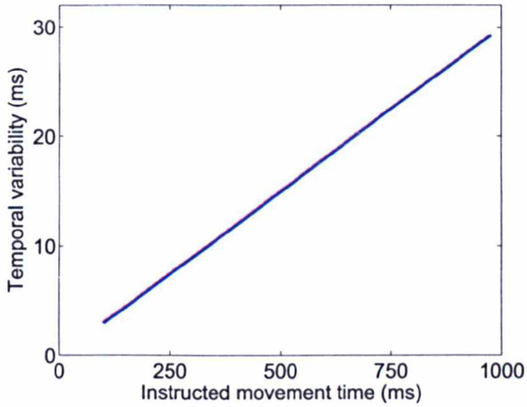

Figure 2.3: General form of the relationship between temporal variability and instructed movement time (adapted from Schmidt[109])

1.4 Velocity and curvature

Another important aspect of human movement is the relationship between velocity and curvature of a movement, often referred to as the two-thirds power law.[78,120,101] This relationship is formalised by equation 2.2.

$$v = g\kappa^{-\beta} \tag{2.2}$$

In equation 2.2, v is the tangential velocity of the hand, κ is the curvature and g is a proportionality constant. The coefficient β has a value around $\frac{1}{3}$ (the name "two-thirds" power law comes from the original formulation of the law in terms of angular velocity[101]).

The following section provides details of a number of computational models that have been developed to explain why the motor system would exhibit the relationships described here.

2 Computational Models

A majority of computational neuroscience models that seek to explain the characteristics given in the previous section are based on the assumption that they arise from the optimisation of some criterion, or criteria, by the human motor system.[17,79,42,80] A notable exception is the equilibrium-point hypothesis and its variations.[8,9,49,92,54]

Within the class of optimisation models, it is not clear which aspects of movement should be optimised. A range of criteria have been proposed, such as minimum time of movement, minimum energy expenditure, minimum commanded-torque-change[93,121] and the well-known minimum jerk[41] and minimum torque-change models.[119] Many of these optimisation criteria have been evaluated against actual human arm movements by previous studies.[51]

In this section, a basic description of the equilibrium-point hypothesis is given for completeness, before the wider-class of optimisation models is explored.

2.1 Equilibrium-point hypothesis

Muscles are the motors responsible for limb movement. They are more than simple force generators however, and their spring-like behaviour has long been recognised as a key element in the control of limb movement. One theory of motor control, the *equilibrium point hypothesis* (EPH)[8,9,49,92] is predicated on the assumption that the central nervous system can control the equilibrium position established by the balance of forces in these muscle-springs.[54]

There are several variations on the basic hypothesis, of which the most well-known is the λ-model. It was proposed, based on force measurements of human muscles, that the force response of those muscles is exponential with respect to perturbation from a target length. Flexor-extensor pairs of muscles behave like exponential springs where the parameters (the λ values, which determine the length threshold at which a muscle begins to generate force) set the target angle of the joint. For a motion between two postures, the λ values are interpolated linearly between the settings consistent with the desired initial and target positions.[51] The equilibrium-point hypothesis thus offers an explanation for how a reference trajectory can be achieved by guiding limb movement, but does not explain how such a trajectory could be produced in tasks more complex than pointing.[116]

As well as this lack of application to more complex tasks, there is also experiment evidence against the theory as well. Gomi and Kawato[49] report on experiments to measure human arm stiffness during movement using a high-precision manipulandum. From these measurements, and from the actual hand trajectory and generated torques, they reconstructed the equilibrium-point trajectory of the movement. They found that using the measured arm stiffness produced an equilibrium-point trajectory with an incorrect velocity profile. Further, a set of experiments performed by Hinder and Milner[54] tested the EPH against the theory that the CNS learns and uses an internal dynamics model of a task. Their results show that predictions made by the EPH were inconsistent with observed data, supporting the internal model theory.

Because of the apparent evidence against the theory, and based as it is on detailed proprioceptive information about the stretch of muscles in the arm, the EPH is unsuited for implementation on a simple robotic platform. It would be interesting to adapt the theory to control a robot arm based on artificial muscles, but these are expensive compared to servo-motors.

This means it is necessary to look at other theories of how the CNS performs the computations required for movement planning and execution. Amongst these theories, those most suitable for implementation on a robotic platform are the ones based on control engineering methods, specifically in the field of optimal control.

2.2 Optimisation models

Optimal control theory has been well studied and forms the basis for most modern control solutions. The principles of optimal control theory have also proved to be useful for applications outside the domain of control engineering, the most relevant of which for this thesis is the problem of human trajectory planning and arm movement.[79,117,116,80]

Rather than specifying a desired path, optimal solutions to control problems work by assigning a performance index based on the parts of the system that the designer wishes to optimise, such as amount of time passed or energy expenditure. This performance index, or cost function, usually takes the form of a summation or integral which must be minimised over a given duration; both finite and infinite (steady state) horizon problems can be addressed.

Optimisation criteria for modelling limb movements and hand trajectories generally fall into one of two categories - kinematic or dynamic solutions. In kinematic solutions the cost function is based upon the geometric or time-based properties of the motion and the state of the limb could be represented, for example, in terms of joint angles or Cartesian position of the hand. In dynamic solutions the cost function is based on the dynamics of the arm and the state could be represented, for example, in terms of joint torques or forces acting on the hand.

One of the major differences between the two types is in the way they represent the planning and execution processes. For kinematic models, movements are specified in terms of the positions and velocities of the arm as a function of time which must then be converted into motor commands to move the arm. This implies a separation of the planning and execution processes. In dynamic models, however, motor commands are specified directly, effectively combining planning and execution into a single process.[51]

Distinction can also be made between intrinsic and extrinsic spaces in which planning occurs. For example, planning in joint angle space is intrinsic to the human or robot, while planning in Cartesian space is extrinsic.[51] Since actual movements can only be specified intrinsically, but many goals of movement are specified extrinsically (e.g. picking up an object), one of the major problems in sensorimotor planning and control is converting between these two frames of reference.

The following sections describe several optimisation criteria that have been suggested as possible explanations for the characteristic properties of human movements. This is not a comprehensive review, but covers a number of the most successful and important theories. Each is evaluated in terms of the features it captures and its applicability for transferring to control of a robotic system.

2.2.1 Minimum energy

Minimisation of energy is an interesting criterion for movement, as it is potentially applicable to many movements performed by different parts of the body. It also has a sound biological basis, as it deals with the metabolic energy expended by the muscles when moving.

The minimum metabolic energy cost hypothesis was modelled by Alexander[2], using equations for the metabolic rate of uni-articular muscles derived from a number of empirical studies.[81,2] The model uses a two-link arm operating in a vertical plane, with two uni-articular muscles (a flexor and extensor) for both the shoulder and elbow joints. Experiments are also carried out on an arm using biarticular muscles to control the elbow.

The metabolic energy cost for muscles shortening or being stretched at known rates is calculated in this paper as a function of the moments and angular velocities of the joints of the arm. The metabolic rate P of a uni-articular muscle while it is shortening at a rate that gives its joint angular velocity $\dot{\theta}$ is given by 2.3.

$$P = M_{iso}\dot{\theta}_{max}\Phi\left(\frac{\dot{\theta}}{\dot{\theta}_{max}}\right) \tag{2.3}$$

where M_{iso} is the moment the muscle would exert if contracting isometrically, and $\dot{\theta}_{max}$ is the angular velocity corresponding to the muscle's maximum (unloaded) shortening speed. Data for the function Φ comes from Ma and Zahalak[81], and are well-fitted by equations 2.4 and 2.5. When the muscle is doing positive work (when the moment it exerts and its angular velocity have the same sign), the function Φ is:

$$\Phi\left(\frac{\dot{\theta}}{\dot{\theta}_{max}}\right) = 0.23 - 0.16\exp\left(\frac{-8\dot{\theta}}{\dot{\theta}_{max}}\right) \tag{2.4}$$

When the muscle is doing negative work (when the moment it exerts and its angular velocity have different signs), the function Φ becomes:

$$\Phi\left(\frac{\dot{\theta}}{\dot{\theta}_{max}}\right) = 0.01 - 0.11\left(\frac{\dot{\theta}}{\dot{\theta}_{max}}\right) + 0.06\exp\left(\frac{23\dot{\theta}}{\dot{\theta}_{max}}\right) \tag{2.5}$$

For some movements only some of the muscles motor units need to be activated. To use equation 2.3, the isometric moment for the part of the muscle that is activated at each time step is needed. The faster the muscle is shortening, the more it must be activated to exert a given moment. Alexander[2] converts standard force-velocity equations into moment-angular velocity equations, and rearranges them to give the isometric moment for the part of the muscle that must be activated to generate a required moment and angular velocity (equations 2.6 and 2.7).

As when calculating the function Φ above, different equations are used depending on whether the muscle is doing positive or negative work. When the moment and the angular velocity have the same sign (positive work), the isometric moment is:

$$M_{iso} = \frac{M\left(\dot{\theta}_{max} + G\dot{\theta}\right)}{\dot{\theta}_{max} - \dot{\theta}} \tag{2.6}$$

When the moment and angular velocity have different signs (negative work), the isometric moment is:

$$M_{iso} = \frac{M\left(\dot{\theta}_{max} - 7.6G\dot{\theta}\right)}{\dot{\theta}_{max} - 13.6G\dot{\theta} - 0.8\dot{\theta}} \tag{2.7}$$

The factor G in equations 2.6 and 2.7 is set by Alexander[2] to be 4, described as a typical value for moderately fast muscles. Empirical values of $\dot{\theta}_{max}$ are given as 22 rad/s for flexion of the elbow, and 28 rad/s for extension - it is noted that these values were determined during maximum effort and are likely to reflect the properties of the fastest muscle units. Less forceful movements would probably be performed by slower muscles, so a value for $\dot{\theta}_{max}$ of 15 rad/s is used in the paper for both flexion and extension of both the elbow and shoulder joints.

The equations above allow the metabolic rate P (equation 2.3) to be calculated at each time step, given the angular velocity of the joint that the muscle is moving. This requires that the angular velocity profile for a movement is calculated. For a two-link planar arm moving between two points, joint angle trajectories are produced using a general Fourier series to describe the time course of the angular velocities $\dot{\theta}$. Two terms of the Fourier series are shown to be adequate, leading to an equation for the velocity profile of each joint based on its start and target values (equation 2.9). The joint angles (equation 2.8) and angular accelerations (equation 2.10) are then calculated by integrating and differentiating this equation respectively.

$$\theta = \theta_{start} + 0.5\left(\theta_{target} - \theta_{start}\right)\left[1 - \cos\left(\frac{\pi t}{T}\right)\right] + 0.5D\left[1 - \cos\left(\frac{2\pi t}{T}\right)\right] \tag{2.8}$$

$$\dot{\theta} = \left(\frac{\pi}{T}\right)\left[0.5\left(\theta_{target} - \theta_{start}\right)\sin\left(\frac{\pi t}{T}\right) + D\sin\left(\frac{2\pi t}{T}\right)\right] \tag{2.9}$$

$$\ddot{\theta} = \left(\frac{\pi}{T}\right)^2\left[0.5\left(\theta_{target} - \theta_{start}\right)\cos\left(\frac{\pi t}{T}\right) + 2D\cos\left(\frac{2\pi t}{T}\right)\right] \tag{2.10}$$

In equations 2.8, 2.9 and 2.10, T is the movement time, θ_{start} is the joint angle at time $t = 0$, and θ_{target} is the required joint angle at time $t = T$. All three equations can be applied to both the shoulder and elbow joints of a two link arm. The variable D determines the exact trajectory between the two joint angles by effectively changing the timing of the movements. If D is zero, the joint angular velocity $\dot{\theta}$ follows the form of a sine wave, rising to a peak at time $t = \frac{T}{2}$ and falling again. If D is positive $\dot{\theta}$ reaches its peak early in the movement, while if D is negative the opposite occurs, as shown in Figure 2.4.

Using the equations given by Alexander[2], it is possible to calculate the metabolic energy used by the muscles for a given trajectory characterised by a value of D for each joint. The optimisation process for a given set of start and target angles involves varying these values of D and recording the total metabolic energy used by all the muscles of the arm. For two joint angles, this gives a 2D landscape whose minimum gives the values of D that produce the minimum metabolic energy cost for the given task.

Comparisons with movement data from human subjects[57] show that it produces optimal trajectories that are similar to the observed trajectories for fast movements when operating on a biarticular arm model. However, it shows marked differences when perform-

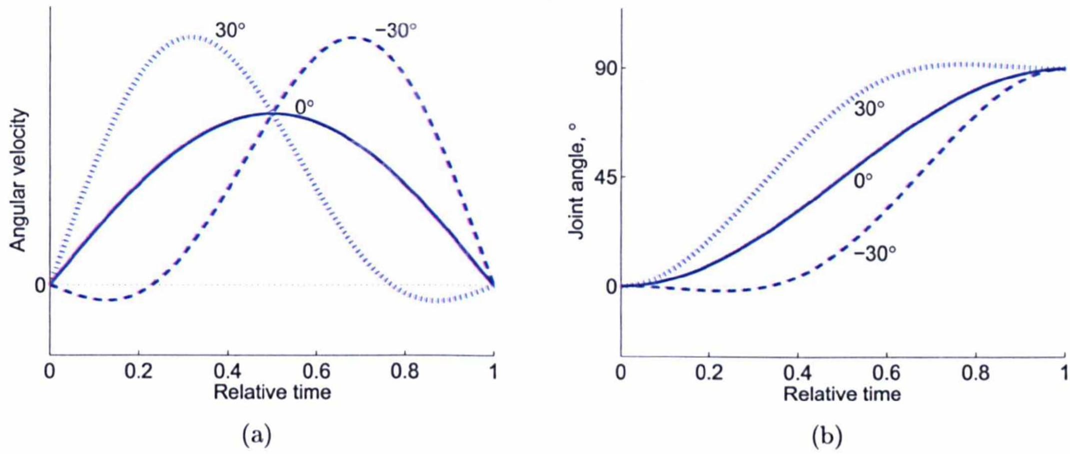

Figure 2.4: Plot showing the effect of the parameter D on trajectories produced by the minimum metabolic energy model. Positive values of D cause the peak velocity to occur earlier in the movement, while negative values cause it to occur later. A zero value for D puts the peak velocity exactly half-way through the movement. (a) Angular velocity profiles for three different values of D, and (b) their corresponding trajectories for a joint movement of 90 degrees.

ing slow movements due to the assumptions made about the maximum angular shortening speeds that the muscles can use. Also, as noted by Alexander[2], task performance is often a more plausible criterion than simple energy economy.

Although energy minimisation can not account for much of the behaviour observed in arm movements or eye movements, it is often used in conjunction with a smoothness cost such as minimum jerk,[116] described in the following section.

2.2.2 Minimum jerk

The minimum jerk model is an example of a purely kinematic cost function. These would seem to be good candidates for explaining human movement, as most targets for reaching are specified in external visual coordinates; it follows that movement planning could also take place in extrinsic coordinates.

It has been suggested that smooth, straight hand paths can be explained if smoothness of movement is an explicit goal of the system.[41] A good measure of smoothness is the jerk of the movement, defined as the derivative of the Cartesian hand acceleration (the third derivative of the hand position). The cost function of the minimum jerk model is given by equation2.11.

$$C_{jerk} = \frac{1}{2}\sum_{n=0}^{T}\left((\dddot{x}_n)^2 + (\dddot{y}_n)^2\right) \tag{2.11}$$

In equation 2.11, T is the number of time steps in the movement and $\dddot{x}$ and $\dddot{y}$ represent the jerk of the movement along each axis. Results for this model show a good match between predicted trajectories and most actual trajectories. The hand paths are indeed smooth and straight. Not all features of movement are captured by the minimum jerk model however, including the slight asymmetry in the velocity profile and the speed-accuracy trade-off, since the model does not include any disturbances.

Figure 2.5 shows simulation hand paths and velocity profiles for ten movements performed between similar points in one area of the arm's workspace. These simulations were performed by an implementation of minimum jerk model using the optimal control scheme described in the next chapter. The specific details of the minimum jerk implementation of this control scheme are given in Appendix A.

As can be seen in Figure 2.5(a), the movements predicted by the minimum jerk model fit the criterion for straight hand trajectories described in section 1.1. The trajectories are smooth with characteristic bell-shaped velocity profiles[41] (Figure 2.5(b)). However, they lack the slight curvature typical of human movements. As stated previously, the minimum jerk model also lacks an accuracy constraint.

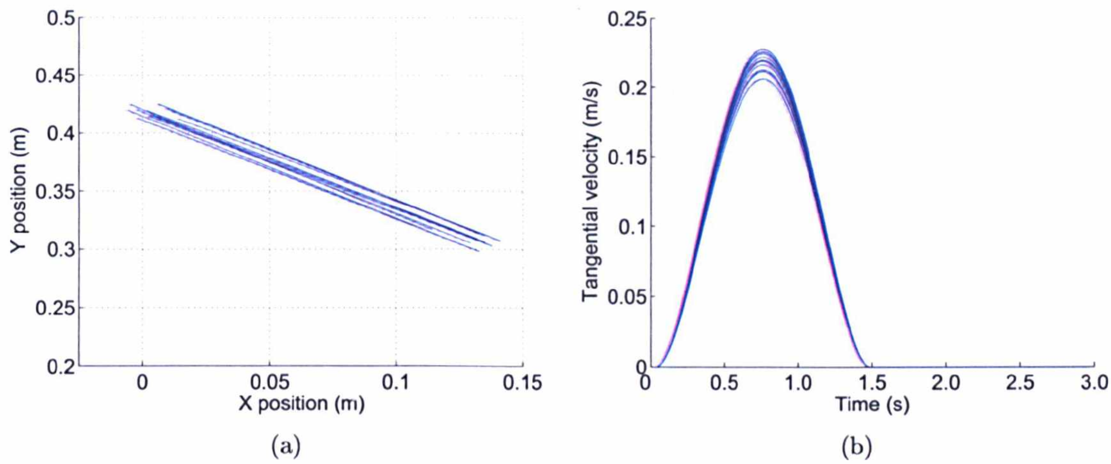

Figure 2.5: Ten typical trajectories produced by the minimum jerk model in simulation: (a) Hand paths; (b) Tangential velocity profiles

A major consideration for using this model on a robot arm is the fact that Cartesian positions and velocities have to be converted into angles and angular velocities at each time step to control the robot arm. This is not difficult or computationally expensive with a two-link planar arm, but a more complicated arm model would have a correspondingly more complicated inverse kinematics function. There are several existing inverse kinematics algorithms, working in a variety of different ways (including iterative methods), that could be used to deal with this increased complexity. Inverse kinematic functions are also one-to-many functions, meaning that the arm configuration calculated at each time step would have to be checked against the configuration at the previous time step to ensure joint angle continuity.

2.2.3 Higher-order derivatives

Jerk is not the only derivative of Cartesian position that has been explored as an optimisation criterion. Trajectories involving the fourth derivative of hand position ("snap") and beyond have been produced, as shown in Figure 2.6. The general hypothesis for higher-order derivatives states that minimising the nth derivative of hand position gives a continuous profile for the $(n-1)$th derivative and a smooth profile for the $(n-2)$th derivative.

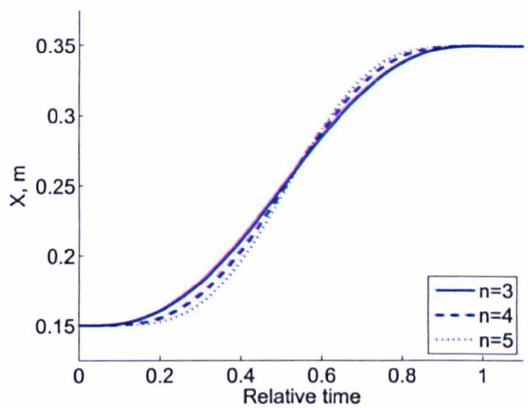

(a)

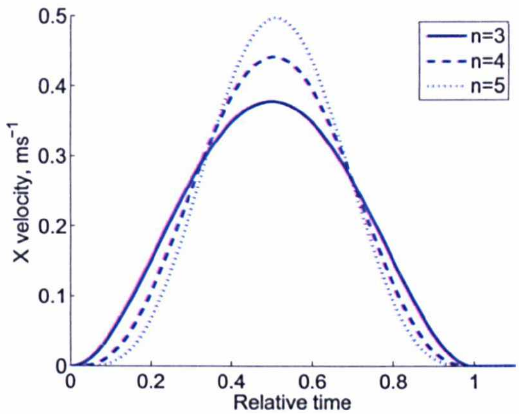

(b)

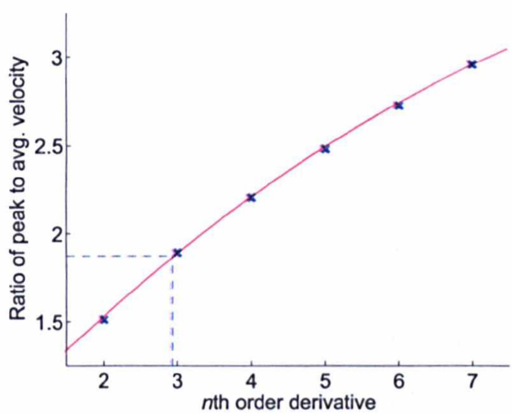

(c)

Figure 2.6: Plots showing (a) x-axis trajectories and (b) x-axis velocity profiles for 20cm movements of duration 1s where different derivatives of hand position have been minimised; (c) Plot showing the relationship between derivative order n and the ratio between peak velocity and average velocity r. The dashed line shows the how the experimentally derived value for humans, $r = 1.875$, relates to the derivative order.

As the value of n gets higher, the optimal trajectory tends to a step function and the velocity profile gets correspondingly narrower and taller. The change in the velocity profile can be measured as the ratio r of peak velocity to average velocity. As shown in Figure 2.6(c), the value of r increases with n. However, psychophysical experiments have shown that in human subjects r is about 1.875 (shown as a dashed line in Figure 2.6(c)) and therefore produce trajectories that are closest to minimum jerk trajectories. Very little is gained in terms of similarity to human movement by taking derivatives above jerk, and it is also unclear how the brain would calculate these higher-order derivatives.[51]

2.2.4 Minimum angle jerk

An obvious problem with the minimum jerk criterion as outlined above is that the optimisation is not carried out in an intrinsic space, thus requiring transformations between coordinate systems in order for the optimal trajectory to actually be performed. The equally obvious response is to perform minimum jerk optimisation of the joint angle trajectories rather than the hand trajectory itself. The cost function for this criterion is given by equation 2.12.

$$C_{angle-jerk} = \frac{1}{2}\sum_{n=0}^{T}\left(\sum_{i=1}^{N}(\dddot{\theta}_{i,n})^2\right) \tag{2.12}$$

Here, T is the number of time steps in the movement, and $\dddot{\theta}_{i,n}$ is the third derivative of the ith joint angle of N joints. As for the minimum jerk model, trajectories produced using equation 2.12 are smooth, but in addition show the slight curvature associated with unconstrained point-to-point reaching movements by humans, as shown in Figure 2.8.

Despite this, minimum angle jerk does not fully explain human reaching behaviour. In the same way that minimising the jerk of the hand leads to straight paths in hand space, so minimising the jerk of joint angles leads to straight paths in joint space. This is not what is observed in actual human reaching, where joint angles do not change monotonically but can invert part way through the movement - as when moving the arm from outstretched to the side, to outstretched in front of the body. In the same way as the minimum hand jerk model, the minimum angle jerk model also fails to take into account any of the forces

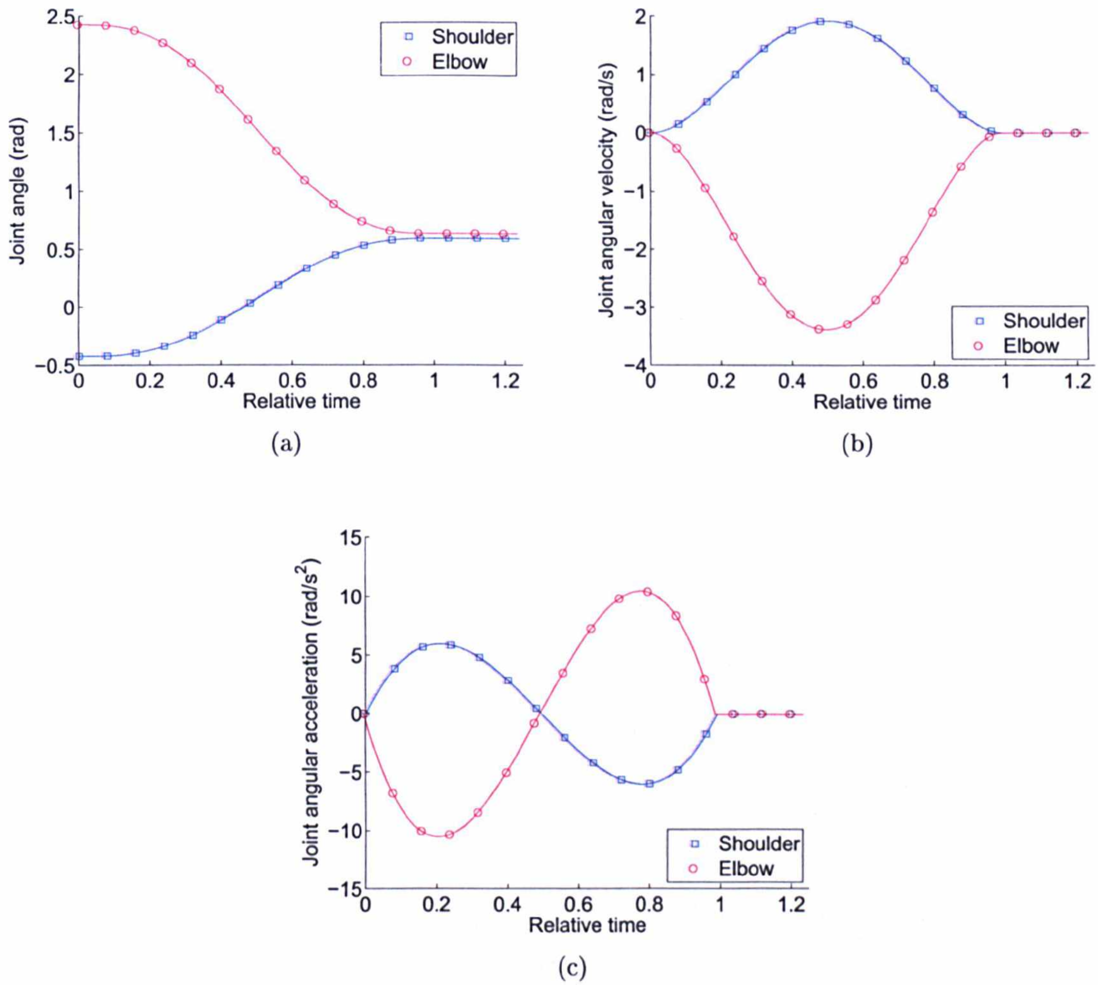

Figure 2.7: Joint angle trajectories for ten movements performed using the minimum angle jerk evaluation function: (a) The changes in joint angle are smooth, as required; (b) The joint angle velocities have the required bell-shape; (c) The joint acceleration profiles are also smooth and have no discontinuities.

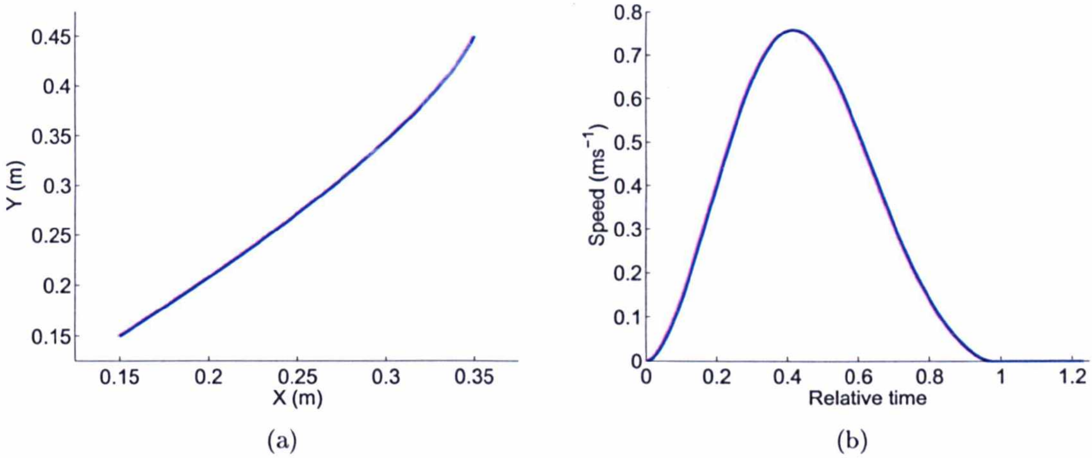

Figure 2.8: Minimum angle jerk hand path and velocity profile: (a) The hand path is smooth and roughly straight, with a slight degree of curvature; (b) The hand velocity profile has the required bell-shape

or other dynamics that act on the arm.

2.2.5 Minimum torque-change

In contrast to the purely kinematic minimum jerk models, the minimum torque-change model[119] uses a dynamic cost function. While the minimum jerk model captures some of the general behaviour of reaching movements (such as smooth movement and a generally straight hand path), it is unlikely that movements are determined independently of dynamic quantities of the arm such as length, load, torque or external force. To account for this, it was suggested that the change in the joint torques be used as a cost function, as shown by equation 2.13.

$$C_{torque-change} = \frac{1}{2}\sum_{n=0}^{T}\left(\sum_{i=1}^{N}(\dot{\tau}_{i,n})^2\right) \tag{2.13}$$

T is again the number of time steps in equation 2.13, while $\dot{\tau}_{i,n}$ is the derivative of torque at the ith joint of N joints, for each time step n. Torque *change* is used rather than minimisation of joint torque itself, as this is known to generate discontinuities in acceleration which are inconsistent with smooth movement.[69]

Uno et al.[119] calculated joint torques using the dynamics equations for a two-joint manipulator acting in the horizontal plane, equations 2.14 and 2.15. Given these highly non-linear dynamics, the trajectories that minimised the cost function could not be calculated analytically in the same way as those for the minimum jerk model, but required an iterative learning scheme.[119]

$$\tau_1 = \left(I_1 + I_2 + 2M_2L_1S_2\cos\theta_2 + M_2(L_1)^2\right)\ddot{\theta}_1 + \left(I_2 + M_2L_1S_2\cos\theta_2\right)\ddot{\theta}_2$$

$$-M_2L_1S_2\left(2\dot{\theta}_1 + \dot{\theta}_2\right)\dot{\theta}_2\sin\theta_2 + b_1\dot{\theta}_1 \tag{2.14}$$

$$\tau_2 = \left(I_2 + M_2L_1S_2\cos\theta_2\right)\ddot{\theta}_1 + I_2\ddot{\theta}_2 + M_2L_1S_2\left(\dot{\theta}_1\right)^2\sin\theta_2 + b_2\dot{\theta}_2 \tag{2.15}$$

In these equations, M_i, L_i, S_i and I_i are the mass, length, distance from the centre of mass to the joint, and the rotary inertia of the link i around the joint, respectively. b_i is the coefficient of viscosity and τ_i is the torque, both for the joint i. The values used for these parameters are given in Uno et al.[119].

The trajectories produced by the dynamic minimum torque-change model are closer to those produced by humans than the trajectories of the purely kinematic minimum jerk model: they are not perfectly straight but are instead slightly curved. The hand paths are still smooth however.

The hand paths predicted by the model agreed with those predicted by the minimum jerk model in areas close to and in front of the body. Significant differences were predicted however in areas further out and to the side of the body, where the dynamics of the arm differ from those in front of the body. This is a feature of human movement which is captured by models where the hand kinematics are not independent of the physical system used to generate them.[91,119] One clear example of this feature is the inversion of the elbow joint angle during some movements; this inversion is captured by the minimum torque-change model but not, as described above, by the minimum angle-jerk model.

In a similar way to the minimum angle jerk model, the minimum torque-change model is more appropriate for controlling the robot arm than the minimum Cartesian jerk model.

The hand position is calculated using the the forward kinematics which are much less computationally expensive than the inverse kinematics. They are also many-to-one functions, so there is no ambiguity about the position of the hand. The required joint angles can be easily translated to the required angles of the motors of the robot arm. However, it still does not fully account for all the features of human movement. In particular, it does not predict any change in the temporal position of the peak velocity; that is, the minimum torque-change velocity profiles are always symmetric and never skewed to either the start or the end of the movement.[114]

This model also still does not account for disturbances to the system and lacks an accuracy constraint. It has the added disadvantage that the criterion it optimises is difficult to measure and calculate compared to a quantity such as jerk, since the inverse dynamics are non-linear equations.

2.2.6 Minimum commanded torque change

The term *commanded* torque refers to the torques that control muscle tension, and hence muscle torque. The commanded torque compensates for the damping caused by muscle viscous properties, i.e. to generate actual torque, the motor commands controlling the muscle tension must overcome the muscles inherent viscosity. By considering muscle properties in addition to the link dynamics used by the minimum torque-change model, the commanded torque can be thought of as a better representation of the motor signals used by the central nervous system (CNS) than the actual torque.[93]

In this model, the cost function is the same as that of the minimum torque-change model (equation 2.13).[119,93,66] However, Nakano et al.[93] address a number of issues regarding the torque equations given by Uno et al.[119], including parameter values for inertia I and viscosity b. They use slightly modified equations for the joint torque, and include a term that accounts for the acceleration due to gravity when movements are performed in the vertical plane.

The minimum commanded torque-change model is based on the idea that the characteristics of human movement can be captured if smoothness constraints are put on the motor system at the level of motor commands generated by the CNS. Since these are at a high level in the motor hierarchy of motor neurons-muscle tensions-torques-joint angles-hand position, the constraints are passed on to each level, reducing the natural indeterminacy of the system. As stated above, in the minimum torque-change model the link dynamics are regarded as the controlled object, while the minimum commanded torque change model uses signals that control muscle tensions to control both the link dynamics and muscles.

For movements in both the horizontal and sagittal planes, the minimum commanded torque change model produces trajectories that match well with the spatial characteristics of observed trajectories. In particular, the trajectories of the model capture the magnitude and direction of movement curvature better than either the minimum torque-change model or the minimum jerk model.

One of the drawbacks of the model from the point of view of controlling a robot is that it is computationally difficult to reliably calculate the optimal trajectories.[66]

Summary

Computational models of human movement vary considerably in the observable characteristics of such movement that they capture and in their applicability to controlling a robot arm. In this chapter the focus has been on optimisation models. It has been demonstrated that they can be successful in capturing and explaining some characteristic features of human arm movements. Their applicability to the control of a robot arm has also been discussed briefly.

The models described in this chapter have focused on producing arm movements with straight hand paths and bell-shaped velocity profiles, but few have addressed the issue of the speed-accuracy trade-off. Many do not include a specific accuracy constraint or do not include any form of disturbance as part of their model. A further point is that few models include a convincing explanation as to why their particular characteristic should be optimised by the motor system, other than the predicted trajectories.

In the next chapter the minimum variance criterion, a model that sets out to specifically addréss these issues, is introduced and implemented for control of a robot arm.

Chapter 3

Minimum Variance Model

It was stated in the previous chapter that the stereotypical features of human movement hold true between individuals and between repeated movements for the same individual. However, all movements are subject to noise which causes deviations from the desired trajectory. The models mentioned previously do not account for these deviations, or assume them to be negligible. By contrast, the minimum variance model[52] specifically allows for disturbances to the hand trajectory caused by noise on the motor command signal.

The goal of the model is to minimise the variance in the hand position caused by this noise during some post-movement period. In this chapter this explanation is expanded, and it is explained how the model accounts for the speed-accuracy trade-off and smooth arm movements. Details are then given of the implementation of this model using an optimal control scheme. The extension to more complex trajectories involving via-points is outlined, and trajectories are presented for both simple point-to-point reaching movements and via-point trajectories.

1 Minimum Variance Model

Starting from the fact that all neuronal signals are subject to signal-dependent noise (noise whose variance is proportional to the signal amplitude), it follows that such noise on the neuronal motor signals sent to muscle units results in deviations from the desired path. Moving rapidly necessarily requires motor signals with large amplitudes and hence high levels of noise, causing greater deviations. Over the course of the movement these deviations accumulate, leading to inaccuracy of the final arm position and possibly causing failure of the movement goal. Moving as fast as possible is therefore sub-optimal from a goal-achievement point of view. Since different tasks require different levels of spatio-temporal precision, an optimal movement would be one that balances the speed-accuracy trade-off to accomplish the task.

It was therefore proposed that the goal of motor planning is to minimise the variance of the arm's position in the presence of signal-dependent neuronal noise.[52] In this model the movement time is chosen to achieve a given movement accuracy constraint. In the formulation of the model expressed by Harris and Wolpert[52], the optimisation criterion to produce goal-directed movements is defined in terms of reaching a target position and maintaining it for a post-movement period, during which the summed positional variance should be minimised.

$$C_{variance} = \sum_{t=T}^{T+N} \left(\sigma_x^2(t) + \sigma_y^2(t)\right) \tag{3.1}$$

In equation 3.1, T is the number of time steps in the movement and N is the number of time steps in the post-movement period. The definition of the variance at each time step $\sigma_x^2(t)$ is

$$\sigma_x^2(t) = E\left[(x(t) - \bar{x}(t))^2\right] \tag{3.2}$$

where $x(t)$ is the hand x-axis position subject to signal-dependent noise and $\bar{x}(t)$ is the position of the hand if the system was noiseless. $E[\dots]$ represents the expected value over repeated movements. For time steps during the period $t = T, \dots, T+N$, the mean position $\bar{x}$ should be the target position x_{tgt}. The same definition applies for the y-axis. This means equation 3.1 can be rewritten as

$$C_{variance} = \sum_{t=T}^{T+N} \left(E\left[(x(t) - x_{tgt})^2\right] + E\left[(y(t) - y_{tgt})^2\right]\right) \tag{3.3}$$

Alternatively, since the sum of expected values is the same as the expected value of the sum, this can written as

$$C_{variance} = E\left[\sum_{t=T}^{T+N} \left((x(t) - x_{tgt})^2 + (y(t) - y_{tgt})^2\right)\right] \tag{3.4}$$

which is the discrete version of the integral cost function for the minimum variance model given in Miyamoto et al.[86]. As in equation 3.1, in equation 3.4 T represents the number of time steps in the movement and N is the number of time steps in the post-movement period. $x(t)$ and $y(t)$ are the hand coordinates positions, x_{tgt} and y_{tgt} are hand target positions, and $E[\ldots]$ is the expected value over repeated movements.

The principle of the minimum variance model can be thought of as moving to a target as accurately as possible in the presence of signal-dependent noise. The model achieves this for individual movements by producing a control law that aims to minimise the spread of end-points about the target of *all* movements between two points.

It is not sufficient to add signal-dependent noise to a feedback-system whose optimisation criterion involves moving precisely to a target. In this situation the noise on the control signals would cause deviation from the optimal trajectory, which would in turn cause corrective actions through the feedback mechanism. The end result would be that individual movements would end as close to the target as possible, given their own independent (and random) noise profile. However, as the noise was not included as part of the original set of optimisation criteria there is no guarantee that the standard-deviation of all independent movement end-points about the target would be in any sense optimal.

Also, any control law produced without allowing for the noise in the system will produce the same trajectories regardless of the relative level of that noise. This means that movements cannot be adapted to maintain a required level of task performance if the system noise changes.

As mentioned above, a key assumption of the model is that the control signals are corrupted by random noise during movement. Based on studies of the standard deviation of motor-neuronal firing,[84] this noise is assumed to have a normal distribution with zero mean and variance proportional to the amplitude of the control signal.[52] This form of the noise is also used in other (non-optimisation) models that include some measure of deviation from a planned trajectory.[14] The exact form of the noise is discussed further in chapter 6.

This model has been shown to produce the roughly straight, smooth movements[52,86] observed in humans.[91] Smooth movements are a clear consequence of the optimisation criterion, as non-smooth movements require larger motor commands which have higher amplitude noise, increasing the cumulative variance.

The speed-accuracy trade-off observed in human movement can also be shown to be a property of minimising the movement variance: fast movements require large control signals, which are subject to higher amplitude noise than slower movements requiring small control signals. Trials with a computational model demonstrate that the two-thirds power law also emerges as a result of minimising the variance of the hand position.[52]

One of the further implications of using end-point accuracy as a criterion for movement is that different trajectories emerge when the goal area is not uniform in all dimensions. For example if the goal area is a rectangle, greater constraints are placed on movements coinciding with the narrow axis of the rectangle than with movements along the wide axis. Depending on the exact task requirements, these different constraints lead to different trajectories.

This aspect of minimising the end-point variance has been formalised by Todorov and Jordan[117]. Their experiments and mathematical models of noisy human movement indicate that trajectories are chosen so that the inevitable variation in a movement is shifted to task-irrelevant dimensions, consequently minimising the variance in task-specific dimensions.

As well as reliably capturing the important features of human arm movements, the minimum variance model has further advantages. Unlike other models, it offers a principled explanation as to why the motor system should have evolved to produce movement in this way. Also, the variance of the hand position over repeated trials is a readily observable quantity that can be reliably estimated from visual and proprioceptive information, in contrast to more complex derivative terms such as jerk or joint torque. The concept of a distribution of movements around a mean is in line with the growing application of probabilistic and Bayesian models to neuroscientific studies.[76,72]

1.1 Previous Implementations

The minimum variance model has been implemented in various forms. The original formulation[52] used a combination of muscle and skeletal models for the arm, combined with optimisation of cubic splines to determine the minimum variance trajectory. Other approaches include the combination of a minimum jerk trajectory generator and a recurrent network to produce the required movements[86] and a Kalman filter method with a muscle model, used to examine appropriate feedback control laws.[117] An analytic solution to the minimum variance problem has also been proposed.[35,36]

Another study that should be mentioned is that of Burdet and Milner[14]. They propose a model where a single movement is produced through the superposition of several smooth submovements. A particular feature of this model is that it allows for deviation of the overall movement by making the amplitude of each submovement variable. This has the effect of making the deviation proportional to the mean velocity of the submovement. As each submovement is able to correct for the deviations introduced by previously submovements (subject to sensory uncertainty about the current deviation and the variability introduced by the submovement itself) greater accuracy is achieved with a greater number of submovements.

This model captures many of the same features of movement as the minimum variance model, including the slightly asymmetric velocity profile of point-to-point movements and the speed-accuracy trade-off. It also introduces other aspects of movement, including learning to perform a given movement more accurately by adjusting parameters over multiple trials.[14]

The most appropriate implementation for this work was the Kalman Filter optimisation scheme of Todorov and Jordan.[117] This feedback control scheme allows rapid movement planning and is suitable for controlling a robot arm. As well as the specific application of controlling a robot arm, a further consideration in using this scheme is its suitability for extension other domains, especially that of action perception. As discussed further in chapter 5, the optimisation scheme and implementation described in detail below fitted well with the principles underlying a model for robotic imitation and action perception.[30,31] The next section details how the Kalman Filter optimisation scheme for producing minimum variance movements was implemented.

2 Implementation

2.1 The arm model

The model used to represent a robot arm in this work is a two link arm with two rotational degrees-of-freedom (DOF), restricted to movement in a plane (Figure 3.1). The forward and inverse kinematics of this model are well defined, allowing both extrinsic and intrinsic optimisation criteria (see chapter 2) to be investigated using the same model.

This is a relatively straightforward multi-joint arm, but it represents a good trade-off between realistic human movement and model complexity. It is sufficient to show details of the movement model and the trajectories it produces without being subject to the difficulties of working with the complex kinematics of an arm with more DOFs.

Many studies have used a manipulandum to restrict a person to move their arm in a plane, providing data for comparison between the movement of this robot arm model and actual human movement.[91,41,119,88,15]

The optimisation scheme described below actually performs all calculations by modelling the hand as a 2-D point mass. It is straightforward to convert the position of this point-mass to the corresponding joint angle changes required to move the hand from its starting position to a target.

2.2 Optimal control algorithm

The algorithm for the optimal control scheme used in this work is described in the following section. This description is largely based on the supplementary notes to Todorov and Jordan[117].

2.2.1 Modified Linear-Quadratic-Gaussian (LQG) System

A general control model takes the form:

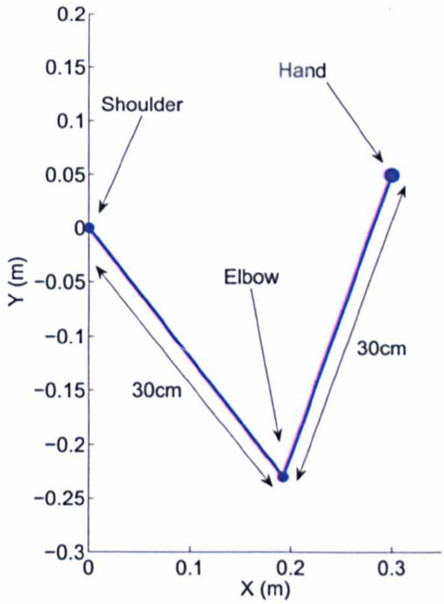

(a)

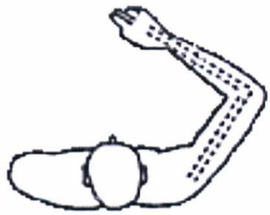

(b)

Figure 3.1: The two link planar arm model with two rotational degrees of freedom used in this work. The forward and inverse kinematics for this arrangement are well defined, allowing extrinsic and intrinsic optimisation criteria to be examined.

$$\mathbf{x}_{t+1} = A\mathbf{x}_t + B\mathbf{u}_t \tag{3.5}$$

$$\mathbf{y}_t = H\mathbf{x}_t \tag{3.6}$$

$$0 \leq \mathbf{x}_t' Q_t \mathbf{x}_t + \mathbf{u}_t' R \mathbf{u}_t \tag{3.7}$$

where equation 3.5 represents the dynamics, equation 3.6 represents the feedback, and equation 3.7 is the control cost. The terms used in these equations are the state vector $\mathbf{x}(t)$, the control signal vector $\mathbf{u}(t)$ and the output vector $\mathbf{y}(t)$. The definitions of the matrices A, B, H, Q and R are given below. To account for multiplicative (signal-dependent) noise in the system, this dynamic and feedback equations of the general model are modified a shown below:

$$\mathbf{x}_{t+1} = A\mathbf{x}_t + B\mathbf{u}_t + \sum_{i=1}^{k} C_i \mathbf{u}_t \varepsilon_{i,t} \tag{3.8}$$

$$\mathbf{y}_t = H\mathbf{x}_t + \omega_t \tag{3.9}$$

In these equations, $\varepsilon_{i,t}$ are independent standard normal variables, C_i are constant matrices, and ω_t is a vector of independent multivariate normal random variables with mean 0 and covariance matrix Ω^{ω}, also defined below. An important point to note here is that, through the inclusion of the C_i matrices, the presence of noise on the control signals is directly included in the optimisation algorithm (see section 2.2.2, below).

The Linear Quadratic Gaussian (LQG) problem is to find the control law which minimises the expected cumulative cost over a given time interval, given the matrices specified above. It has a well-known solution when the noise is additive rather than multiplicative. To solve the problem when the noise is multiplicative, Todorov and Jordan[117] derived an iterative algorithm using a modified Kalman filter, which takes the following form.

2.2.2 Kalman filter

For a given control law L_t, the corresponding Kalman filter K_t is

$$\begin{aligned}
\hat{\mathbf{x}}_{t+1} &= A\hat{\mathbf{x}}_t + B\mathbf{u}_t + K_t(\mathbf{y}_t - H\hat{\mathbf{x}}_t) && (3.10)\\
K_t &= A\Sigma_t^e H' (H\Sigma_t^e H' + \Omega^{\omega})^{-1} && (3.11)\\
\Sigma_{t+1}^e &= (A - K_t H)\Sigma_t^e A' + \sum_n C_n L_t \Sigma_t^{\hat{x}} L_t' C_n' \ ; \ \Sigma_1^e = \Sigma_1 && (3.12)\\
\Sigma_{t+1}^{\hat{x}} &= K_t H \Sigma_t^e A' + (A - BL_t)\Sigma_t^{\hat{x}}(A - BL_t)' \ ; \ \Sigma_1^{\hat{x}} = \hat{\mathbf{x}}_1\hat{\mathbf{x}}_1' && (3.13)
\end{aligned}$$

In the set of equations 3.10 to 3.13, $\hat{\mathbf{x}}$ is the estimated state vector and matrices K_t, Σ_t^e, and $\Sigma_t^{\hat{x}}$ correspond to the Kalman gain, the expected estimation error covariance, and the non-centred covariance of the state estimate. Computing the unknown matrices in this set of equations requires a single forward pass through time.

For a given Kalman filter K_t, the corresponding control law L_t is

$$\begin{aligned}
\mathbf{u}_t &= -L_t\hat{\mathbf{x}}_t & (3.14)\\
L_t &= \left(B'S^{\mathbf{x}}_{t+1}B + R + \sum_n C'_n\left(S^{\mathbf{x}}_{t+1} + S^{e}_{t+1}\right)C_n\right)^{-1} B'S^{\mathbf{x}}_{t+1}A & (3.15)\\
S^{\mathbf{x}}_t &= Q_t + A'S^{\mathbf{x}}_{t+1}\left(A - BL_t\right)\ ;\ S^{\mathbf{x}}_T = Q_T & (3.16)\\
S^{e}_t &= A'S^{\mathbf{x}}_{t+1}BL_t + \left(A - K_tH\right)'S^{e}_{t+1}\left(A - K_tH\right)\ ;\ S^{e}_T = 0 & (3.17)
\end{aligned}$$

In the set of equations 3.14 to 3.17, S^e_t and $S^{\mathbf{x}}_t$ are the parameters specifying the optimal cost-to-go function. Computing the unknown matrices in this set of equations requires a single backward pass through time. To find the Kalman filter and control law that are optimal with respect to one another, the sets of equations 3.11 to 3.13 and 3.15 to 3.17 are iterated until convergence. It has been shown that iteration always converges exponentially, and to the same answer regardless of initialisation.[117]

As such, for the simulations shown in this thesis L_t was set to zero for the first pass through equations 3.11 to 3.13, taking the value calculated by equations 3.15 to 3.17 thereafter.

2.2.3 State vector

As described in section 2.1, following Todorov and Jordan[117] the hand was modelled as a point-mass with position (p^x_t, p^y_t). The movement of the hand is accomplished through actuators producing forces f^x_t and f^y_t. This forces are calculated by applying a second-order linear filters with time constants $\tau_1 = \tau_2 = 0.04s$ to the noisy control signals u^x_t and u^y_t.

As the plant model is an inertial system, the state vector has to include the position and velocity of the point mass. The linear filters used to calculate the actuator forces have their own states, which must be included as well (since the filters are second-order, two state variables per actuator are needed). Finally, the target position (g_x, g_y) is needed so that the task error can be defined as a function of the state, as per equation 3.7 (see section 2.2.5, below).

With a single target it is acceptable to include the goal coordinates in the state vector. However, if multiple via-points are defined as part of the task, this structure can become inefficient and unwieldy. To make the state vector simpler in this situation, the goal coordinates can be encoded in the state cost matrix Q_T. The state vector then has two "1"s appended to it for each required positional constraint (an x-axis goal coordinate and a y-axis goal coordinate). For a single target, this gives a ten-dimensional state vector $\mathbf{x}_t$:

$$\mathbf{x}_t = \begin{bmatrix} p_t^x & p_t^y & \dot{p}_t^x & \dot{p}_t^y & f_t^x & f_t^y & \tilde{f}_t^x & \tilde{f}_t^y & 1 & 1 \end{bmatrix}' \tag{3.18}$$

In equation 3.18, $\tilde{f}_t^i$ is the internal state variable required to implement the second-order filter.

2.2.4 Dynamics matrices

Having defined the state vector, it is now appropriate to define the constant matrices used in the dynamics and feedback equations: A, B, C_n and H.

Sensory feedback to the system only requires position, velocity and force information, so the internal state variables for the second-order filter and the positional "1"s do not need to be included in the feedback vector $\mathbf{y}_t$. This sets the feedback matrix $H = \begin{bmatrix} I_{6x6} & 0_{6x4} \end{bmatrix}$. Putting this H matrix into equation 3.9 gives the state feedback vector as:

$$\mathbf{y}_t = \begin{bmatrix} p_t^x & p_t^y & \dot{p}_t^x & \dot{p}_t^y & f_t^x & f_t^y \end{bmatrix}' + \omega_t \tag{3.19}$$

AS mentioned previously, the sensory noise terms in the vector ω_t are independent Gaussians with a mean of zero, and standard deviations:

$$\sigma_s \begin{bmatrix} 0.01m & 0.01m & 0.1ms^{-1} & 0.1ms^{-1} & 1N & 1N \end{bmatrix}'$$

σ_s is a weighting term that sets the overall sensory noise magnitude. It was set to 0.4 for the simulations shown here. The relative magnitudes of the standard deviation terms given above were set by the fact that, for the movements tasks carried out in this work velocities are an order of magnitude larger than displacements and forces are an order of magnitude larger than velocities.

The discrete time dynamics of the system $\mathbf{x}_{t+\Delta t} = A\mathbf{x}_{t+\Delta t} + B\mathbf{u}_t + C_1\mathbf{u}_t\varepsilon_t^1 + C_2\mathbf{u}_t\varepsilon_t^2$ is given by the following set of equations (the subscripts x and y have been removed from the equations for position, velocity and force for clarity. Each equations applies equally to movement of the hand on the x- and y-axis):

$$p_{t+\Delta t} = p_t + \dot{p}_t \Delta t$$

$$\dot{p}_{t+\Delta t} = \dot{p}_t + \frac{f_t \Delta t}{m}$$

$$f_{t+\Delta t} = e^{-\frac{\Delta t}{\tau_1}} f_t + e^{-\frac{\Delta t}{\tau_1}} \tilde{f}_t$$

$$\tilde{f}^x_{t+\Delta t} = e^{-\frac{\Delta t}{\tau_1}} \tilde{f}^x_t + u^x_t + \sigma_u \left(u^x_t \varepsilon^1_t + u^y_t \varepsilon^2_t\right)$$

$$\tilde{f}^y_{t+\Delta t} = e^{-\frac{\Delta t}{\tau_1}} \tilde{f}^y_t + u^y_t + \sigma_u \left(u^y_t \varepsilon^1_t - u^x_t \varepsilon^2_t\right)$$

In these equations, σ_u is a scaling factor for the signal-dependent noise. Together, the two parameters σ_u and σ_s set the overall variability of the optimal control law. For similar movements to those shown here, Todorov and Jordan set these parameters to adjust the overall variability to match their experimental observations of human movement. The values they selected were $\sigma_s = \sigma_u = 0.4$.

Given these equations and equation 3.8, the remaining dynamics matrices A, B, C_1 and C_2 can now be specified:

$$
A = \begin{bmatrix}
1 & \cdot & \Delta t & \cdot & \cdot & \cdot & \cdot & \cdot & \cdot & \cdot \\
\cdot & 1 & \cdot & \Delta t & \cdot & \cdot & \cdot & \cdot & \cdot & \cdot \\
\cdot & \cdot & 1 & \cdot & \frac{\Delta t}{m} & \cdot & \cdot & \cdot & \cdot & \cdot \\
\cdot & \cdot & \cdot & 1 & \cdot & \frac{\Delta t}{m} & \cdot & \cdot & \cdot & \cdot \\
\cdot & \cdot & \cdot & \cdot & e^{-\frac{\Delta t}{\tau}} & \cdot & e^{-\frac{\Delta t}{\tau}} & \cdot & \cdot & \cdot \\
\cdot & \cdot & \cdot & \cdot & \cdot & e^{-\frac{\Delta t}{\tau}} & \cdot & e^{-\frac{\Delta t}{\tau}} & \cdot & \cdot \\
\cdot & \cdot & \cdot & \cdot & \cdot & \cdot & e^{-\frac{\Delta t}{\tau}} & \cdot & \cdot & \cdot \\
\cdot & \cdot & \cdot & \cdot & \cdot & \cdot & \cdot & e^{-\frac{\Delta t}{\tau}} & \cdot & \cdot \\
\cdot & \cdot & \cdot & \cdot & \cdot & \cdot & \cdot & \cdot & 1 & \cdot \\
\cdot & \cdot & \cdot & \cdot & \cdot & \cdot & \cdot & \cdot & \cdot & 1
\end{bmatrix}
$$

$$
B = \begin{bmatrix} 0_{6x2} \\ I_{2x2} \\ 0_{2x2} \end{bmatrix}
$$

$$
C_1 = B \begin{bmatrix} \sigma_u & \cdot \\ \cdot & \sigma_u \end{bmatrix}; \; C_2 = B \begin{bmatrix} \cdot & \sigma_u \\ -\sigma_u & \cdot \end{bmatrix}
$$

2.2.5 Cost function matrices

The cost function matrices are the mathematical interpretation of the task. In the case of the minimum variance model, the task is to come to rest as close to a specified end-point (g_x, g_y) as possible, in time T. The cost is the defined as the amount of error in accomplishing this task, as shown in equation 3.20.

$$
\frac{1}{3} \sum_{i=x,y} \left(\left(g_i - p_T^i\right)^2 + \left(w_v \dot{p}_T^i\right)^2 + \left(w_f f_T^i\right)^2 \right) \tag{3.20}
$$

Here, the first term is the error between the final hand position p_T and the goal, and the second and third terms ensure that the hand comes to a halt at the end of the movement. The weighting terms w_v and w_f scale the velocity and force values so that all terms in the cost function have equal weighting. Again following Todorov and Jordan, these weights had the values 0.1 and 0.01 respectively, again reflecting the fact that velocities are an order of magnitude larger than displacements and forces are an order of magnitude larger than velocities.

A scale factor of $\frac{1}{3}$ is introduced as there are three task constraints - one positional, one velocity and one force. In the case of via-points being specified for a trajectory as well as an end-point target, the number of positional constraints will increase (see section 2.3, below). For P positional constraints ($P-1$ via-points and the end-point goal), the scale factor is $\frac{1}{P+2}$.

An interesting aspect of the minimum variance model over other optimisation models is that strict boundary conditions, when the errors in position, velocity and acceleration of the start and end points are required to become strictly zero, are no longer necessary. Since the final state will vary from the target state due to the noise, the goal of the algorithm is not to reach the exact target point at the end of the movement, but rather to move the hand to the target with a certain level of task-dependent variance.[86] This flexibility means that velocity constraints at the target position can also be relaxed, allowing movements such as catching a ball to be performed in the same way as reaching to a static target.

It should be noted here that although the movement time T is an input parameter of this system, determined to some extent by the required accuracy, in the human motor system movement time is more likely to be an integrated part of the optimisation process.[55] This point is discussed further in chapter 6.

Also, the optimal control scheme of Todorov and Jordan[117] does not include a post-movement period. Instead, the goal is to minimise the variance across all movements at the exact end of the movement. This does not fundamentally change the principle of the implementation, or the trajectories it produces.

As well as penalising task error, optimisation requires that the control signal energy, or effort, is also penalised. The term added to the cost function to do this is shown in equation 3.21.

$$\frac{r}{T}\left(\sum_{t=1}^{T}\left(u_t^x\right)^2+\left(u_t^y\right)^2\right) \tag{3.21}$$

Here, the scalar r represents a tradeoff between task error and effort. If the effort penalty is much larger than the task error the optimal strategy is to keep the control signals as small as possible, meaning the target may not be reached at all. With the model parameters described in the previous sections, a value of $r = 0.002$ provided a good tradeoff between error and effort. The effort penalty is also divided by the movement time T to average out the cost of the control signals over the entire course of the movement.

Converting the linear equations 3.20 and 3.21 into the appropriate matrix form for the Kalman Filter algorithm given above is straightforward. The LQG cost function (equation 3.7) specifies a state cost matrix Q and a control signal cost matrix R.

The control signal part of the cost function takes the form $\mathbf{u}_t' R \mathbf{u}_t$, where $\mathbf{u}_t = \begin{bmatrix} u_t^x & u_t^y \end{bmatrix}'$ is the control signal vector. Converting equation 3.21 into the form of equation 3.7 gives:

$$R = \frac{r}{T} I_{2x2} \tag{3.22}$$

where I_{2x2} is the 2x2 identity matrix.

The state part of the cost function takes the form $\mathbf{x}_t' Q_t \mathbf{x}_t$, where $\mathbf{x}_t$ is the state vector given in equation 3.18. Because the task error is only measured at the end of the movement ($t = T$), $Q_t = 0,\ 0 < t < T$. The only exception to this is when the task goal requires the trajectory to pass through specified via-points (see section 2.3, below). As specified by equation 3.20, the only non-zero state cost matrix is Q_T:

$$Q_T = \frac{1}{3}\begin{bmatrix} 1 & . & . & . & . & . & . & . & -g_x & . \\ . & 1 & . & . & . & . & . & . & . & -g_y \\ . & . & w_v & . & . & . & . & . & . & . \\ . & . & . & w_v & . & . & . & . & . & . \\ . & . & . & . & w_f & . & . & . & . & . \\ . & . & . & . & . & w_f & . & . & . & . \\ . & . & . & . & . & . & . & . & . & . \\ . & . & . & . & . & . & . & . & . & . \\ -g_x & . & . & . & . & . & . & . & (g_x)^2 & . \\ . & -g_y & . & . & . & . & . & . & . & (g_y)^2 \end{bmatrix} \qquad (3.23)$$

As an example of how this matrix reproduces equation 3.20, the positional constraint for the x-axis is expanded here:

$$\begin{aligned} \mathbf{x}_T' Q_T \mathbf{x}_T &= \begin{bmatrix} p_T^x & . & . & . & 1 & . \end{bmatrix} \begin{bmatrix} 1 & . & . & . & -g_x & . \\ . & . & . & . & . & . \\ . & . & . & . & . & . \\ . & . & . & . & . & . \\ -g_x & . & . & . & (g_x)^2 & . \\ . & . & . & . & . & . \end{bmatrix} \begin{bmatrix} p_T^x \\ . \\ . \\ . \\ 1 \\ . \end{bmatrix} \\ &= \begin{bmatrix} p_T^x - g_x & . & . & . & -p_T^x g_x + (g_x)^2 & . \end{bmatrix} \begin{bmatrix} p_T^x \\ . \\ . \\ . \\ 1 \\ . \end{bmatrix} \\ &= (p_T^x)^2 - p_T^x g_x - p_T^x g_x + (g_x)^2 \\ &= (p_T^x)^2 - 2p_T^x g_x + (g_x)^2 \\ &= (p_T^x - g_x)^2 \end{aligned}$$

The y-axis positional constraint is calculated in exactly the same way.

2.3 Complex Trajectories and Via-points

While point-to-point reaching movements are the simplest types of movements, humans normally carry out tasks that require more complex trajectories. These complex trajectories are characterised by one or more via-points.[121,87]

Each via-point V has two parts: its spatial coordinates and its temporal location n in the course of the movement, as shown in equation 3.24.

$$V = (p_n^x,\ p_n^y),\ 0 < n < T \tag{3.24}$$

This is no different from the start and target points, except in those cases the temporal information is unimportant ($t = 0$ for the start point and $t = T$ for the target point, where T is the duration of the movement). However, via-points must be dealt with differently to start and target points, as their temporal position within the course of the movement effects the trajectory as much as their spatial coordinates (Figure 3.2(a)). Despite this, small differences between the temporal locations of via-points (10-100ms) can produce trajectories that are sufficiently similar for most purposes (Figure 3.2(b)).

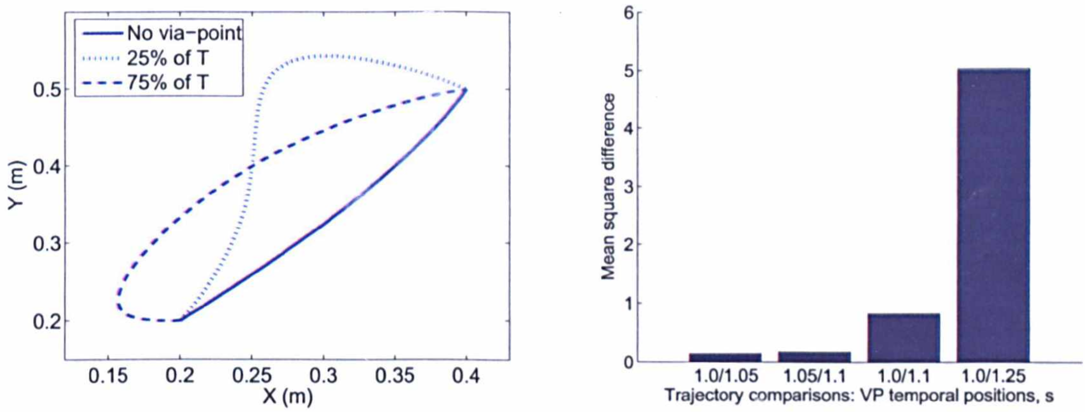

(a) (b)

Figure 3.2: The position of a via-point within the time course of a movement has a significant impact on the shape of the resulting trajectory.
(a) A simple point-to-point reaching movement with a single via-point is performed. In the first movement (dotted line) the via-point occurs at 25% of the movement time. In the second (dashed line) it occurs at 75% of the movement time. The solid line shows the reaching movement without the via-point;
(b) This chart shows mean square differences for movements with the same target and via-point as in (a). Mean square differences are shown for trajectories with via-points at the times shown on the x-axis. It is clear that differences in via-point temporal position up to about 100ms do not significantly alter the trajectory.

Via-points are added to a movement by first appending "1"s to the state vector, and then changing the state cost matrix Q_t (usually set to 0 for all t less than the movement time T) at time step $t = n$ to reflect the spatial location of the via-point. Q_t at $t = n$ takes a form similar to that of Q_T (equation 3.23). Constraints can be placed on the velocity or force when passing through the via-point, but generally these constraints are not imposed ($w_v = w_f = 0$ for Q_t) . The task error equation for a movement with P via-points can then be written:

$$\frac{1}{P+2}\sum_{i=x,y}\left(\sum_{n}\left(v_n^i - p_n^i\right) + \left(g_i - p_T^i\right)^2 + \left(w_v \dot{p}_T^i\right)^2 + \left(w_f f_T^i\right)^2\right) \tag{3.25}$$

The important differences to note between equation 3.20 and equation 3.25 are the extra term for the via-point positional errors and the change to the cost function scaling factor.

Single via-points can be useful for tasks such as obstacle avoidance, while more complex

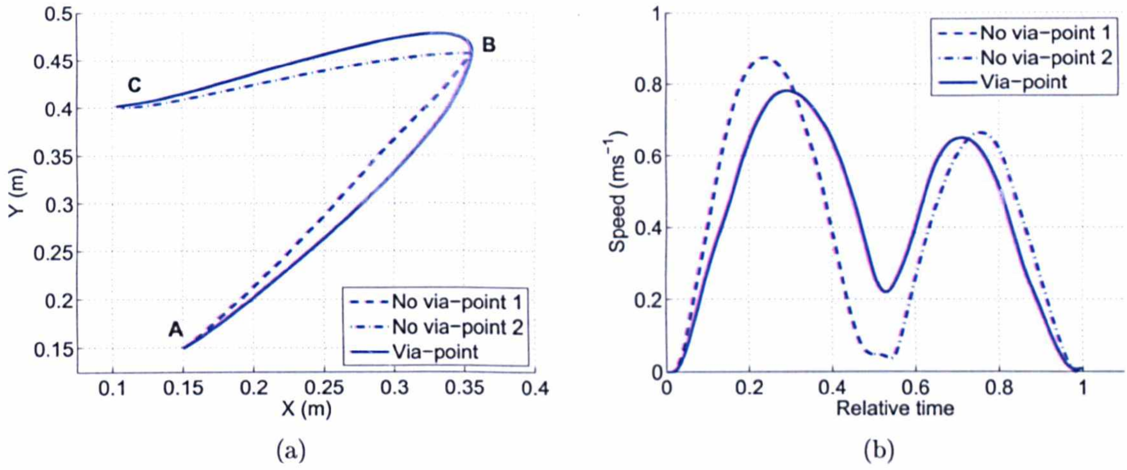

Figure 3.3: Plots showing how the target of a movement can be turned into a via-point to merge two discrete movements.
(a) Shows the trajectories of the two discrete movements and the composite movements. Movement 1 between points A and B, and movement 2 between points B and C have no via-points. Movement 3 between points A and C has a via-point at B;
(b) The velocity profiles for the three movements, clearly showing the contributions of the two discrete movements to the composite movement.

trajectories can be built up using multiple via-points. Via-points can also play a role in combining movements: instead of the target of one movement being the final position, it could be turned into a via-point for a movement that then continues into a second distinct movement, as can be seen in Figure 3.3.

Another use for via-points is to provide a reduced representation of a movement, by recording the spatial and temporal relationships between each point. The movement is then defined by its start, end and via-points. Depending on how the via-points of the movement are chosen, this can result in a compact and adaptable representation. Appendix 2.3 provides further information on how via-points could be determined to provide this sort of representation, and how this could then be used to generalise movements both spatially and temporally.

This completes the description of the Kalman Filter optimal control implementation of the minimum variance model. The following section presents the trajectories produced by the model given above, for both simple point-to-point movements and more complex trajectories with one or more via-points.

3 Trajectories and Parameter effects

3.1 Trajectories produced by the model

Example trajectories and demonstration of the speed accuracy trade-off for a simple reaching movement performed using the Kalman Filter LQG implementation of the minimum variance model are shown in Figures 3.4 and 3.5.

The trajectories predicted by this version of the model exhibited the required features of human movement. For individual point-to-point reaching movements without via-points the trajectories were slightly curved in the same way as human arm movements (Figure 3.4(a)), matching those of the dynamic minimum torque-change model without an explicitly dynamic cost function. The average of a large number of these noisy movements is a straight line between the start point and the goal point, as expected from the zero-mean Gaussian profile of the noise added to the control signals.

In addition to roughly straight smooth movements, the addition of signal-dependent noise on the control signals results in changing end-point standard deviation for different required movement times. Figure 3.5(a) clearly shows the decrease in end-point standard deviation with increasing movement time predicted by the model, and this is confirmed by the decreasing spread of distances from the target-point shown in Figure 3.5(b). This speed-accuracy trade-off matches that of Fitts' Law in human movement.

3.2 Via-point trajectories

The optimisation scheme can be extended to more complex trajectories through the inclusion of one or more via-points, as discussed in the previous section. Figure 3.6 shows trajectories and velocity profiles for reaching movements consisting of two via-points. The end-point standard deviation for repeated movements between the same points, but with different movement times, is shown in Figure 3.7(a) to demonstrate that the speed-accuracy trade-off still applies for complex trajectories.

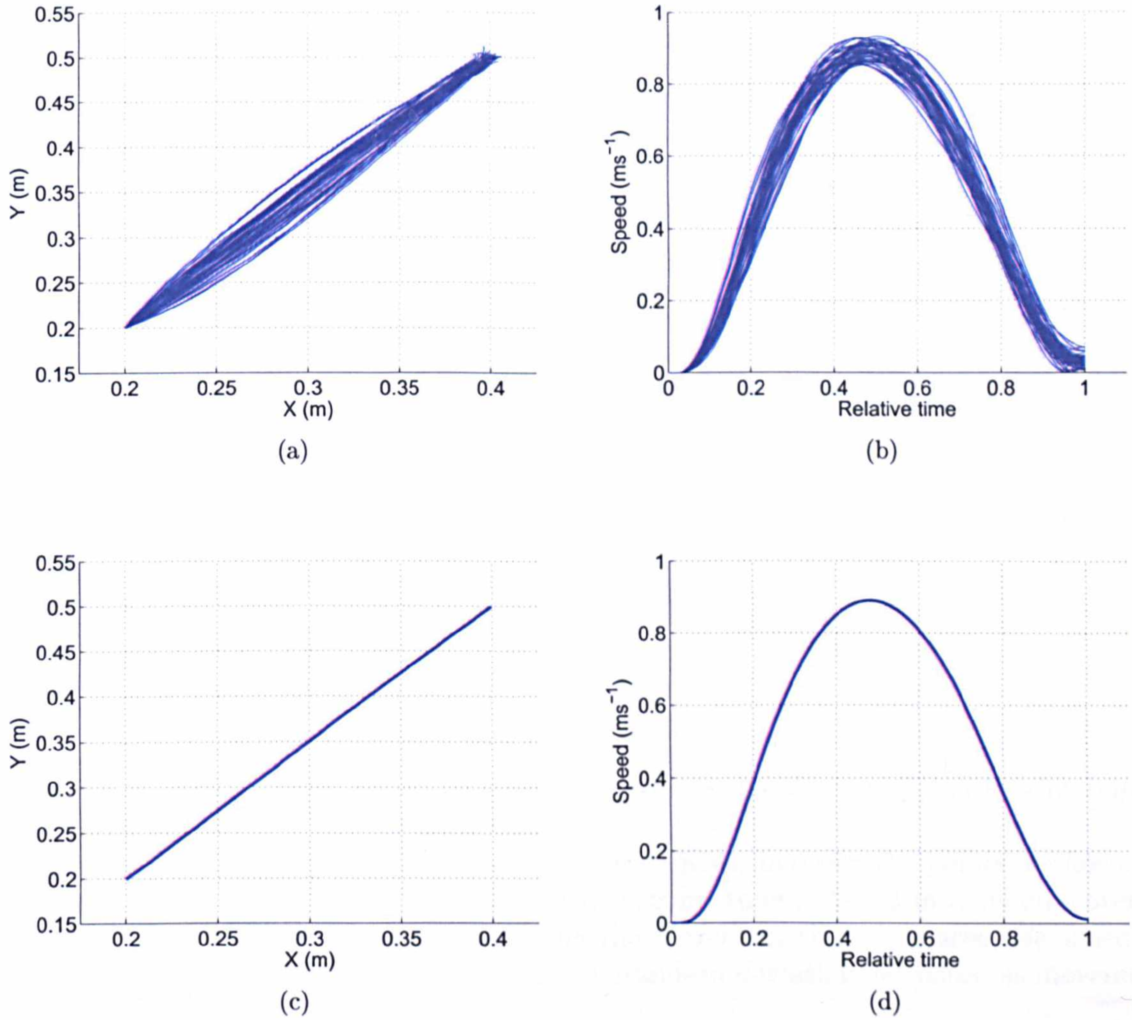

Figure 3.4: These plots show the trajectories and velocity profiles of a typical point-to-point movement of the hand, between (0.2,0.2) and (0.4,0.5) (with the shoulder at (0,0)).
(a) 50 repeated example trajectories. Signal-dependent noise on the control signal results in slightly different trajectories for repeated movements, but each trajectory is still smooth and roughly straight;
(b) The velocity profiles for the movements. The velocity curves follow the characteristic bell-shape of reaching movements;
(c) The average hand path of the fifty movements shown in (a). The average trajectory is a straight line between points, as expected when the movement noise in the system is Gaussian white-noise with zero mean. The addition of movement noise also causes individual movements to exhibit a slight curvature;
(d) The average velocity profile of the fifty profiles shown in (b).

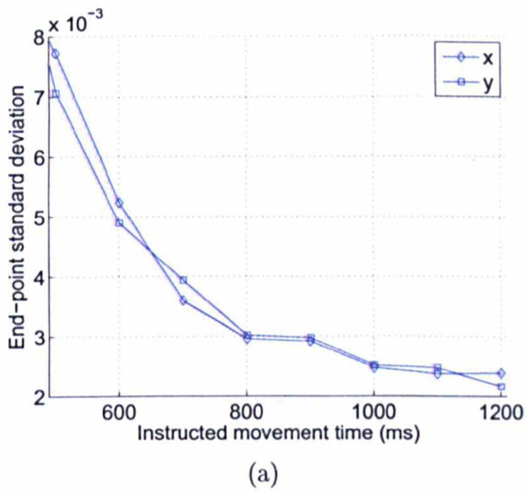

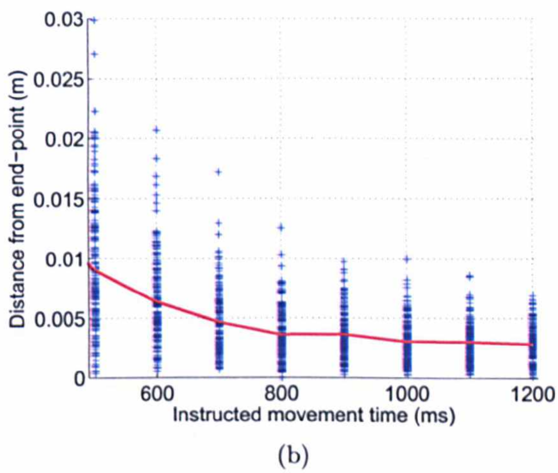

Figure 3.5: A demonstration of the speed-accuracy trade-off as exhibited by this implementation of the minimum variance model.
(a) The end-point standard deviations of 200 movements between the points as shown in Figure 3.4 were calculated for a variety of movement times. As all movements covered the same distance in hand-space, increasing the movement time decreased the speed of movement. As seen in this plot, the end-point standard deviation decreased as movement speed decreased;
(b) The end-point linear distances from the target coordinates are shown for each of the movements used to calculate the standard deviation. This confirms that the spread of deviations from the average distance decreases as the speed decreases, and also shows that the average distance from the end-point gets smaller as the speed decreases.
(Each cross represents a single trajectory's distance from the target point at the end of the movement. The line follows the average of 200 movements performed at durations of 500, 600, 700, 800, 900, 1000, 1100 and 1200ms).

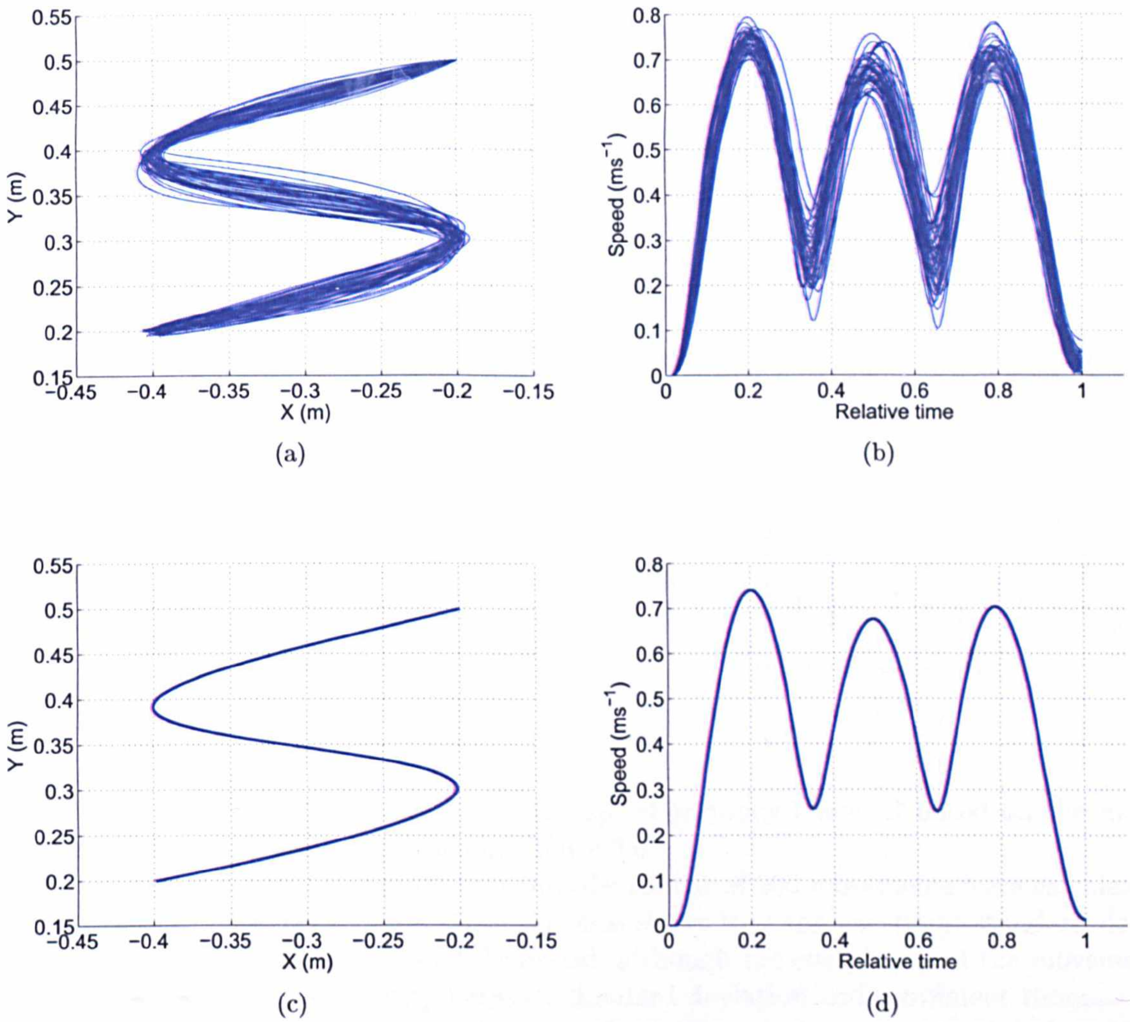

Figure 3.6: These plots show the trajectories and velocity profiles for a point-to-point movement between (-0.2,0.5) and (-0.4,0.2), with a pre-specified via-point at (-0.4,0.4) and another at (-0.2,0.3), forming an 's' figure. The first via-point was set to occur at 25% of the movement time and the second was set to occur at 75% of the movement time.
(a) 50 repeated example trajectories. As for the point-to-point movement without via-points shown in Figure 3.4, signal-dependent noise on the control signal results in different trajectories for repeated movements;
(b) The velocity profiles for the movements. The velocity curves follow the characteristic bell-shape of reaching movements, for the three straight sections of the movement, with slowing at the bends of the 's';
(c) The average hand path of the fifty movements shown in (a);
(d) The average velocity profile of the fifty profiles shown in (b).

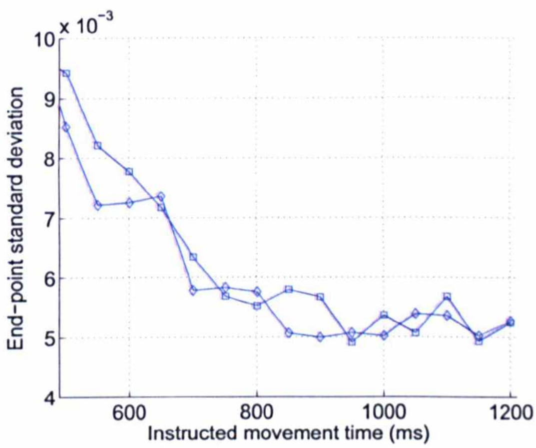

(a)

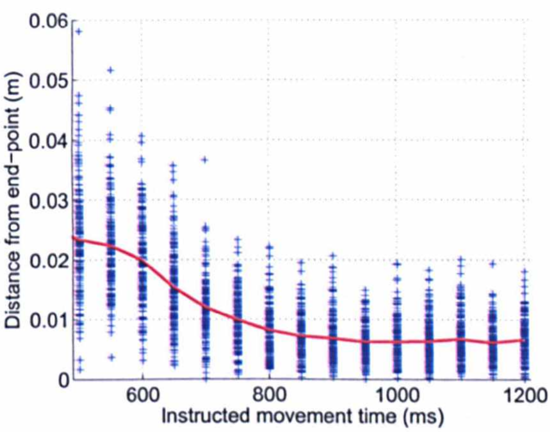

(b)

Figure 3.7: A further demonstration of the speed-accuracy trade-off based on the more complex via-point movement shown in Figure 3.6.
(a) As in Figure 3.5, the end-point standard deviations of 200 movements were calculated for a variety of movement times. This plot also shows that the end-point standard deviation decreased as movement speed decreased, although the complexity of the movement results in a less clear relationship between standard deviation and movement time;
(b) As before the end-point linear distances from the target coordinates are shown for each of the movements used to calculate the standard deviation. Again, the complexity of the movement results in a less clear relationship, but the decrease in average distance from the target can easily be seen.
(As before, each cross represents a single trajectory's distance from the target point at the end of the movement. The line follows the average of 200 movements performed at durations of 500, 600, 700, 800, 900, 1000, 1100 and 1200ms).

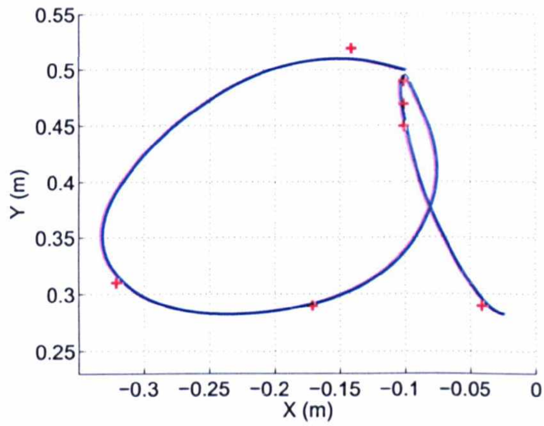

(a)

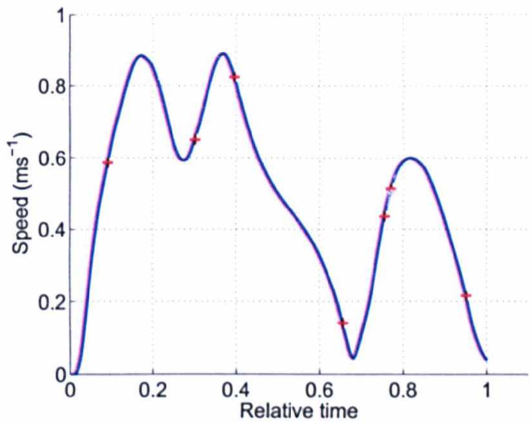

(b)

Figure 3.8: A movement with several via-points arranged to draw out the letter 'a'.
(a) The hand path, showing the positions of the via-points;
(b) The velocity profile for the movement, showing the temporal relationships between via-points. The point of reversal, where the velocity drops to zero, can also be clearly seen at approximately 70% of the movement time.

In a similar way, Figure 3.8 shows the same plots for a reaching movement consisting of several via-points, arranged in such a way that the movement draws the letter 'a'. This highlights another use of via-points, in that they can be used to define more meaningful action that simple reaching movements. In this example, the spatial and temporal relationship between these via-points could easily be stored, allowing the letter 'a' to be redrawn anywhere in the arm's workspace, or with a different movement time, and yet still remain recognisably an 'a'.

A comparison between this arrangement of via-points performed at different movement speeds is shown in Figure 3.9. The shape is maintained even when the velocity is increased as the order and relative times between via-points is kept the same.

Summary

The minimum variance model has been shown to address many of the issues that are not covered by previous movement models, including noise, biological basis, accuracy constraint, as well as a unified explanation of smooth movement and the speed-accuracy

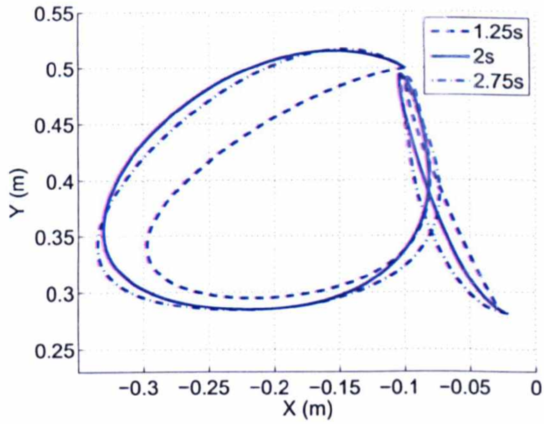

(a)

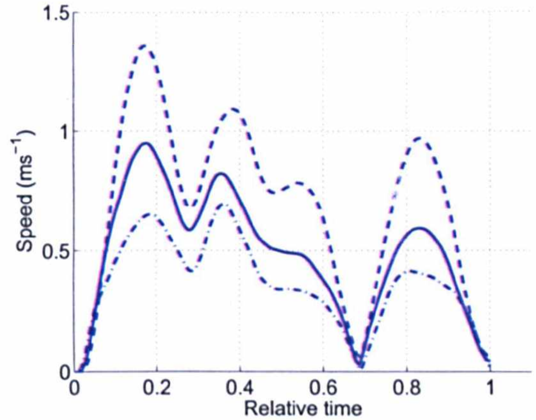

(b)

Figure 3.9: The same movement as shown in Figure 3.8, repeated with three different movement times.
(a) The hand trajectories are clearly very similar, as the order of the via-points is the same. The path performed at the highest speed is clearly cruder than the others, as there are fewer time steps between via-points and the higher velocity is subject to higher noise; (b) The velocity profiles have the same shapes, with the fastest movement subject to greater levels of noise.

trade-off.[52] In this chapter an optimal control scheme implementation of the model has been described, and it has been demonstrated that this implementation produces trajectories that capture the essential features of human point-to-point movements. This model has also been extended to cover complex trajectories through the use of via-points.

In the next chapter the model is extended further to cover reach-to-grasp movements, and it is shown how minimum variance trajectories can capture the essential features of grasping movements.

Chapter 4

Grasping Using the Minimum Variance Model

Reaching to grasp an object is a complex motor task involving the movement of many joints and the coordination of several end-effectors. In much the same way as multi-joint reaching movements, studies of the kinematics of grasping[59,60,56,77,65,18] have revealed characteristic patterns of behaviour. Among the most well established of these is the observation that maximum grip size (between the thumb and the finger) increases with the size of the object,[59] with a slope of approximately 0.8. A further observation is that the maximum grip aperture occurs at around 60-80% of the movement time.[60]

The general description of grasping behaviour is based upon the separation of the grasp into two visuomotor channels: one for the transport component (moving the hand to the object) and one for the grip (moving the fingers to grip the object).[59] This separation implies that the two components are planned independently, but executed together to form a single coordinated movement.[56]

More recently, Smeets and Brenner[113] suggested the alternative view that grasping movements are carried out as smooth pointing movements of the thumb and finger to target positions on the object. They used the minimum jerk model of arm movement to successfully predict finger- and thumb-tip trajectories towards an object, however deliberately avoiding any consideration of the mechanics of limbs and joints.[113]

1 Minimum variance grasping

In the preceeding chapters an implementation of the minimum variance model of human reaching using an optimal control scheme suitable for controlling a robot arm has been described. Following the general idea that grasping can be described as pointing movements performed by the finger and thumb, in this chapter it is shown that this implementation is suitable for examining the behaviour of grasping as well.

Grasping is an interesting task on which to apply the minimum variance model, as there are two sources of variance effecting the finger-tip position: that produced by the movement of the wrist and that produced by the movement of the fingers.[77]

To correctly model the minimum variance trajectory, signal-dependent noise must be applied to the control signals of the arm (and digit) actuators. It is not possible therefore to eliminate the mechanics of the arm from the model. Instead, this approach builds on both the "classical" view of grasping and on the view of Smeets and Brenner[113]. In this chapter, reaching-to-grasp is viewed as two separate processes (the transport and the grip) that are nonetheless planned using the same computational model for pointing, under the same temporal constraints.

In the following section the extension of the reaching model to include a gripping mechanism is described. An analysis of the impact of several different parameters on the end-point accuracy of the digits' trajectory is carried out, identifying in each case the trend in that parameter that leads to the lowest level of inaccuracy. Using the identified values of the parameters, the resulting trajectories are examined as to whether they capture the characteristic features of grasping.

The model presented here allows for the study of the nature of the variance over the whole course of the movement, for both the transport and grip components. This chapter goes on to show how these are effected by changes in object size, movement time and transport distance.

1.1 Implementation for Grasping

Following the effector model of the preceeding chapters, and other motor control studies[41,119], the arm is still modelled as a two-link planar device with two rotational degrees-of-freedom.

A gripping mechanism is then added at the wrist of the arm, modelled as smaller two-link devices, as shown in Figure 4.1. The links of the arm are set to be 30cm in length and the links of the digits to be 10cm in length, values chosen as approximations to the proportions of a human arm. Overall the arm-and-gripper model has six joints which are controlled directly by the optimisation scheme. The focus here is on the kinematics of the movements, without explicit consideration of the dynamics of the arm or modelling arm muscles. More complex models of the hand have been examined for grasping (for example, Meulenbroek et al.[85]), but this model is sufficient to demonstrate the required principles, and strikes a balance between these approaches and the simple model of Smeets and Brenner[113].

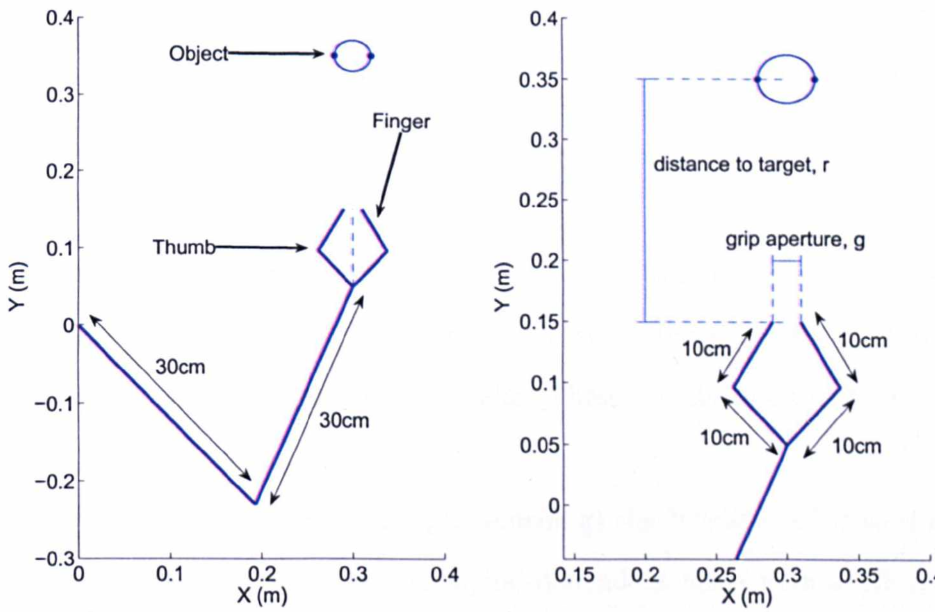

(a) (b)

Figure 4.1: The initial set up of the arm, hand and object. The link lengths for the arm and gripper are shown, and the distance to object r and grip aperture g are defined. The digit target positions on the surface of the object are shown as dots. The model used here for the arm is the same as that used in the previous chapter.

From the given position of the object, the wrist target position is specified as being 6cm vertically below the centre of mass of the object. For the experiments presented here, the distance between the wrist target position and the centre of the object is kept constant at this value. Examining the effects of this variable on the digit trajectories is therefore outside the scope of this work, but is a clear candidate for future work.

As for the reaching experiments described in the previous chapter, the Cartesian wrist target is converted into target joint angles using the inverse kinematics for a two-link planar arm (equations ?? and ??). Following the optimal control scheme algorithm also described in the previous chapter, the "cost-to-go" is then calculated for the reaching part of the movement.

Target points are then specified on the object, using a disk for simplicity. The digit target positions are specified as being on the surface of the object, connected by a line that is perpendicular to the surface and passes through the centre of mass of the object. There has been much recent work on the placement of digits on an object and the resulting quality of the grasp.[90,16] However, the assumption made here (and also made by Smeets and Brenner[113]) is that for the simple cylindrical object, a precision grip is used that aims to place the fingers on opposite sides of the object at points in line with the centre of mass.

These target points are translated into the hand frame of reference by subtracting the wrist target position. Again the inverse kinematics are used, with appropriately link lengths, to get target joint angles for the digits. These are also used to create a "cost-to-go" for each digits movement.

From the starting point (with the digits touching) the "cost-to-go" is used to generate motor commands for each joint, adding signal-dependent noise with a 1% coefficient of variation and updating the state at each time step. As the movement is executed the forward kinematics are used to specify the Cartesian positions of the wrist and the tips of the digits, given the appropriate joint angles.

Having described the mechanism used to extend the minimum variance model to grasping, the next section identifies a number of tests to show that the extended model replicates the important features of reach-to-grasp movements described in the introduction to this chapter.

1.2 Experiments to be performed

The model of Smeets and Brenner[113], which uses the minimum jerk trajectory, does not account for the natural inaccuracies of human movement introduced by neural noise. Instead, they empirically discuss why finger-tip trajectories that approach the surface of the object perpendicularly result in more accurate grasping than those that approach tangentially. Accordingly, they introduce an "approach parameter" which constrains the minimum jerk trajectory to approach the surface of the object perpendicularly.

The minimum variance model has no equivalent parameter to model this perpendicular approach to the object. As described above, this implementation of the model does, however, allow the introduction of one or more via-points into the trajectory. A via-point is therefore introduced into the planning of the digit movements to cause the trajectory to approach the target positions perpendicularly. As the digit planning takes place from the target position of the wrist, close to the object, these via-points are specified relative to the object. When the movement begins the digits follow the joint trajectory specified by the target and via-points. However, since the reach and grip components are executed together, the digit end-point trajectories do not pass through the via-point spatial positions relative to the object.

Given this separation of planning and execution, the first set of results determine where this via-point should be located, both relative to the target points on the object and within the time course of the movement, by selecting the values of these parameters that result in the lowest variance of the digit end-point - that is, the highest accuracy when making contact with the object.

Following this, analysis is carried out to determine whether the minimum variance model of pointing, with the introduction of these via-points, can actually reproduce the characteristic features of grasping as previously identified: a maximum grip aperture proportional to the size of the object, decreasing with a slope of approximately 0.8 as the object size increases; and a time for that maximum aperture at between 60-80% of the movement time.[59,60] Specifically an attempt is made to match predictions three and four of Smeets and Brenner[113]:

- The maximum grip increases and occurs *later* for larger disk sizes

- The maximum grip size increase and occurs *earlier* if the via-point is located further away from the object

Here, the first prediction is the same as prediction three of Smeets and Brenner[113], while the second prediction matches prediction four of Smeets and Brenner[113], but with a modification to account for the via-point implementation.

Aspects of the task that may effect the contributions of the different components to the end-point variance of the digits in the reach-to-grasp movement are then looked at. Specifically it is shown how the movement time, the object size and the distance of the object from the start position of the hand effect the variances of the wrist and grip aperture.

Experimental work in this area has been carried out by Kudoh et al.[77], who recorded the spatiotemporal variability of the two segments when both distance to the object and the object size were manipulated. Their results indicate that object size had a significant impact on the variability of both the transport and the grasp components, while a change in starting distance mostly effected the transport component. They also found that the peak wrist variability depended on distance but not object size, while the peak aperture variability depended on both distance and object size. Variability in grasping has also been studied by Girgenrath et al.[47], who observed a clear speed-accuracy trade-off in prehension as well as reaching.

The next section describes how these predictions are to be tested using the minimum variance model extended for grasping.

2 Grasping trajectories

Before the predictions made in the previous section can be properly tested, the position of the via-point of the grip component must be specified. The following section identifies the via-point height and temporal position that minimises the variance of the final digit positions, and presents the resulting trajectory that forms the basis for the experiments that test the predictions.

2.1 Via-point Position

Each via-point consists of three parameters: its spatial coordinates on the plane of the arm, and its temporal location within the time course of the movement. To confirm whether a perpendicular approach to the surface of the object is line with the minimum variance principle two factors are examined:

- The vertical position of the via-point relative to the target positions on the object.
- The point at which the via-point occurs during the course of the movement (referred to as the temporal position of the via-point).

These parameters have the greatest effect on the angle of approach: the vertical position of the via-point determines whether the digits approach the object from above, below or level with the target positions; the temporal position of the via-point determines the balance between the movement towards the object and the final approach.

To do this, one parameter is changed at a time and 500 movements are repeated for each value. Two measures of the end-point accuracy are observed - the Cartesian distance of the end-point from target position for each trajectory and the standard deviation about the target position of all 500 end-points for a given parameter value.

The model is set up to perform a reach-to-grasp movement on a disk located 20cm directly in front of the starting position of the arm and hand, with via-points located 1cm horizontally from the object, as shown in Figure 4.1. Each movement was performed on an object of diameter 4cm and took place over 1000ms.

2.1.1 Via-point vertical position

First the vertical distance of the via-points (defined as the distance between the line connecting the target positions and the line connecting the via-points. For example, a vertical distance of -1.0cm would indicate the line connecting the via-points was 1.0cm below the line connecting the target positions. This is illustrated Figure 4.2(a)) is varied. For these movements, the via-points occurred after 70% of the movement time, or 700ms into the movement.

The accuracy of the digit trajectories was measured as both the standard deviation of digits movement in the x and y axes, and as the mean distance of the digit trajectory end-point from the target position on the object.

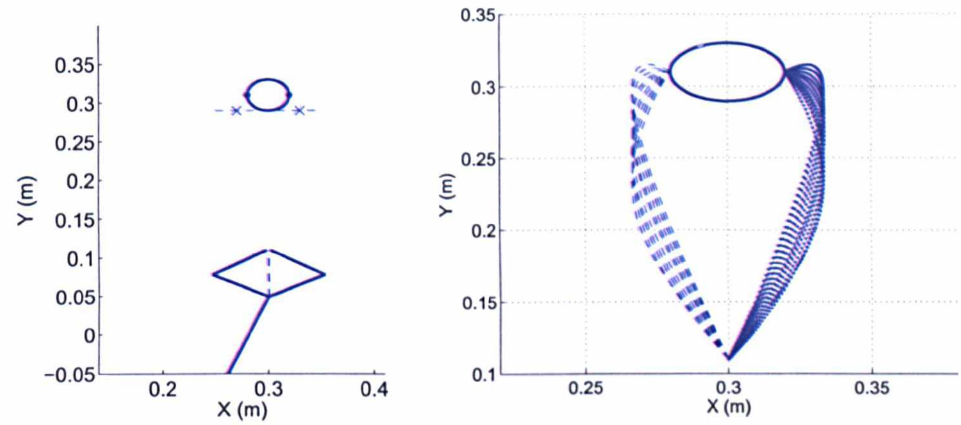

(a) (b)

Figure 4.2: Changing the vertical position of the digit via-point relative to the digit target position on the object.
(a) An illustration of the starting position of the hand and the relationship between the line connecting the via-points and the line passing through the target positions;
(b) The average digit trajectories for each value of the via-point y-coordinate. To reduce clutter, the changing positions of the via-points are not shown. Thumb trajectories are shown as dashed lines, finger trajectories as dotted lines.

Figures 4.3(a) and 4.3(b) show that the distance between the end-point of each digit trajectory and the target position for that digit on the object decreases as the via-point position comes level with the target positions, before increasing again as the via-point position goes above the target positions. This indicates that a perpendicular approach of the digits to the object results in a more accurate movement.

From the results shown in Figure 4.3(c) and Figure 4.3(d), it is clear that the lowest end-point standard deviation for each digit is found when the via-points are located at the same level as the target positions on the object in the wrist target frame of reference. Together, these two results are in line with the argument given in Smeets and Brenner[113]

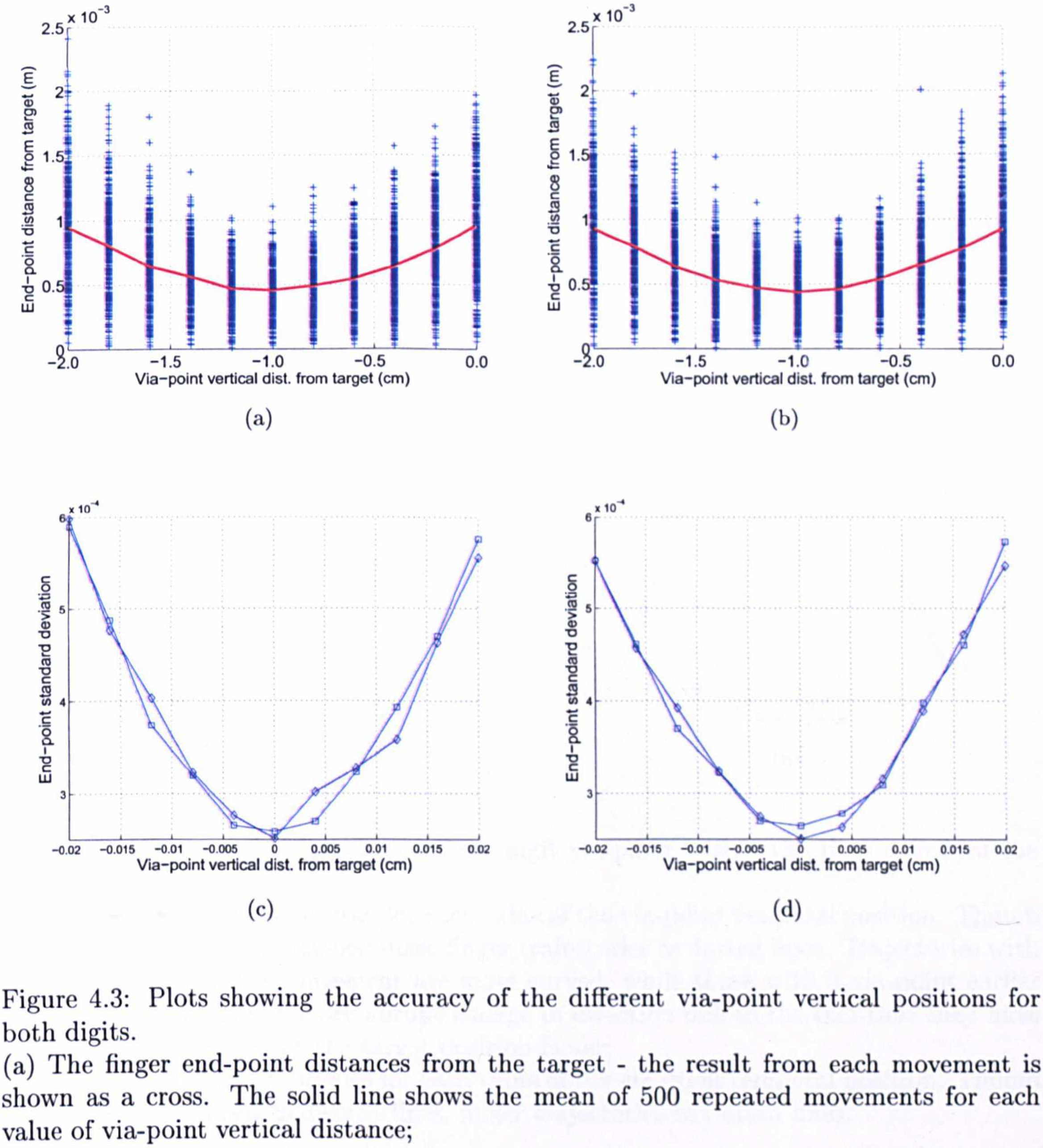

Figure 4.3: Plots showing the accuracy of the different via-point vertical positions for both digits.
(a) The finger end-point distances from the target - the result from each movement is shown as a cross. The solid line shows the mean of 500 repeated movements for each value of via-point vertical distance;
(b) The thumb end-point distances from the target (again, the result of each movement is shown as a cross). The solid line shows the mean of 500 repeated movements for each value of via-point vertical distance;
(c) Finger end-point standard deviations in both the x and y axes for each value of via-point vertical distance;
(d) Thumb end-point standard deviations in both the x and y axes for each value of via-point vertical distance.

relating a greater perpendicular approach of the digits to increased accuracy of the final grip position and less variation between repeated movement.

2.1.2 Via-point timing

The position of the via-point within the time course of the movement was then varied. The same movement parameters were used as for the previous experiment. Following those experiments, the via-points were placed along the line passing through the target positions.

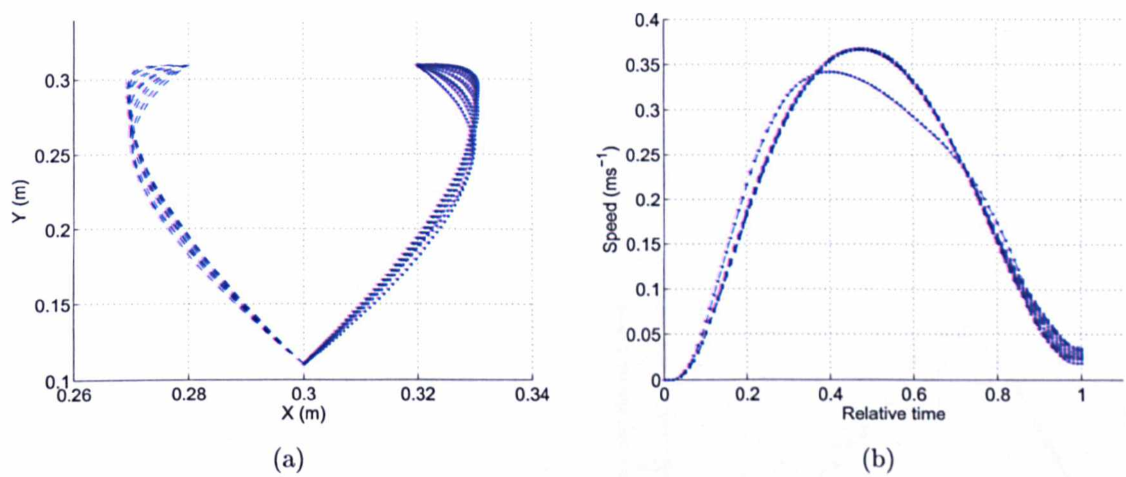

Figure 4.4: Changing the position of the digit via-point within the time course of the movement.
(a) The average digit trajectories for each value of the via-point temporal position. Thumb trajectories are shown as dashed lines, finger trajectories as dotted lines. Trajectories with a via-point later in the movement are more curved, while those with a via-point earlier in the movement show a more abrupt change in direction due to the fact that they have reached a point level with the target position faster;
(b) The average velocity profiles for each value of the via-point temporal position. Thumb trajectories are shown as dashed lines, finger trajectories as dotted lines.

The results shown in Figures 4.5(c) and 4.5(d) indicate that a via-point late in the movement increases the inaccuracy of the digit trajectory end-point, with a peak in the end-point standard deviation at approximately 87%. Past this point the standard deviation decreases. This can be explained as the declining weight of the via-point in the optimisation scheme relative to the target point, as the via-point temporal position approaches the end of the movement.

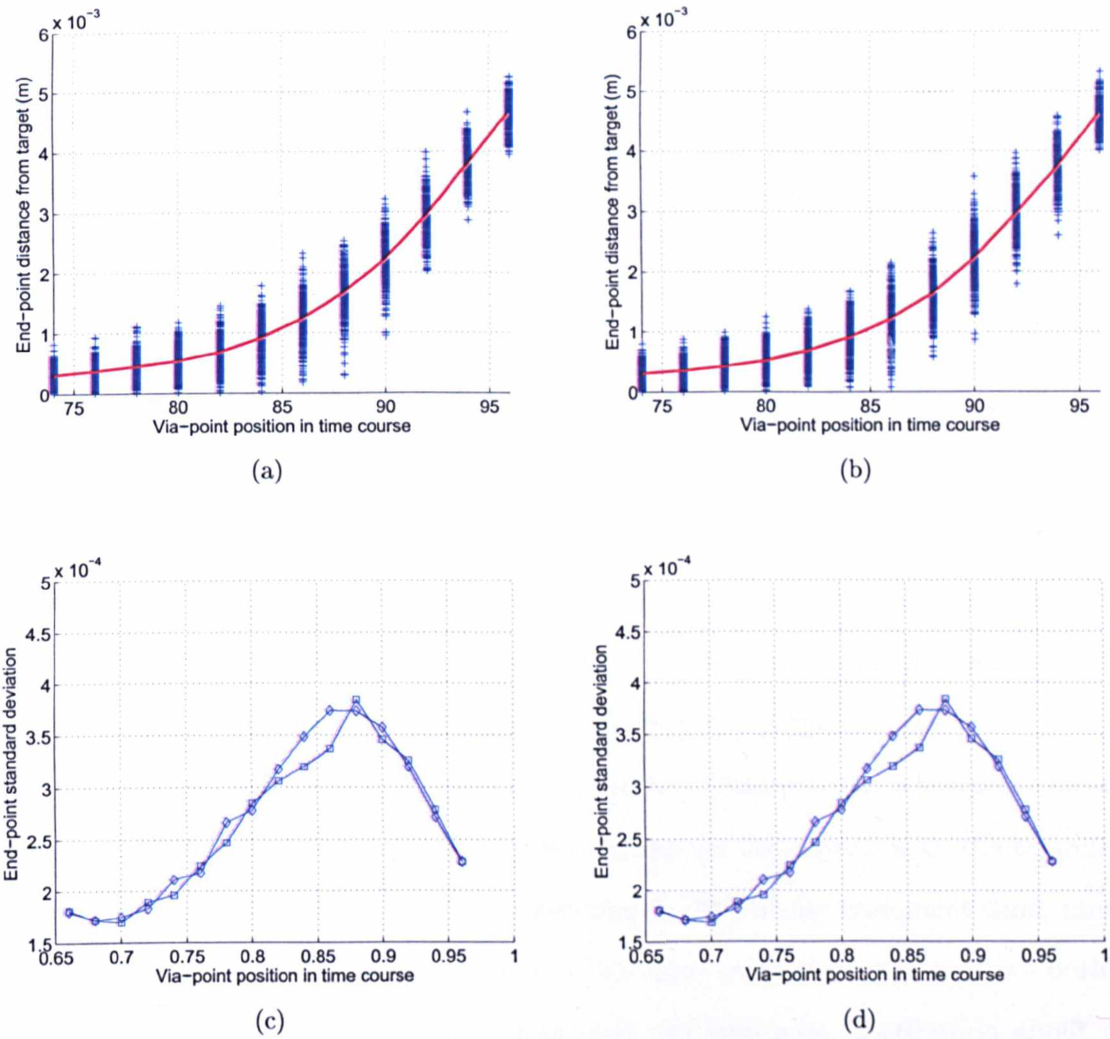

Figure 4.5: Plots showing the accuracy of the different via-point temporal positions for both digits.
(a) The finger end-point distances from the target (shown as crosses) and the mean of 500 repeated movements for each value of via-point temporal position (shown as a solid line);
(b) The thumb end-point distances from the target (crosses) and the mean of 500 repeated movements for each value of via-point temporal position (solid line);
(c) Finger end-point standard deviations in both the x and y axes for each value of via-point temporal position;
(d) Thumb end-point standard deviations in both the x and y axes for each value of via-point temporal position.

The decrease in standard deviation below 87% is a product of the increasingly perpendicular approach of the digits to the object as the via-point temporal position decreases - as the digit reaches the via-point (which is level with the target position) earlier in the movement, it has longer to move along the perpendicular line joining the via-point and the target position.

However, via-point temporal positions below approximately 70% of the movement time show an increase in standard deviation. This is likely to be due to the increased speed (and increased noise) that is required to cover the distance to the via-point so early in the movement. Although the a perpendicular approach indicates reduced variance at the end-point, the transport of the digits to a point where an accurate final approach can be made must also be taken into account.

Results from Figures 4.5(a) and 4.5(b) indicate that below approximately 80% the via-point temporal position has little effect on the distance of the end-point from the target position. This climbs sharply beyond 85% as the digit trajectories approach the target position at a greater and greater deviation from the perpendicular.

From the results of Figures 4.3 and 4.5, it can be concluded that a via-point located perpendicularly along the axis of the target positions on the object, with the trajectory required to pass through that point at approximately 70% of the movement time, results in trajectories that maximise the accuracy of the digit trajectories end-points - both in terms of end-point distance from the target and the end-point distribution about the target.

Typical digit trajectories, and their velocity profiles, produced using these parameters are shown in Figure 4.6.

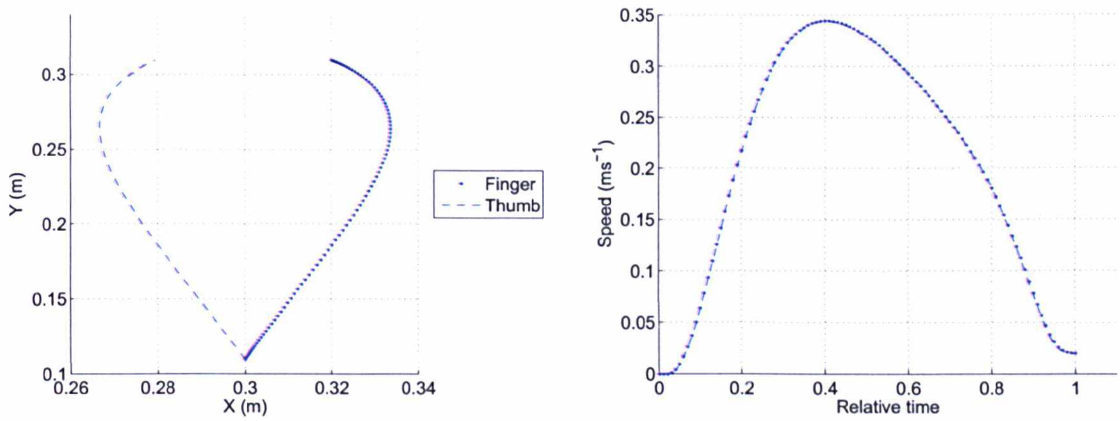

(a) (b)

Figure 4.6: Plots showing: (a) Typical trajectories for the finger and thumb with via-points level with the axis of the target positions and occurring at 70% of the movement time. The via-points were located 1cm horizontally from the object and the movement took place over 1000ms.

The next section looks at whether these digit trajectories actually match the features of human grasping (and the predictions discussed in the previous section) in a quantitative manner.

2.2 Grasping Predictions

Using the parameters identified in the previous set of results, the model is set up to test the predictions given above (see section 1.2). These predictions examine the characteristic form of grasping movements, specifically the maximum grip aperture and the time at which it occurs within the course of the movement. Initially two sets of movements are performed: in one the via-point horizontal distance from the object is varied, while in the other the object size is varied. For both sets of experiments, each movement again took place over 1000ms. The via-point was located along the orientation of the grip and occurred at 70% of the movement time, or 700ms into the movement, in line with the results above.

2.2.1 Via-point horizontal position

The first set of results, shown in figures 4.7 and 4.8, show five grasping movements to an object of diameter 4cm. Via-point distances from the object were set at 0.0cm, 0.5cm, 1.0cm, 1.5cm and 2.0cm. For each of these values, 500 repeated movements were made. Figure 4.7 shows the mean digit paths, the mean digit velocity profiles and the time course of the grip aperture for each via-point value.

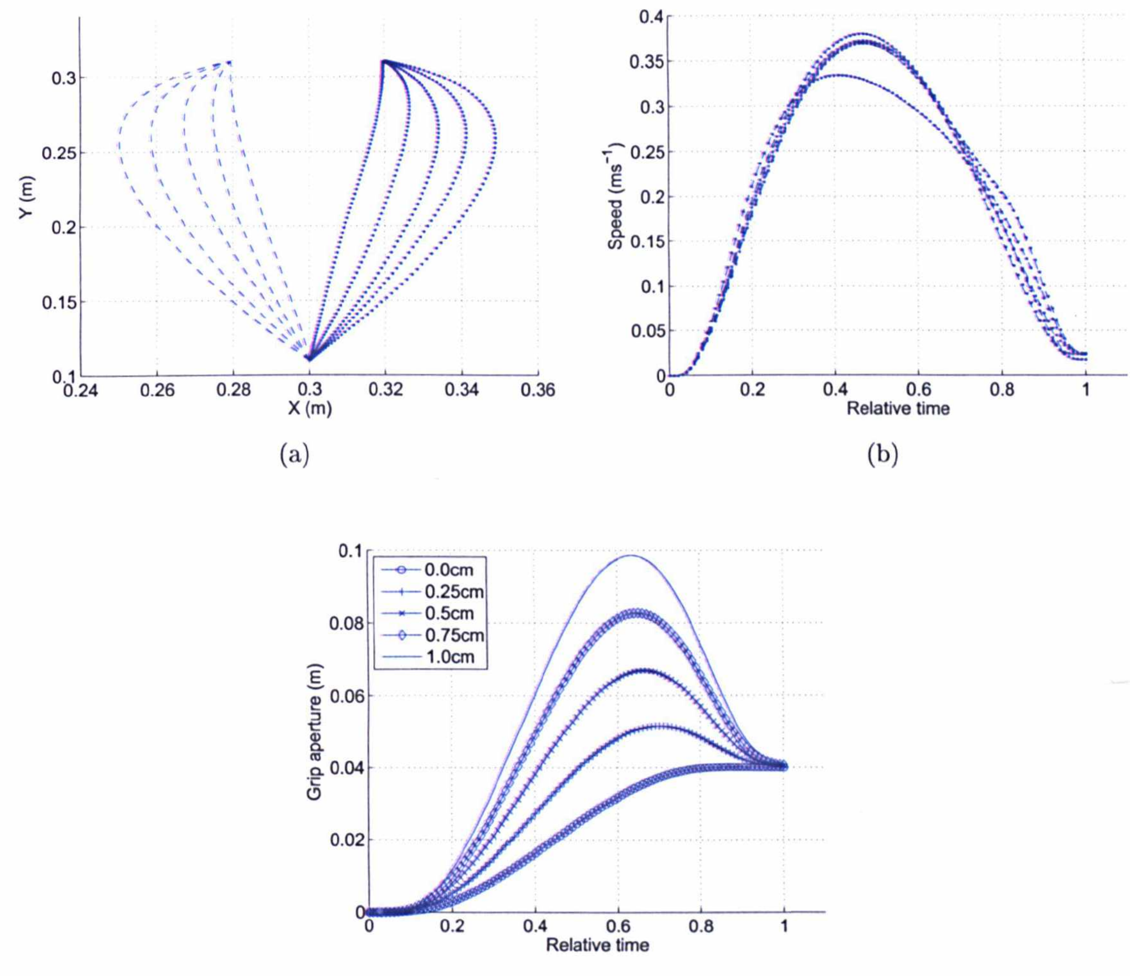

Figure 4.7: Grasping movements performed to a disk of diameter 4cm, with via-points at horizontal distances 0.0cm, 0.25cm, 0.5cm, 0.75cm and 1.0cm from the object.
(a) Movement paths for the thumb (dashed line) and finger (dotted line);
(b) Velocity profiles for the digits;
(c) Time course of the grip aperture.

From these movements it was possible to plot the via-point distance against both the maximum grip aperture and the time at which that maximum occurred, as shown in Figure 4.8.

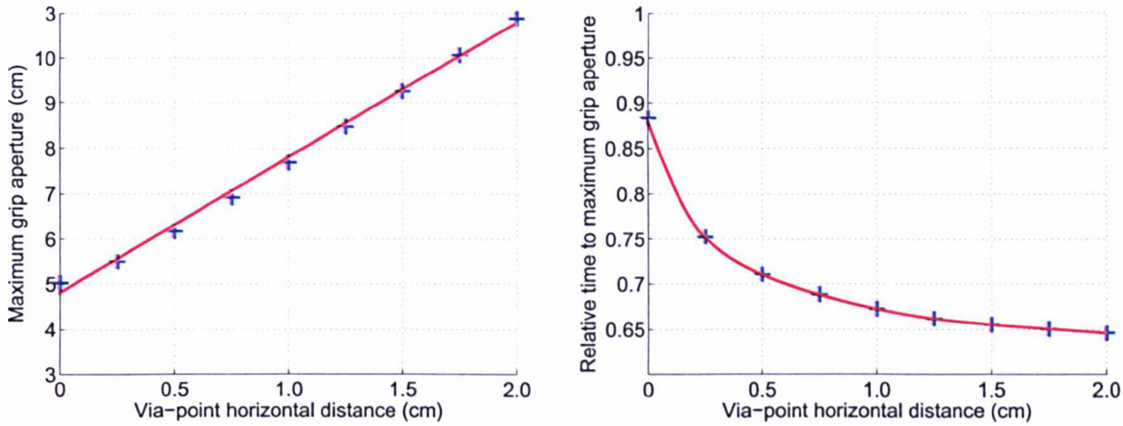

(a) (b)

Figure 4.8: Plots showing:
(a) The relationship between via-point horizontal distance from the object and maximum grip aperture;
(b) The relationship between via-point horizontal distance and the relative time at which the maximum grip aperture occurs.
These show the results for ten grasping movements to an object of 4cm, including the five shown in Figure 4.7. These plots confirm the prediction that the grip size *increases* and occurs *earlier* if the via-point is located further away from the object.

The results shown in Figure 4.8 clearly confirm the second prediction given in the previous section: that grip size increases and occurs *earlier* if the via-point is located further away from the object.

2.2.2 Object size

The second set of movements were performed to objects of varying sizes, with the via-point distance fixed at 1.0cm from the object. All other parameters were kept the same as for the first set of movements. The grasps were performed on objects of size 0.0cm, 2.0cm, 4.0cm, 6.0cm and 8.0cm. Again, 500 repeated movements were made to obtain the mean trajectories for each value of the object size. Figure 4.9 shows the digit paths, the digit velocity profiles and the time course of the grip aperture for each object size.

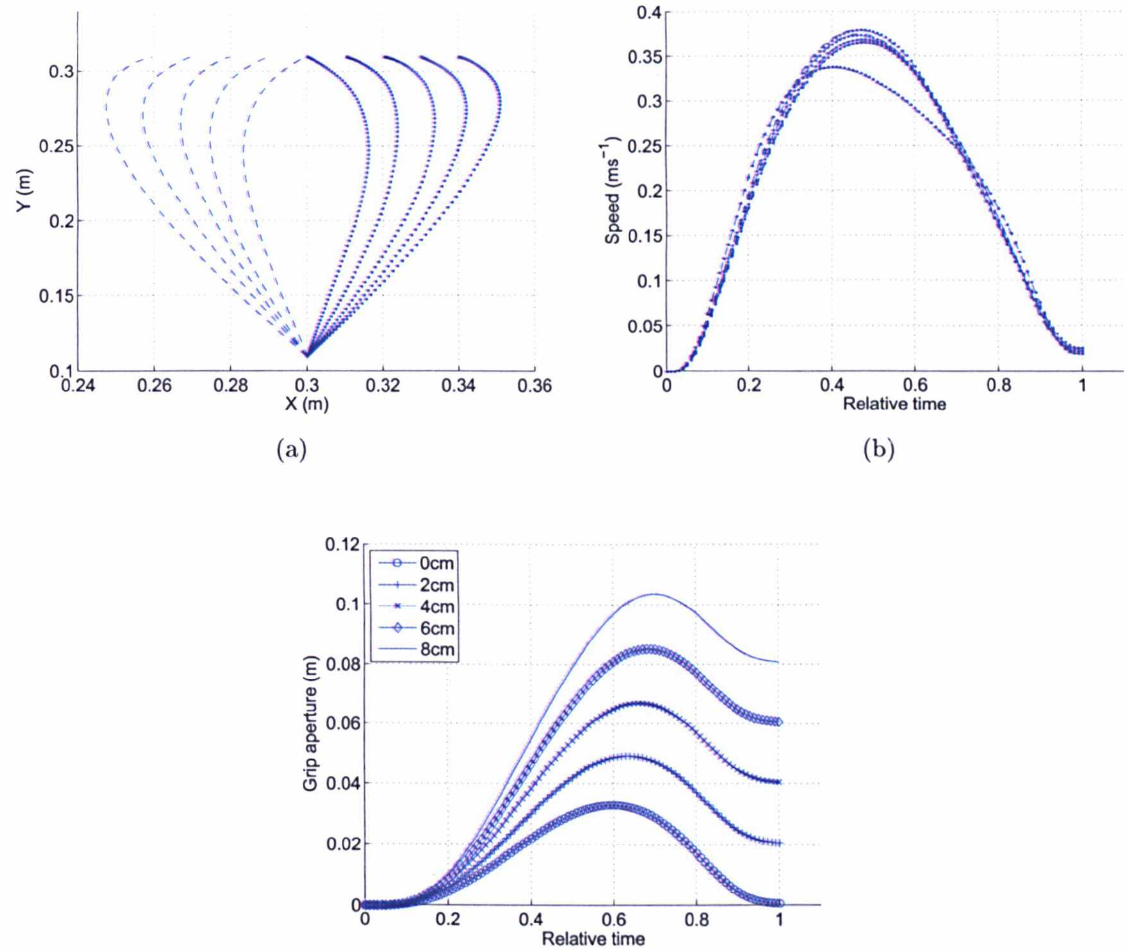

(a) (b) (c)

Figure 4.9: Grasping movements performed to disks of diameter 0.0cm, 2.0cm, 4.0cm, 6.0cm and 8.0cm, with via-points at horizontal distance 1.0cm from the object.
(a) Paths for the thumb (dashed line) and finger (dotted line);
(b) Velocity profiles for the digits;
(c) Time course of the grip aperture.

In the same way as the first set of movements, these trajectories were used to examine the relationship between object size and maximum grip aperture, and between object size and the time at which that grip aperture occurs, as shown in Figure 4.10.

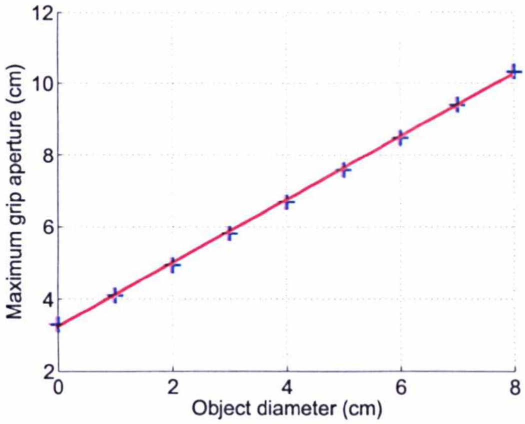

(a)

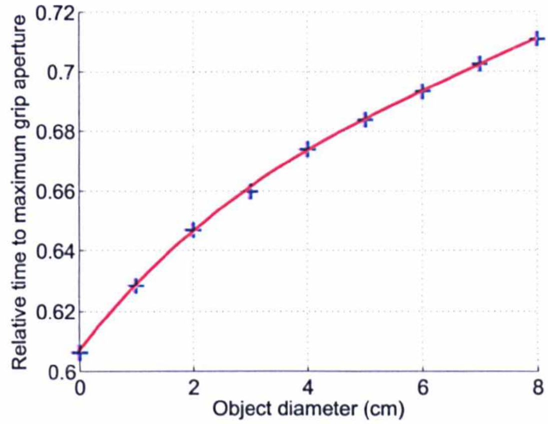

(b)

Figure 4.10: Plots showing:
(a) The relationship between object size and maximum grip aperture, along with the equation for the line of regression for 9 different object sizes, from 0cm to 8cm;
(b) The relationship between object size and the relative time at which the maximum grip aperture occurs.
These plots confirm that the prediction that the grip size *increases* and occurs *later* for larger object sizes.

From these plots, it is clear that the model confirms the first prediction from section 1.1, that grip size increases and occurs *later* for increasing object sizes. In addition, Figure4.10a shows the equation for the line of regression between the points. This line has a slope of 0.92, which is larger than the average value reported in Fig. 6A and Fig. 7A of Smeets and Brenner[113], but still well within the range of maximum grip slopes from the numerous experimental studies of grasping shown in those figures.

The second plot, Figure 4.10b, shows a range of relative times for the maximum grip aperture, with values between 60-80% of the movement time for the object sizes examined here. These values and the form of the regression line are also well within the range of values reported in Figure 6B and Figure 7B of Smeets and Brenner[113].

2.3 Transport and Grip Variability

Having demonstrated that the grasping model captures the experimentally observed features of human movement, it can now be used to study the contributions to the end-point digit variance made by the two components of the reach-to-grasp movement. The three variables considered were the effect of movement time, object size and distance to the object from the start position of the hand.

As in the previous sets of experiments movements were performed with a via-point located 1cm from the object along the line joining the target positions on the surface of the object, and occurring at 70% of the movement time. The variability of the movement was analysed by performing 500 repeated grasps for each parameter change, plotting both the standard deviation of the wrist trajectories and the standard deviation of the grip apertures at each time step. As well as looking at the overall variance in this way, the magnitude of the peak standard deviation and the time within the course of the movement that it occurred were also used as measurements of the variance. These values were plotted against the parameter values and a one-way analysis of variance (ANOVA) was used for each parameter to determine whether that parameter had an effect on movement variability.

2.3.1 Movement time

The first variable to be considered was the impact of movement time. As shown in Figure 3.4(d) the variability of both components is expected to decrease as the movement time increases, for movements over the same distance. The grasping movements were performed on an object of 4cm diameter, located 20cm in front of the hand, with via-points placed as described above. The movement times were 600ms, 700ms, 800ms, 900ms, 1000ms, 1100ms and 1200ms.

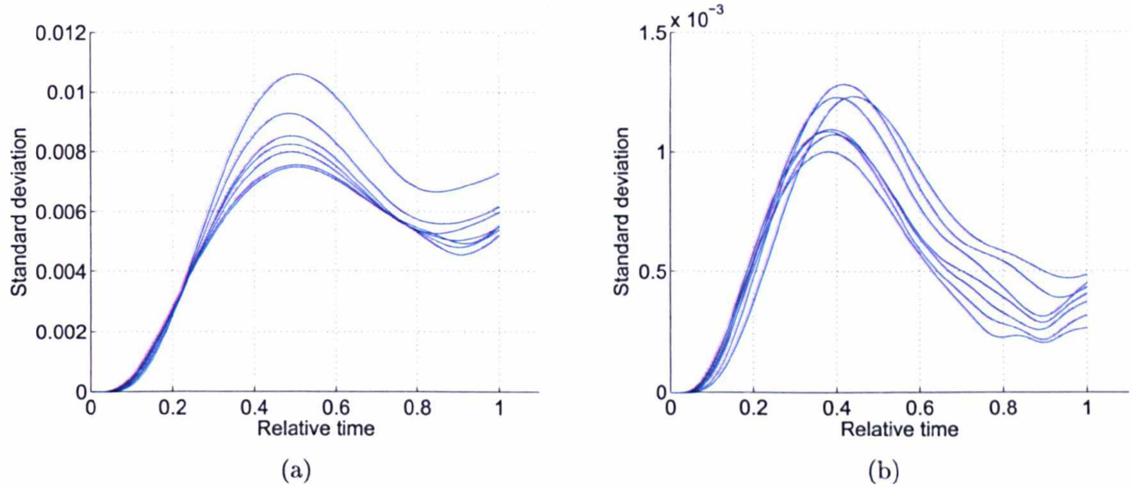

Figure 4.11: Plots showing the time course of (a) the wrist standard deviations and (b) the grip aperture standard deviations of 500 movements repeated for each movement time. The time courses have been normalised for ease of comparison.

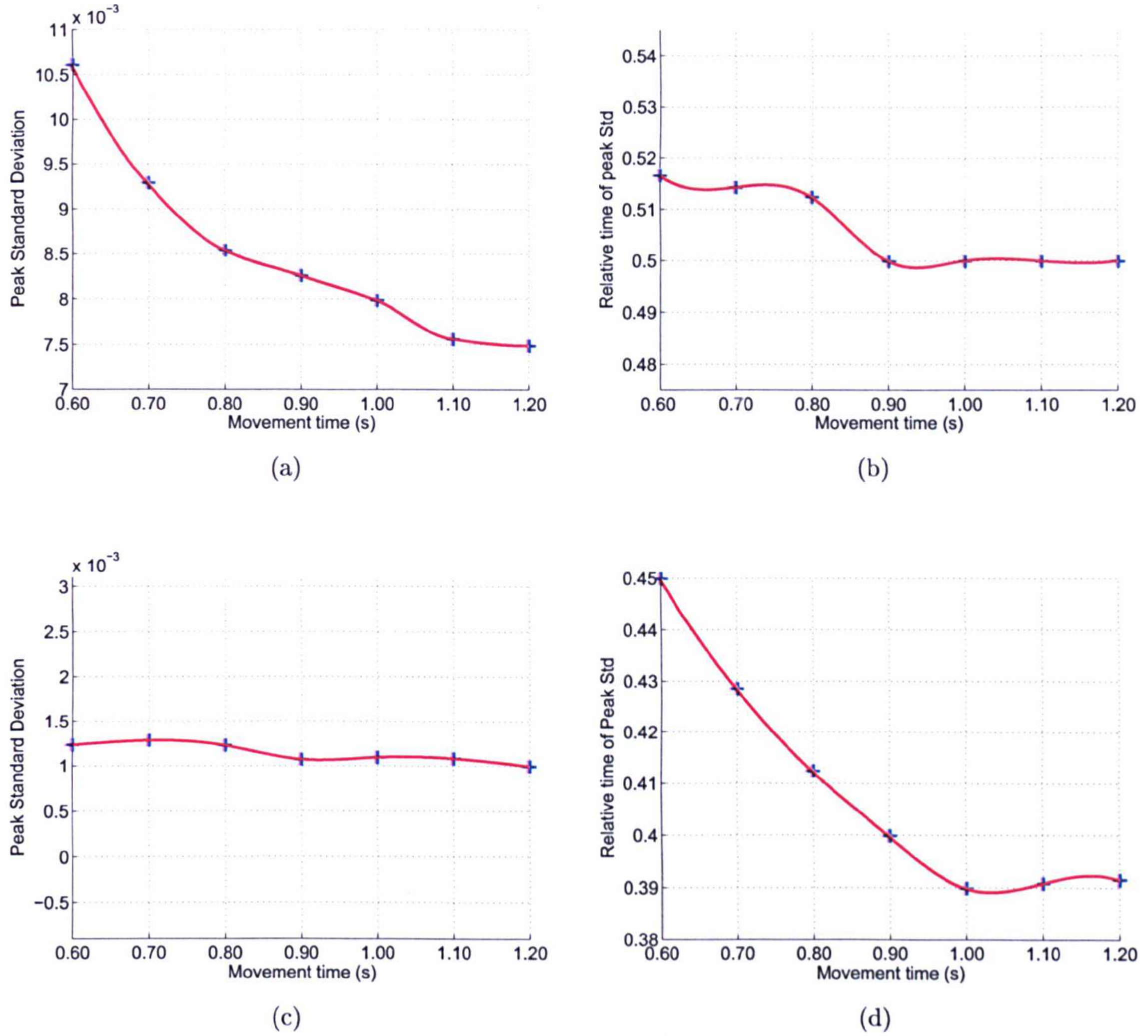

Figure 4.12: Plots showing the change in peak standard deviation and relative time of peak standard deviation of 500 movements for each value of the movement time.
(a) Wrist peak standard deviation and (b) relative time of peak standard deviation;
(c) Grip aperture peak standard deviation and (d) relative time of peak standard deviation.

The results shown in Figure 4.11 confirm that increasing the movement time decreases the overall variability of the movement for both the wrist (transport component) and the grip aperture (grasp component). The variability of the grip aperture (Fig. 4.11(b)) shows a change in the slope of the variability just after the via-point (70% of the movement time). This can also be seen in Fig. 4.13(b) and Fig. 4.15(b) below.

The change in slope of the standard deviation after the via-point is caused by a reduction in constraints acting on the trajectory. After the via-point has been reached, the dominant term acting on the trajectory is the target position, which must be reached in the remaining movement time. This leads to an increase in velocity (and hence variability) just after the via-point.

From Figure 4.12(a) and Figure 4.12(c) it can be seen clearly that peak standard deviation decreases as movement time increases. Figure 4.12(b) and Figure 4.12(d) show that the movement time also had an effect on the time at which the peak standard deviation occurred during the movement. Generally, an increased movement time resulted in the peak variability occurring earlier in the movement.

These results are expected, as according to Fitts' Law[37,82] an increased movement time for a movement over a fixed distance will result in lower velocities. Since the standard deviation of the movements is signal-dependent, lower velocities (which require lower control signals) result in lower standard deviations for both the digits and the wrist. These results also follow those of Girgenrath et al.[47], who specifically showed that prehension is subject to the same speed-accuracy trade-off as reaching.

2.3.2 Object size

The next variable examined was the effect of object size on the variability. As before grasping movements were performed on an object located 20cm in front of the hand, with the movement time set to be 1000ms. The object size was varied as 0cm, 2cm, 4cm, 6cm and 8cm.

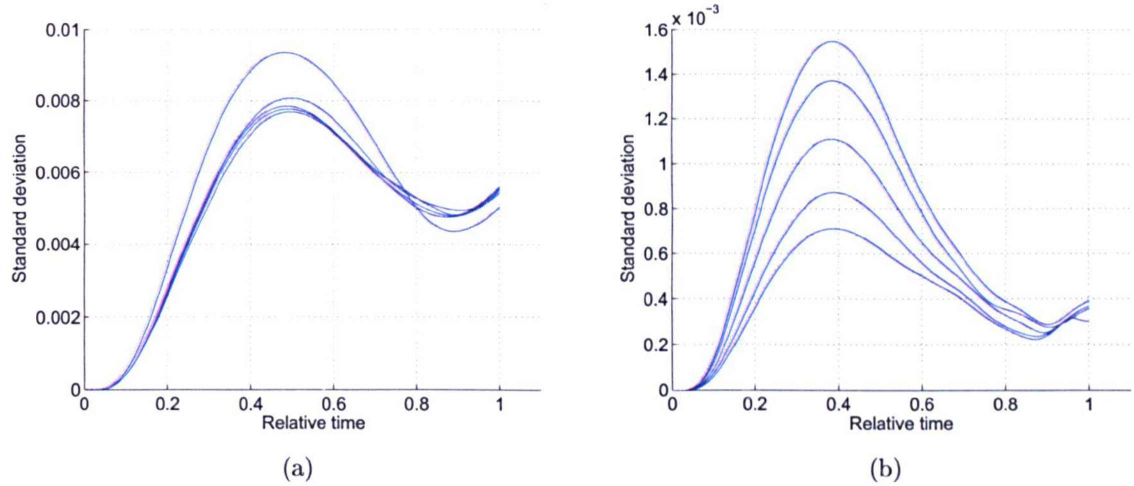

Figure 4.13: Plots showing the time course of (a) the wrist standard deviations and (b) the grip aperture standard deviations of 500 movements repeated for each object size.

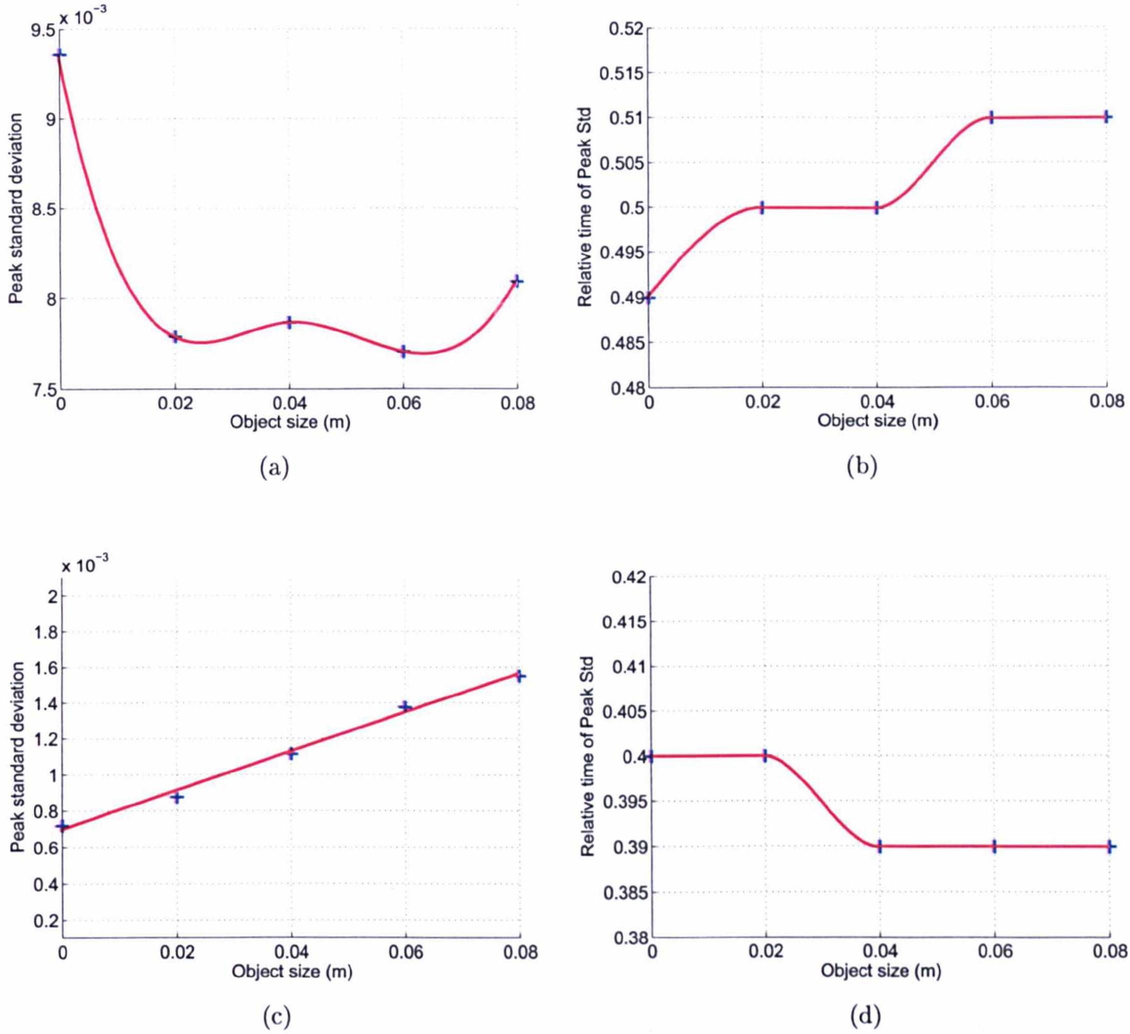

Figure 4.14: Plots showing the change in peak standard deviation and relative time of peak standard deviation of 500 movements for each object size.
(a) Wrist peak standard deviation and (b) relative time of peak standard deviation;
(c) Grip aperture peak standard deviation and (d) relative time of peak standard deviation.

The results shown in Figure 4.13(a) indicate that object size has no significant effect on the peak standard deviation except in the case where no object was present (object size of 0cm), when the peak standard deviation was much higher. This is confirmed by Figure 4.14(a). Figure 4.14(b) shows that the peak standard deviation occurs slightly later in the movement for larger object sizes.

By contrast, Figure 4.14(c) shows a strong linear correlation between peak standard deviation and grip aperture as object size increases. This can also be seen in Figure

4.13(b). For the object sizes used in this experiment, the timing of the peak standard deviation of grip aperture does not vary significantly with object size.

This is largely in line with the results of Kudoh et al.[77] which showed similar effects of increasing object size on the grip aperture at a significant level, but no effect on the wrist movement.

2.3.3 Transport distance

Finally, the effect of starting distance between the hand and the object was examined. Movements were performed to an object of 4cm diameter, over 1000ms. The distance to be moved was set as 8cm, 12cm, 16cm, 20cm and 24cm.

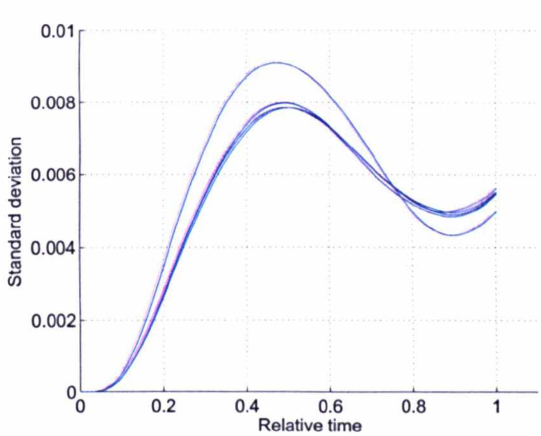

(a)

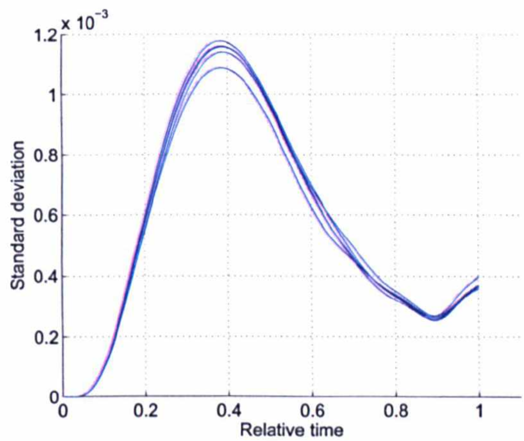

(b)

Figure 4.15: Plots showing the time course of (a) the wrist standard deviations and (b) the grip aperture standard deviations of 500 movements repeated for each movement distance.

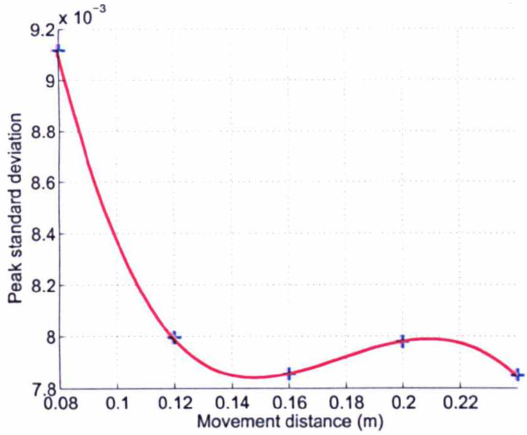

(a)

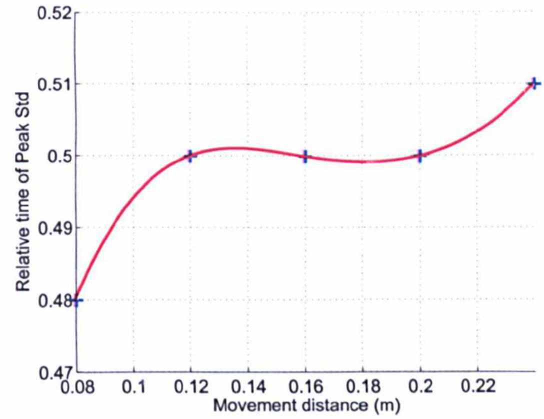

(b)

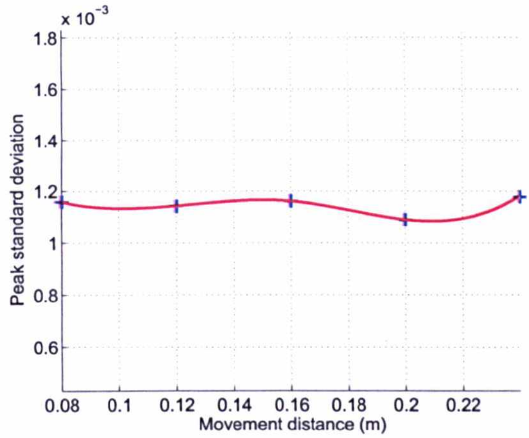

(c)

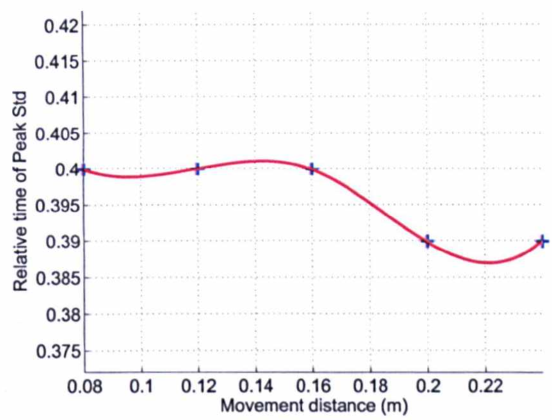

(d)

Figure 4.16: Plots showing the change in peak standard deviation and relative time of peak standard deviation for 500 movements for each movement distance.
(a) Wrist peak standard deviation and (b) relative time of peak standard deviation;
(c) Grip aperture peak standard deviation and (d) relative time of peak standard deviation.

As can be clearly seen in Figure 4.15, increasing the movement distance decreases the overall standard deviation of the wrist movement, but has no effect on the standard deviation of the grip aperture. This is also clear from Figure 4.16(a) and Figure 4.16(c).

These results were also largely in line with those of Kudoh et al.[77], in that the effect of increasing movement distance on wrist variability was highly significant. However, their study also showed a significant effect on grip aperture variability which is not replicated using the model presented in this thesis.

Summary

In this chapter, a model of grasping based on both the "classical" dual visuomotor channel view and on a new view that attempts to explain reaching-to-grasp as pointing movements with the digits has been put forward. Using the implementation of the minimum variance model described modified to allow grasping movements, described in previous chapters, it has been shown that the model captures many of the characteristic features of human grasping.

In particular, it was demonstrated that the model exhibits an increase in maximum grip aperture for increasing object size, with a slope of approximately 0.8. The maximum grip aperture produced by the model was also shown to occur at around 60-80% of the movement. Both of these results follow observations made by a large body of experimental studies.

Furthermore, the contribution of each component (the transport and the grip) to the variability of grasping movements was studied, by analysing the effects of changing three task-related parameters: the movement time, the movement distance, and the object size. The results produced by the model again follow the experimental studies carried out in this area.

Overall then, the approach presented here seems to support the view that reaching and grasping are planned using the same motor principle. However, as it is still not known whether the human motor system acts in this way, further biological and neuroscientific studies are needed to clarify this.

As a condition of the movement model it was found necessary to retain elements of the "classical" view of grasping as two separate visuomotor processes. Experiments presented in this chapter were thus able to analyse the contribution of each of the components in a unified manner through the application of the minimum variance principle, computationally confirming human experimental studies.

Chapter 5

Action Perception

The previous chapters have described the minimum variance model, an implementation of the model for a robotic platform and demonstrated that this implementation can successfully capture key features of human reaching and grasping movements. In this chapter, the model (as extended for grasping) is tested in the domain of action perception. Like grasping, this is both an important validation of the human-like qualities of the trajectories produced by the model and a useful application in its own right.

1 Coupling between action observation and execution

Much recent work in action perception has focused on the possible role played by the motor system in perception. The motor theory of perception suggests that actions are perceived and understood by using the motor system "offline" (i.e. without sending commands to the system actuators) to simulate potential actions and then comparing the predicted movements with the actual observed movements of the demonstrator.[38] The theory has gained support with the discovery of mirror neurons in monkeys;[102,50] neurons in area F5 of the monkey cortex, an area associated with motor control, have been shown to fire both when the monkey observes an action and when the monkey performs the action itself. There is growing evidence for a similar system in humans,[103,104] although it is thought to be considerably more complex than this simple definition suggests.

There is also a growing interest in computational mechanisms that allow robots to observe, imitate and learn from human actions.[107,7,12] As robots are required to perform tasks of greater and greater complexity, and to cooperate with humans on tasks in human-centric environments, there is a clear need for easier methods of programming robot movements. This need has resulted in a number of computational architectures that allow the matching of demonstrated actions to the observer robot's equivalent motor representations.[6,26,3] If the robot is to learn from human demonstrations by invoking its own motor system, it is intuitive that its own motor system should produce movements similar to human movements.

In the work presented in the previous chapters, the robot's motor representation is the scheme for producing human-like movement features using the minimum variance model. In this chapter, this is combined with part of an existing model for robotic learning from demonstration,[26] the goal being to couple action observation to the action observation system, where the execution system is suitable for robot control and produces the qualities of human-like movement.

When presented with a demonstration, the system compares its predicted trajectories with those of the demonstration and produces a confidence value based on how closely the two match. Here, the system is presented with normal grasps and grasps that show deviation from the normal pattern. A comparison of the relative levels of the confidence profiles aims to show that the system produces significantly higher confidences when presented with normal grasps, thus providing evidence that the system could successfully be used as part of a scheme for robotic learning from human demonstration.

The confidence profiles produced by the system are then compared qualitatively with transcranial magnetic stimulation (TMS) data from humans during the passive observation of similar grasping movements.[45] This comparison aims to show that the importance of temporal coupling between action observation and execution in humans (see below) is matched by its importance to the imitation scheme presented here.

1.1 Temporal coupling between action observation and execution

While imaging studies have demonstrated the existence of a mirror system in humans,[50] the temporal resolution limitations of brain scanning technology means that far less is known about the temporal aspects of the mirror system. However, recent experiments with transcranial magnetic stimulation (TMS) have shed some light into the temporal coupling between action observation and execution.[45,44] Previous computational models of the mirror system have shown that such temporal coupling is crucial.[22,26,96] For example, Demiris[22] derived a set of testable predictions, most important of which was that monkey mirror neurons would not fire (or fire less) when the demonstrated movement was performed at speeds unattainable by the observer monkey. In Gangitano et al.[44] it was shown that the amplitude of the motor evoked potentials (MEP) induced by TMS in humans observing a reach-to-grasp action was modulated by the amount and timing of the observed grip aperture. A strict temporal coupling between cortico-spinal excitability and the dynamics of the reaching and grasping movement when passively observed was clearly demonstrated.[44]

A follow-up study[45] shed further light into the temporal characteristics of this coupling. The modulation in cortico-spinal excitability profiles during the observation of reach and grasp actions was studied under three experimental visual stimuli:

- Observation of natural reach-to-grasp actions
- Observation of a reach-to-grasp action where the appearance of the maximal finger aperture was significantly delayed.
- Observation of a reach-to-grasp action where an unexpected finger closing and opening action was inserted before the final grasp portion of the demonstration.

The first condition replicated the results of Gangitano et al.[44], in that the observer's cortical excitability profile was in alignment with the kinematic profile of the demonstrated finger movements. The second condition did not show any modulation in the cortico-spinal excitability profile, while for the last condition the initial profile remained the same for as long as the two stimuli remained the same, but upon sight of the unexpected finger closing and opening action there was a slow decay in the initial activation.

This essentially means that familiar grasping dynamics caused greater cortico-spinal excitability than un-natural and unfamiliar patterns, and that the differences between cortico-spinal excitability levels when presented with different stimuli were predictable and directly linked to the dynamics of unfamiliar grasping movements. The experiments presented in this chapter attempt to reinforce this theory by showing that, when presented with the same stimuli, the computational imitation scheme described below produces similar patterns in its confidence profiles.

In the next section the movement model developed over the previous chapters will be integrated with an existing imitation scheme (following the motor theory of perception.[103,124,11,20,28,64,30]) and the combined system will be shown to both match human-like grasping and to place emphasis on the temporal coupling between its predicted action and the observed action.

2 The Imitation Scheme

The scheme to perform action perception used in this chapter is based in part on the Hierarchical Attentive Multiple Models for Execution and Recognition (HAMMER) imitation architecture. This section gives a brief overview of that model and describes how the optimal control scheme described in chapter 3 fits into this model.

The HAMMER family of architectures uses inverse and forward models[94,67,126] as the basic building blocks. An inverse model is a module that takes as inputs the current state of the system and the target goal or goals and outputs the control commands that are needed to achieve those goals. The functionally opposite concept is that of a forward model of a controlled system: a forward model is a module that takes as inputs the current state of the system and a control command and outputs the predicted next state of the controlled system.

Pairing an inverse model with a forward model in the way shown in Figure 5.1 results in a structure that can be used both for executing an action and for perceiving it. When HAMMER simulates or executes an action, the inverse model module receives information about the current state and outputs the motor commands that it judges are necessary to achieve the target goal. The forward model provides an estimate of the upcoming states if these motor commands were to be executed. If, instead of feeding the current state of the imitator to the inverse model, the imitator feeds in the current state of the demonstrator, the inverse mode will generate the motor commands that it would output if it was in that state and wanted to execute this particular action. By inhibiting the motor commands

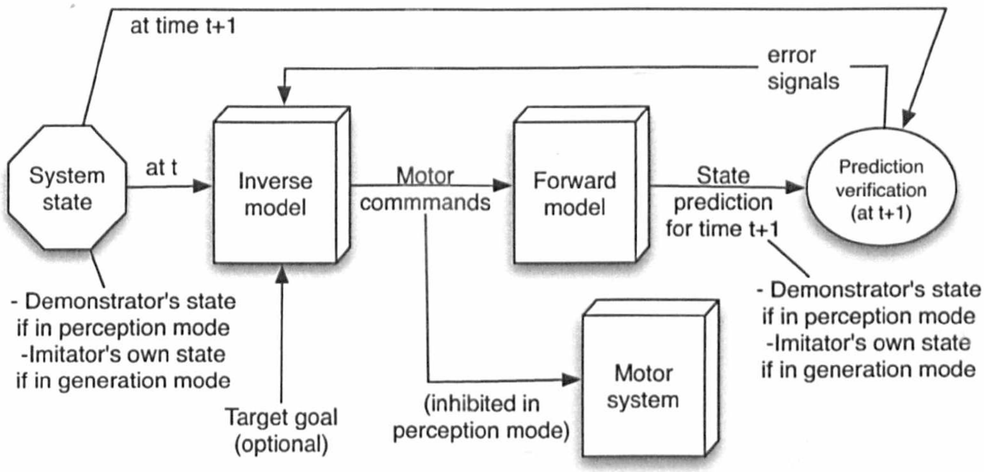

Figure 5.1: The building block of the HAMMER architecture, an inverse model paired with a forward model[26,27]

from being sent to the motor system, the forward model can output an estimated next state, which is a prediction of what the demonstrator's next state will be.

This predicted state is compared with the demonstrator's actual state at the next time step. This comparison results in an error signal that can be used to increase or decrease the behaviour's confidence value, which is an indicator of how closely the demonstrated action matches a particular imitator's action.

The HAMMER architecture in full consists of multiple pairs of inverse and forward models that operate in parallel and in hierarchies.[26] When the demonstrator agent executes a particular action the perceived states are fed into all of the imitator's available inverse models. Following the algorithm described above, this generates multiple motor commands (representing multiple hypotheses as to what action is being demonstrated). The multiple forward models generate predictions about the demonstrator's next state that are all compared with the actual demonstrator's state at the next time step, and the error signals resulting from these comparisons effects the confidence values of the inverse models (see section 3 below for a description of how the confidence values are calculated). At the end of the demonstration (or earlier if required) the inverse model with the highest confidence value, i.e. the one that is the closest match to the demonstrators action is selected.

2.1 Fitting the minimum variance model into the HAMMER architecture

As stated above, the implementation of the minimum variance model presented in chapter 3 is also suitable for producing an instance of the HAMMER architecture.[111] To do this, a movement needs to be encoded as a pair of forward and inverse models. The forward model aspect corresponds to the state dynamics (equation 3.5 - this equation is in fact usually described as a forward model in the control literature). It takes the current state and a motor command and produces a prediction for the next state. The forward model in the HAMMER architecture is therefore stored as the state dynamics matrices A and B.

The inverse model corresponds to the motor command equation. Here, the set of state-feedback gains L and Kalman-filter gains K are stored as the inverse model. Both these and the dynamics matrices can be calculated and stored "offline" without having to execute a movement. They are calculated using the parameters of the movement, such as the target and movement time (or number of time steps).[111]

With these structures in place, the implementation of the minimum variance model can be fitted directly into the HAMMER architecture. This instance of the architecture is termed HAMMER-MV to distinguish it from other instances of the architecture that use a different control system.[26,30] Pairs of forward and inverse models exist for individual movements of individual effectors and can be combined into hierarchical structures.[29,30] Formulating reach-to-grasp movements as a hierarchy is described in the next section.

2.2 Organisation for grasping recognition

The arm model used in these experiments was the same as that used in chapter 4 (see Figure 4.1). The model was a two-link planar arm with two rotational degrees-of-freedom corresponding to the shoulder and elbow. The lengths of the two links were 30cm, which roughly corresponded to the lengths of the upper arm and forearm of the demonstrator. The hand was constructed as before from two similar components, both two-link models with two rotational degrees of freedom. The link lengths were set to 10cm, accounting for

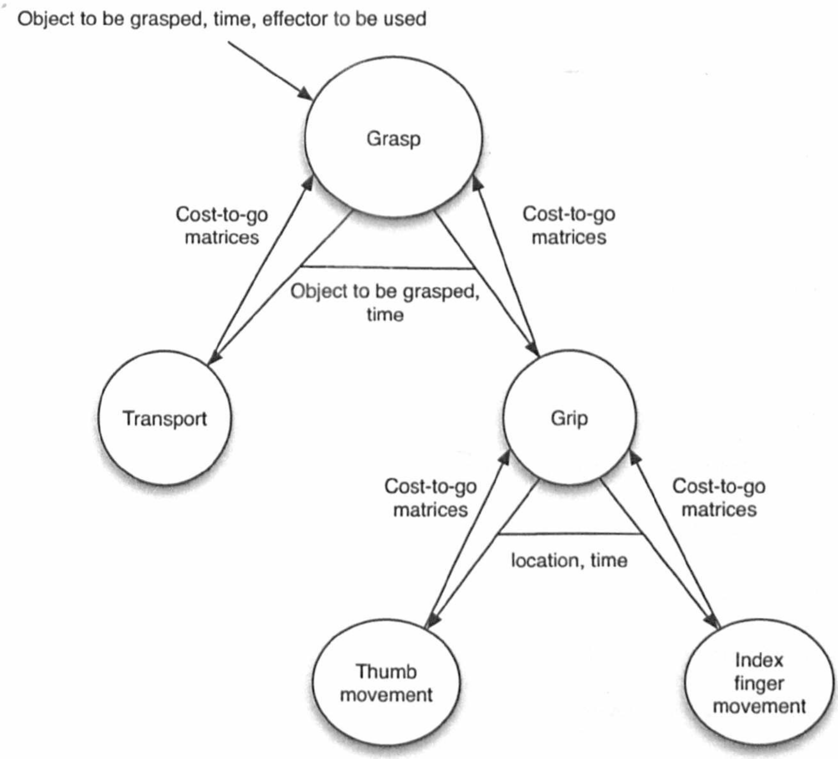

Figure 5.2: A hierarchical representation of the control model for grasping, as described in chapter 4. Each leaf of the hierarchy calculates its own set of state-feedback and Kalman-filter gain matrices for the given task parameters. These take the role of inverse models in the architecture shown in Figure 5.1.

the hand and the digit.

To perform a reach-to-grasp movement using the paired forward/inverse model concept, inverse models of the component parts of the movement are assembled as shown in Figure 5.2, in much the same way as reach-to-grasp movements were planned and executed in the previous chapter. The individual components are parameterised from the highest level using information about the object and the required movement time. This is propagated down to the components of the movement, which then return back the state-feedback gains L and the Kalman-filter gains K for those particular requirements.

3 Confidence

The confidence value associated with a predicted trajectory is a measure of how closely the prediction matches the observed action. Confidence values are calculated at each time step, and the confidence that a given model's prediction matches the observed action can both increase and decrease over the course of a movement. Many movements may begin in a similar way, but differ considerably in their final trajectory, as will be seen with the experiments into grasping recognition described below.

Confidence values from many competing models can be compared, and the model with the highest confidence can be selected to execute its motor commands, thereby replicating the observed action. Selecting the "winning" model in this way does not have to take place at the end of the movement - it can also take place during the observed action if required. For long or complex movements it is unlikely that one model will have the highest confidence throughout the demonstration, and the system is capable of switching between models as confidence values rise and fall. A clear example of this can be seen in Johnson and Demiris[63] where several models exhibit the highest confidence value as a demonstrator performs a sequence of movements.

For the experiments shown below, the following method is used to calculate the confidence for the predicted trajectory against the observed action. When the system is presented with the demonstration trajectory, it uses the state-feedback and Kalman-filter matrices of known movements to produce a prediction of the next state, given its observation of the current state of the observed action. To produce an value for the confidence in the prediction, this is then compared to the demonstrators actual next state, according to equation 5.1.

$$\Delta C_r = sgn\left(r_n - r_{n-1}\right) \times sgn\left(r_n^{pred} - r_{n-1}^{pred}\right) \times \left(r_n^{pred} - r_{n-1}^{pred}\right) \tag{5.1}$$

Here, r_n is the distance between the hand and the target at time step n for the observed action, while r_n^{pred} is the same value for a given inverse model. $sgn(x)$ is the sign function, which returns -1 for $x < 0$ and +1 for $x \geq 0$. The term $n - 1$ indicates the previous time step. Equation 5.1 can be summarised in the following points:

- If the predicted trajectory is moving in the same direction as the observed trajectory (i.e. either towards or away from the target) at a given point in time, we want the confidence value of the prediction to increase. If the predicted trajectory is moving in the opposite direction to the observed trajectory, we want to decrease the prediction's confidence value. From the above definitions, $r_n - r_{n-1}$ is the change in distance between hand and target in one step. If the hand is moving further away from the target, its value will be negative; if moving closer to the target, its value will be positive. Multiplying the sign of the change for the observed action, $sgn\,(r_n - r_{n-1})$, by the sign of the change for the predicted action, $sgn\left(r_n^{pred} - r_{n-1}^{pred}\right)$, in equation5.1 results in a value of +1 (confidence value increase) if the changes are the same or -1 (confidence value decrease) if they are different.

- The third term in equation 5.1 is the velocity of the predicted trajectory; the confidence value increases or decreases by this amount to reflect the fact that a rapidly changing prediction should either have its confidence increased or decreased correspondingly rapidly; if it is moving rapidly in the correct direction its confidence should increase rapidly, while if it is moving rapidly in the *wrong* direction, its confidence should be decreased significantly. By the same argument, a slow moving prediction should have its confidence rise or fall equally slowly.

This confidence update equation can be applied to both reaching and grasping; as described in more detail below, for grasping the term r_n (distance between hand and target) is substituted for grip aperture.

The change in confidence ΔC_r is calculated for each time step, and is used to update the overall confidence C_n that the movement has been correctly recognised, based on the past history of confidence values (equation 5.2).

$$C_n = C_{n-1} + \Delta C_r \tag{5.2}$$

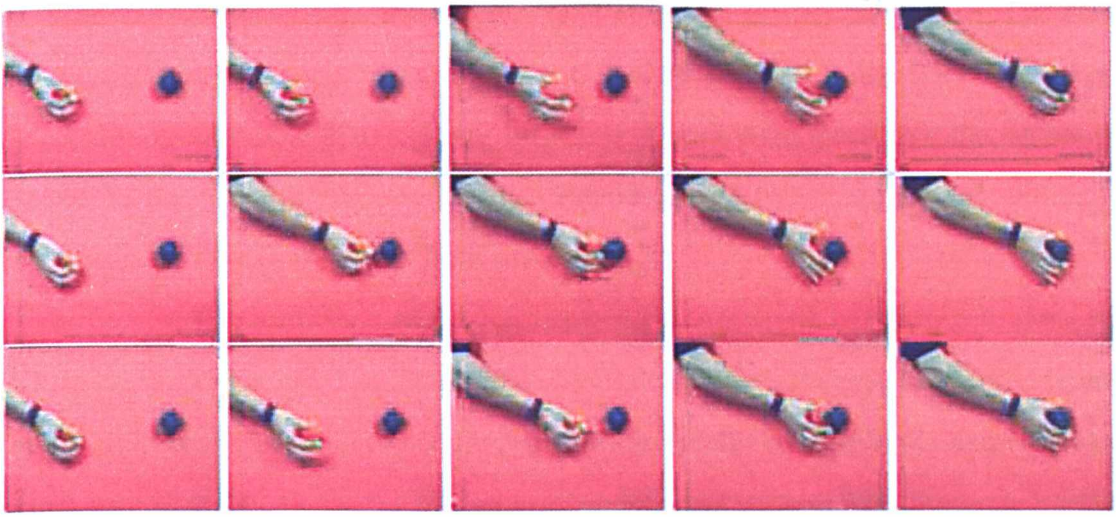

Figure 5.3: Examples of the three different stimuli recorded: the top panel shows a normal grasp action, the middle panel shows a grasp action where the finger opening occurs abnormally late in the process and the bottom panel shows a grasp action with an unexpected finger closure at the point of expected maximum finger aperture; the stimuli closely follow those used in the TMS experiments of Gangitano et al.[45].

4 Grasping Experiments

In this set of experiments, human demonstrations of reaching actions were recorded and given as inputs to the two-dimensional 6 degree of freedom simulated arm, controlled using the scheme described in the previous section. In the following sections, the visual stimuli that make up the demonstrated movement are described, along with the equations governing the matching of the model arm's performance against the human data.

4.1 Visual stimuli

Three different types of reaching and grasping movements were recorded using a human demonstrator as shown in Figure 5.3, closely following the experimental approach and stimuli types of Gangitano et al.[45].

The movements of the human demonstrator were restricted to a 2D plane parallel to the table surface, and a 100mm foam ball was used as the grasping target. Data were captured with a Unibrain firewire camera at the rate of 30 frames per second. Colour markers were placed at the thumb and index fingers of the demonstrator and a coloured arm band at the wrist. These three points (end of thumb and pointer fingers, and centre of mass of the wrist) were tracked using the CamShift algorithm, and the coordinates of these points in successive frames along with time stamps were saved to a file, to be used as input to the action perception scheme. Periods of inactivity at the start and end of the demonstration were removed from the file.

The captured trajectories used in these experiments are shown in Figure 5.4, along with the grip aperture profiles. These show the essential differences between the three types of stimuli, and the similarity between the grip aperture profile of the human demonstrator's normal grip and that produced by the grasp implementation of the minimum variance model.

4.2 Error calculation and confidence update

The confidence was updated at each time step by comparison between the imitator's prediction and the demonstrator's trajectory. Specifically, comparisons were made between the predicted change in both the distance to the target, r, and the grip aperture, g, both shown in Figure 4.1. This meant that the confidence for the top-level of the hierarchy a function of the confidences of its component parts. The first step was to find the coordinates of the mid-point of the grip according to equation 5.3.

$$m_n = \frac{f_n - t_n}{2} + t_n \tag{5.3}$$

where m_n is the position of the grip mid-point, and f_n and t_n are the positions of the tips of the finger and thumb respectively. This was then used to define the distance to the target r (equation 5.4), given as the absolute difference between the coordinates of the centre of the object and the mid-point of the grip (see Figure 4.1).

$$r_n = |object - m_n| \tag{5.4}$$

The absolute value of the grip aperture g (again, see Figure 4.1) was also calculated for each time step according to equation 5.5.

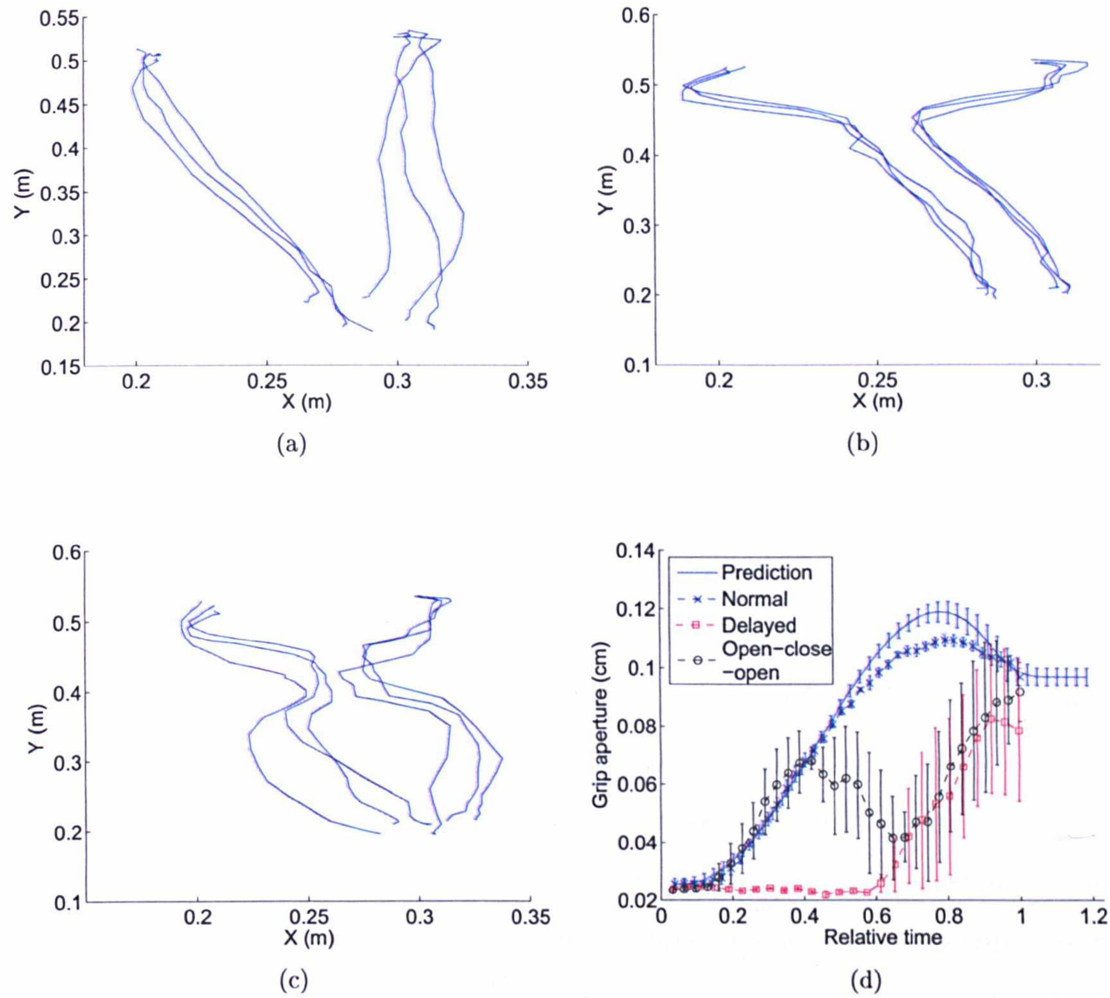

Figure 5.4: Examples of the thumb- and finger-tip trajectories recorded from the human demonstrator: (a) Normal grasping movement; (b) Delayed opening; (c) Opening-closing-opening; (d) Grip aperture profiles for the three different types of stimuli and the minimum variance model grasp. This plot also shows the grip aperture variances, which are understandably greater for the non-natural grips.

$$g_n = |f_n - t_n| \tag{5.5}$$

Using equations 5.3, 5.4 and 5.5, values of m_n, r_n, and g_n were calculated both for the observed trajectory and the predicted trajectory. Given these values, the confidence value at each time step was given as

$$C_n = C_{n-1} + \Delta C_r + \Delta C_g \tag{5.6}$$

where

$$\Delta C_r = sgn\left(r_n - r_{n-1}\right) \times sgn\left(r_n^{pred} - r_{n-1}^{pred}\right) \times \left(r_n^{pred} - r_{n-1}^{pred}\right) \times w_r \tag{5.7}$$

and

$$\Delta C_g = sgn\left(g_n - g_{n-1}\right) \times sgn\left(g_n^{pred} - g_{n-1}^{pred}\right) \times \left(g_n^{pred} - g_{n-1}^{pred}\right) \times w_g \tag{5.8}$$

Here, $sgn(x)$ again represents the sign function. As with the confidence calculations for reaching given in the previous section (equation 5.1), equations 5.7 and 5.8 mean that if both the observed action and the prediction are moving in the same direction *and* the grip apertures of the two are also changing in the same way (i.e. either both opening or both closing), the confidence that the inverse model has correctly recognised the movement will increase. If the two trajectories move in different directions or the grip apertures change in different ways, the confidence will decrease. The change in confidence for both distance-to-target and grip-aperture is modulated by both the step-by-step change in the prediction, as in equation 5.1, and additionally by a weighting term w_r or w_g. These weighting terms are set to ensure that the relative contribution of each component of the movement to the overall confidence is the same, despite the large differences in velocity between arm and digit movements in a combined reach-to-grasp movement. In the confidence plots shown below, $\frac{w_r}{w_g} = \frac{1}{2}$.

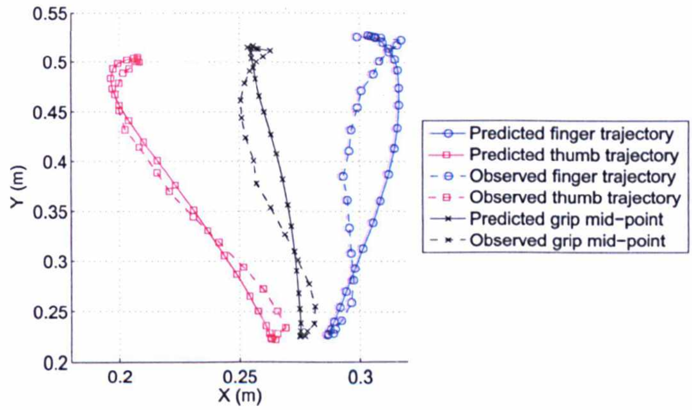

Figure 5.5: Plot showing normal trajectories predicted by the reach-to-grasp model against observed trajectories, when the observed action is of a normal grasping pattern.

4.3 Results

Figures 5.5, 5.6 and 5.7 show the normal trajectories produced the reach-to-grasp model against the demonstrated movements. Figure 5.5 shows how similar the predicted movement is to the observed movement when the demonstrator performs a normal reach-to-grasp action. By contrast, large differences can be seen in Figures 5.6 and 5.7 between the predicted normal movement and the observed movements when the demonstrator performs non-natural actions.

Figure 5.8 shows the confidence plot over time for example trajectories of the three different conditions. Confidence profiles for all the trajectories performed are shown in Figure 5.8.

The results closely follow the characteristics of the data reported by Gangitano et al.[45]. For example, in Figure 5.8(a), the confidence progression during the observation of a *normal* movement over time follows the increasing trend reported by Gangitano et al.[45], reaching its maximum at the point of maximum aperture and subsequently reducing slightly as the movement closes to the end.

The confidence progression during the observation of the second stimuli type (the grasp movement with delayed aperture opening) does not show any significant increase in value during the first half of the observed action, corresponding to the time when the demonstrator's digits are still closed. When the digits start to open they begin to

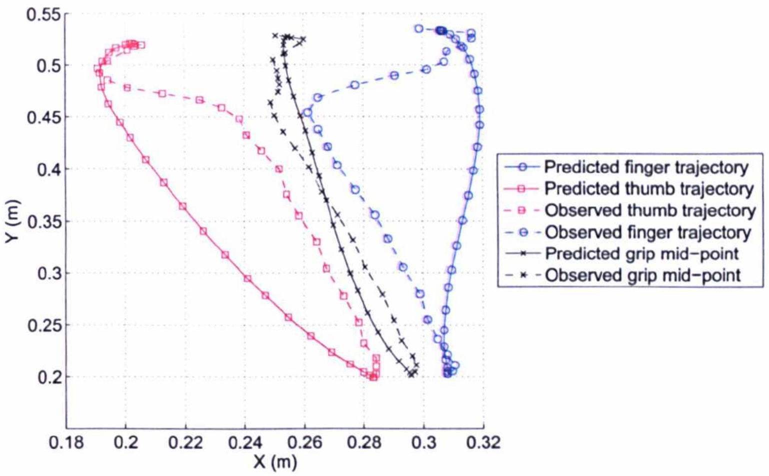

Figure 5.6: Plot showing normal trajectories predicted by the reach-to-grasp model against observed trajectories, when the observed action is of a delayed opening of the digits.

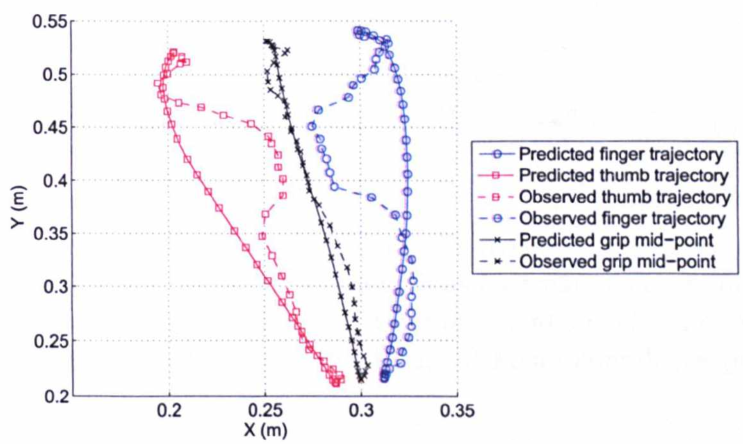

Figure 5.7: Plot showing normal trajectories predicted by the reach-to-grasp model against observed trajectories, when the observed action is of an open-close-open grasping pattern.

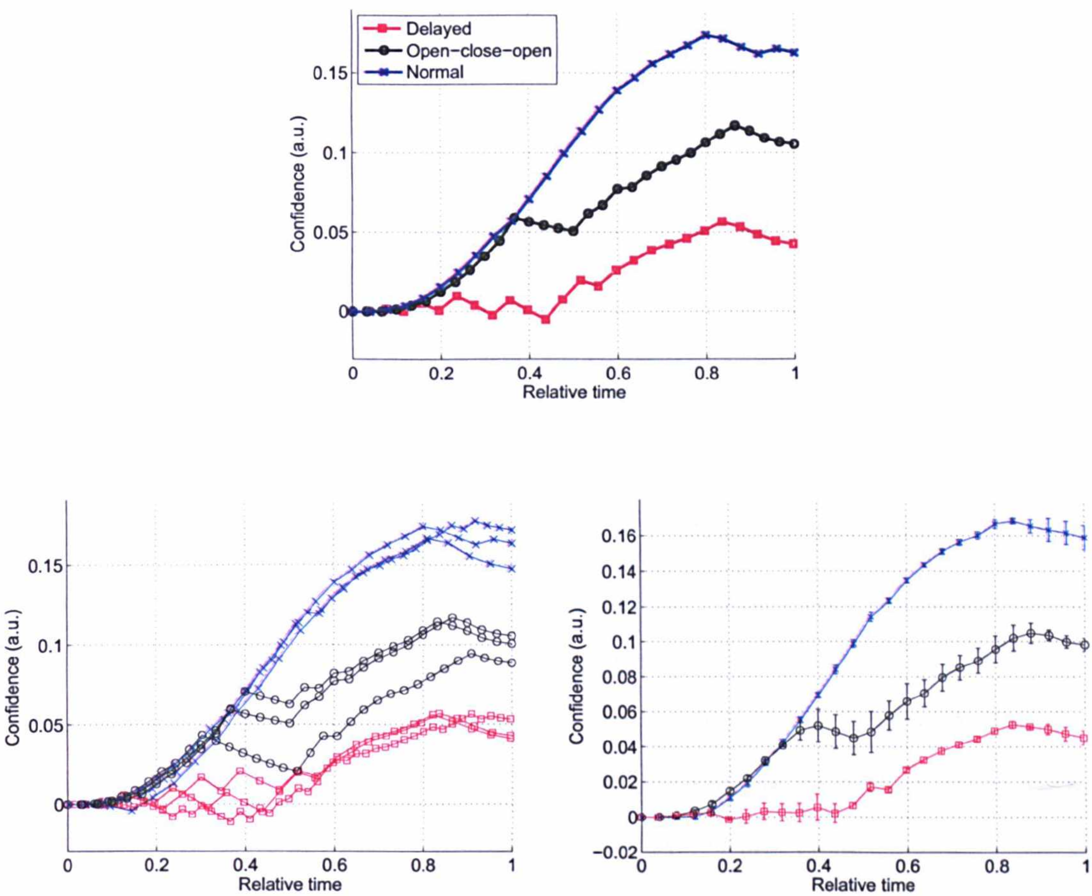

Figure 5.8: (a) Confidence profiles of the predicted movement when executed against single instances of each of the three observed grasp actions (normal, delayed opening, open-close-open); (b) Confidence profiles of the predicted movement for all observed movements: 3 instances each of the three observed conditions; (c) Mean confidence profiles for each of the three observed conditions.

intersect with the digit trajectories of a normal grasping movement, causing a gradual increase in the confidence level of the prediction that still only results in a relatively low final confidence value (again following data reported by Gangitano et al.[45]).

Finally, the confidence progression during the open-close-open grasp closely follows the trend of the normal movement until the point of the sudden digit closure, with a notable descending trend followed by a gradual increase as the digits open and begin to match the normal grasping trajectories, again matching the general trend for this stimuli reported by Gangitano et al.[45]. It can be seen in both Figure 5.8(a) and 5.8(c) that the rate of confidence increase during the second half of the movement is still greater for the prediction against the observed normal grasp than for either of the other two non-normal grasps.

This pattern is reproduced amongst all captured trajectories, as shown by both Figure 5.8(b) and the mean confidence profiles of all observed movements shown in Figure 5.8(c). This figure also shows the variance at select points along the confidence profiles. These bars are small for the prediction against the normal grasp, indicating that the predicted grip is highly consistent with the observed grasping movement. For the non-normal grasps, the predictions show greater variability during the periods where the grasps differ most from the normal movement. For the delayed opening movement, this is during the first half of the movement, before the digits have opened. For the open-close-open grasp, it is at exactly the point where the grasp begins to un-expectedly close.

Summary

The neuro-physiological data mentioned in this chapter lend support to the notion that the human brain does not passively observe actions but actively forms hypotheses and predicts forthcoming states. In Gangitano et al.[45] it was shown that timing is a strong component of these predictions, and thus that there is no temporal dissociation between components of an action plan in the motor representation of an observer.

The computational implementation of a system based on the HAMMER architecture described in this chapter reproduced these results, using a controller based on the minimum variance principle introduced in previous chapters. This system used the controller to generate predictions of the next state for the observed action based on a familiar (natural) grasping pattern, predictions that closely matched the actual digit trajectories of human grasping.

Where the components of the observed action (the reach and the grip) were dissociated to produce an unfamiliar grasp, the system produced reduced confidence profiles whose key differences from the confidence profile for the normal movement were explainable and related to the dynamics of the un-natural movements.

Chapter 6

1 Discussion

1.1 Minimum Variance Model

Computational models of human movement vary in the observable characteristics of such movement that they capture and in their applicability to controlling a robot arm. In chapter 3, focus was given to the minimum variance model and it was demonstrated that not only does this model capture the common characteristics of human arm movements, but that it is also suitable for implementation on a robotic platform, thereby allowing a robot arm to move in a human-like manner.

Previous implementations of the minimum variance model were briefly outlined in chapter 3, and a number of reasons for the differing approach of this work were given. Chief among these was one of the aims of this work, to look at the applicability of models of human movement to the control of a robot arm. A number of the previous approaches were not suitable for this, either due to time consuming computations required for the planning of single movements or due to their computational complexity.

Another consideration when choosing a different approach to previous work was the structure of the optimisation process, and its compatibility with the ideas and principles behind the HAMMER imitation architecture. As described in chapter 5, the LQG implementation outlined here[117] has structures that were able to represent forward and inverse models in the control sense. Since these are required for the prediction and comparison of known movements with an observed demonstration, it was important that the optimal control scheme be able to match these structures.

As well as describing an implementation of the minimum variance model, the resulting trajectories were compared with those produced by two other well-known models. These models capture some, but not all, of the common features of human movement. Their criteria of jerk and torque-change are also less straightforward to calculate and optimise than the readily observable quantity of hand positional variance.

The success of the minimum variance model in predicting and explaining the characteristic features of human behaviour is extensive. It has been shown to capture the form of saccadic eye movements,[52] reaching movements,[52,117,112] and now grasping movements (Simmons and Demiris[110] and chapter 4), and is one of the few models to account for disturbances to the system in the form of noise on the control signal. However, no experiment (behavioural or neurophysiological) has been performed that definitively identifies exactly how the brain plans and executes movements. It is highly likely that more than one criterion is used, or that emphasis is placed on different criteria depending on the task.[116] The direction of research in this area is moving towards combined optimisation criteria, such as that proposed by Matsui and Wada[83].

Despite this, the arguments and theory behind the model make it reasonable that some form of minimum variance or task-level optimisation that accounts for natural disturbances to the system takes place in the planning of movements. As such, it was chosen as a valid model for implementation on a robotic platform to reproduce important characteristics of human movement.

The stochastic nature of the minimum variance model, where the random noise on the control signal is assumed to have variance proportional to the amplitude of the control signal, fits in well with the growing emphasis on probabilistic and Bayesian methodologies in the study of behaviour and brain function.[76] The suggestion put forward by these theories is that the CNS uses previous knowledge to judge likely future outcomes, adjusting its expectation of these outcomes as it accumulates more experience.[25,20] Using this as a basis, a learning scheme can be envisaged whereby the motor system, generating movements through the minimisation of variance in the presence of noise, modifies its output based on its previous experience of the effects of the noise and other disturbances.

An interesting aspect of the minimum variance model not discussed in the preceeding chapters is the actual form that the signal-dependent noise takes in the model, and the effect this has on the trajectories that are produced. For the purpose of this work, the noise has been assumed to be white noise (i.e. random noise drawn from a normal distribution) with zero mean and variance proportional to the square of the control signal amplitude (giving a standard deviation that is linearly proportional to the amplitude of the control signal), as shown below. This is the same assumption made by Harris and Wolpert[52] in their original paper, based on studies that report on the standard deviation of motor-neuronal firing.[84]

$$\tilde{u}_n = u_n + w_n, \;\; w_n \sim N\left(0,\, k(u_n)^2\right) \tag{6.1}$$

Other studies have looked at aspects of this assumption in greater detail, including the type of distribution from which the noise is drawn[35] and the profile of the noise determined by the exponent on the control signal.[58] In their analytic treatment of the minimum variance theory, Feng et al.[35] discuss using a Poisson process instead of a normal distribution for the noise, on the suggestion that neural signals take this form.

Iguchi et al.[58] note that a number of studies suggest that the relationship between the mean of the noise and its standard deviation may be non-linear, implying that the value of the exponent used to calculate the variance in equation 6.1 is not 2. They repeated the experiments of Harris and Wolpert[52], varying the value of the exponent between 0.1 and 3.0, and showed that the match to observed data by the model trajectories depends on the value of the exponent.

1.2 Grasping

Together, the two experiments shown in sections 2.1 and 2.2 confirm that the model of reaching-to-grasp captures the experimentally determined characteristics of human grasping. As stated before, the approach of this chapter was to consider grasping to be two separate processes, planned using the same motor control principle.

Through the addition of a single via-point to each digit's trajectory, the perpendicular approach of the digits to the object target positions observed in grasping has been replicated. Following the minimum variance principle, the spatio-temporal positions of the via-points were determined as those that resulted in the lowest end-point standard deviation of the digit trajectories, quantitatively confirming that a perpendicular approach to the target positions of the object results in a more accurate grasp.

The via-point constrains the trajectory to pass through a set location (or close to it, as the addition of signal-dependent noise means the trajectory is unlikely to pass through the exact spatial location) at a set time during the movement. The via-point imposes no other demands, such as velocity or acceleration constraints, on the system.

The results show that increasing the horizontal distance of the via-points from the object increases the maximum grip aperture of the hand during grasping and causes that maximum to occur earlier in the movement. This follows as a fairly logical consequence, as a via-point further from the object will require a larger grip, which will have to performed earlier if the digits are to successfully reach the target positions on the object in the required movement time.

This work also confirms that the model matches the characteristics observed in numerous experiments on grasping. Both the relationship between maximum grip aperture and object size, and between time of maximum grip and object size were successfully captured by the model. These results compare favourably with the literature summaries reported in Smeets and Brenner[113].

The model presented in chapter 4 allows the contributions to the end-point variance of both components of grasping to be studied. By varying the movement time for a grasping movement over a fixed distance, it was demonstrated that both the transport component and the grip component exhibit reduced variance as movement time increases.[47] Since the model of reaching has been shown to obey the speed-accuracy trade-off of Fitts' Law (see Simmons and Demiris[112] and Figure 3.4), this result is not unexpected.

Experiments to check whether the model matched the findings of an experimental study into the spatiotemporal variability of grasping were also carried out. Following Kudoh et al.[77], both object size and movement distance were varied to observe their effects on the variability of the movement. The model showed that object size has a significant effect on the variability of the grip aperture, but not on the wrist movement. This follows from the separation of the grasping movement into two separately planned components, as the planning of the reaching component takes no account of the object properties.

With regards to changing the movement distance, the results from the model differed slightly from those of Kudoh et al.[77]. The same effect on the transport component was observed; that an increase in movement distance results in an increase in variability. Again, this is a logical consequence of the speed-accuracy trade-off in that a shorter movement distance over the same movement time will require lower velocities and therefore be more accurate.

However, no significant effect of movement distance on the grip aperture variability was observed. Again, the reason for this result is the separation of planning for the reach and transport components. This would generally be the case for models that follow the dual-channel view of grasping, since it proposes that the information processed by the grip channel is intrinsic to the object and not effected by properties that relate to the object and its environment.[59,113] In turn, these extrinsic properties are processed solely by the transport channel.

1.3 Action perception

The hierarchical organisation of the motor representation used in chapter 5 is a useful engineering tool when structuring motor systems. As well as being a natural organisation of the prehension scheme detailed in chapter 4 (the movement consists of reach and grip components, with the grip further consisting of separate digit movements), the hiding of the lower details in higher level structures allows for easier task planning than can be achieved with flat non-hierarchical representations. Only the details of the goal and the desired task parameters need to be supplied and the higher inverse model will recruit and coordinate the appropriate lower level primitives. This is a key feature of the HAMMER architecture, upon which the action perception scheme presented in chapter 5 is based.

Additionally, the higher level models also modulate the contribution of each of the underlying primitives when predicting future states: apart from judging success individually, predictions from lower levels are rated, and modulated according to how much they contribute to the higher goal (equations 5.6, 5.7 and 5.8).

The minimum variance implementation employed was particularly suited for this, since it allows the calculation of the confidence of the lower level level primitives (e.g. digit movements) individually as well as with respect to each other (e.g. grip aperture), and propagates their weighted values upwards to allow higher level nodes to calculate the progress of the overall model towards the final goal. It would also be interesting to see whether other criteria (for example, smoothness of movement) that result in human-like trajectories could also replicate the effects observed in experiments presented here.

Whereas some control schemes can adapt their output during execution, movement planning using the optimal control implementation presented here is performed "off-line". As a result, there are no parameters to be adjusted during execution, and therefore no way to temporally "morph" the plan to more closely match what is being observed. Although that is technically possible using this action perception scheme (as shown in previous instances of the HAMMER architecture that use adaptive PID controllers;[26] these allow online adaptation to different speeds of the demonstration, within limits), the data of Gangitano et al.[45] suggest that humans do not morph the ongoing motor plan temporally, and the minimum variance implementation for action perception captures that aspect more closely than Demiris and Hayes[26].

However, it is possible for the system given here to smoothly switch from one motor plan to another (as opposed to adjusting the current motor plan). An example of when this might be appropriate is when two movements share a common initial trajectory but then diverge; if the confidence value of the correct predicted trajectory is lower, but then rises after the point of divergence while the confidence of the other movement drops away, the system could easily switch which of the predicted trajectories is sent to the motor system.

It is important to note that the comparisons between the results of Gangitano et al.[45] and the computational results reported in chapter 5 rely on the assumption that the confidence of an inverse model can be mapped to changes in motor evoked potentials (MEPs) of the controlled body part in humans. This is based on the intuition that the neural substrate of an inverse model with higher confidence (i.e. a model that better explains the observed movement) will be more active than that of a model with lower confidence. Other work has linked the confidence of inverse models to the attentional resources that are allocated to them.[30] Since attention to action increases activity in prefrontal, premotor and parietal cortices,[105] a potential link between inverse models and MEPs can be drawn, although the exact nature of this link will require more detailed neural modelling than is within the scope of this thesis.

2 Future Work

2.1 Minimum Variance Model

An important aspect for further study based on the work in this thesis is to increase the complexity of the robotic platform. The minimum variance model has been shown to hold for a relatively straightforward arm configuration, but access to more human like arm configurations and devices would allow further study. More degrees of freedom increase the complexity of the model, allowing greater flexibility in the tasks that can be carried out by the arm.

One of the primary differences between the minimum variance theory and other optimisation criteria is that the optimal trajectory is found through costs associated with a post-movement period, rather than costs associated with the movement itself. Framing the movement task as one in which goal accuracy is the most important requirement works well, but not every task can be cast in this way. A common movement goal is to minimise variance during the movement itself, as when moving a glass full of liquid. An obvious experiment to perform with the implementation given in chapter 3 is to place costs on the variance during the movement and observe the resulting trajectories. This has also been proposed by Feng et al.[35], who produced an analytic solution to the minimum variance problem for both post-movement and during-movement variance minimisation.

As mentioned above, the human motor system is unlikely to use a single optimisation criterion to plan and generate movement. An examination of how different criteria can be combined and their different effects would be a profitable area for future work. In particular, the relative weighting given to different criteria in different tasks is of interest.[83]

Along these lines, an improvement to the system presented in this work would be the addition of movement duration to the cost function, following the model proposed by Hoff[55]. Currently, the movement time is an input parameter calculated according to the required movement accuracy, but incorporating it in the terms to be optimised would allow further study of issues related to the timing of movement.

One limitation of the present system is that it is unable to perform obstacle avoidance. A via-point trajectory can be specified that would allow an obstacle in the workspace to be avoided, but there is no principled way to determine exactly what that via-point should be to produce a human-like trajectory. Work has been done by de C. Hamilton and Wolpert[19] analysing obstacle avoidance trajectories, using a spline based optimisation method. They added costs to the minimum variance trajectories such that any part of an ellipse with axes equal to two standard deviations that intersected with the object was penalised. In this way, the degree of uncertainty in position at each point in time during the movement determined the path around the object. Fast movements, with greater variance, take a wider path around an obstacle than slower movements that are subject to less uncertainty.

Outside of the domain of upper limb movements, this method of obstacle avoidance using the minimum variance model could find application in mobile robot navigation. A robot planning a path that reached a target position with as great an accuracy as possible could make use of the minimum variance principle, and use the obstacle avoidance method described above to navigate to the target through a cluttered environment. If this could be implemented, it would be of value to compare the chosen path with human subjects moving through the same environment at a comparable speed, to judge if humans take the uncertainty of movement into account when moving around obstacles.

Looking beyond the system as it exists, an interesting extension would be into the realm of tool use. Movements involving tools often have very specific patterns related to the task being carried out. Analysis of human tool use would have to be performed to acquire relevant data for comparison with model predictions. For generating trajectories from the model, a careful formulation of both the task and the mechanical system would have to be performed, bearing in mind that tasks involving tools are often unstable.[15] Many tasks with tools also involve the application of forces, and a valid extension of the model that was able to accomplish these tasks would also have to extend the model given here to account for the combined arm and tool dynamics.

Another interesting future area of study would be to look into how the system could be extended to learn to improve its trajectories through training or practice. When humans first learn a skilled movement, they often perform it inaccurately and inconsistently. Following Fitts' Law, beginners will usually attempt to increase their accuracy by performing the movement more slowly than a more skilled individual, but through practice and training they are able to increasingly reduce the effects of disturbances and perform movements fast and accurately.

A starting point for extending the model in this direction would be the work of Burdet and Milner[14], as described in chapter 3. Their model of movement as the superposition of multiple submovements accounts for deviations from a planned trajectory by introducing deviations into each submovement. These can then be corrected by subsequent submovements; thus, the greater the number of submovements the greater the accuracy of the overall movement. By adjusting various model parameters according to the outcome of the overall movement, this model effectively learns to improve its accuracy over repeated trials.

2.2 Grasping

The work presented in chapter 4 clearly prompts further investigation into the behaviour of grasping. It supports the view that grasping could be planned as pointing movements of the digits, but this remains to be physiologically or neurologically confirmed.

The results presented in chapter 4 have been achieved even with a relatively simple model for the arm and hand. A more realistic model of the hand, such as that used by Meulenbroek et al.[85], could certainly be introduced to the system without changing its fundamental characteristics. However, different types of grip have been modelled using two "virtual" fingers[97] that are similar to the arrangement for the hand used in this chapter. A further extension of the model would be to move away from planar grasping and model full three-dimensional grasping movements.

One of the assumptions of our model and that of Smeets and Brenner[113] is that the digits begin the movement touching each other. An area for further modelling is to relax this assumption and observe the effect on the digit trajectories of a starting grip aperture that is not zero. Timmann et al.[115] showed that when subjects started the movement with maximum grip aperture, they initially closed the grip before reopening to second maximum and then closing again to grip the object. Current models, including those of Smeets and Brenner[113] and Meulenbroek et al.[85] are unable to account for this, although Smeets and Brenner[113] suggest that additional constraints on their model would conform to the results of Timmann et al.[115].

This work has not touched on the effects of hand orientation or object-to-wrist distance on grasping. Clearly these will have a large influence on the movement of the digits, and will also change the shape of the grasp. The greatest impact of changing the object-to-wrist distance will be to restrict the maximum size of object that can be grasped - the largest object can only have a radius equal to the object-to-wrist distance. A second factor will be a limitation on the size of the maximum possible grip aperture.

Only a single object shape has been considered, while there is evidence that object shape has a large impact on the grasping kinematics.[18,108] Furthermore, only a precision grip between the finger and thumb has been explored - the principle could equally be applied to other types of grip, such as a power grip.

An interesting area of study would be to examine how grasping trajectories produced from pointing models are effected by the presence of obstacles, both in the path of hand and close to the object. Experimental work has already been performed looking at how obstacles influence the speed of grasping movements[5] and how obstacle position in the workspace can change grasping trajectories.[89] As stated above, the effects of obstacles on minimum variance reaching movements have also been examined,[19] allowing obstacle avoidance to be incorporated into a minimum variance grasping model.

2.3 Action perception

Although, as noted above, the motor plan generated off-line by the action perception system can be interrupted and a new one generated to possibly better capture the demonstration, it is unlikely that for short demonstrations such as the ones examined here (and used in the experiments of Gangitano et al.[45]) there is sufficient time to do so. It would be interesting, both for the neurophysiology and the computer modelling sides to repeat such experiments but for longer actions, including possibly sequences of them, to determine whether such a resetting mechanism (as termed by Demiris[24]) is indeed present in humans and study its characteristics.

Perceiving and recognising individual elements within a sequence of movements would also be a challenging task, as any given sequence might be made up of known and unknown movement components. Since an unknown movement might move smoothly and continuously into a known movement, it is not clear at what point the observed action shifts from being a completely unknown single movement to a combination of known and unknown segments.

If the minimum variance model is extended to the domain of tool use, as suggested above, the role of the action perception system would become highly relevant. As well as observing the movement behind the use, the action perception system could be used to extract the *meaning* behind the movement. This would move the system beyond recognising the movement and towards the higher level goal of understanding the intention of the demonstrator. Once this is achieved, the high level cognitive information could conceivably be used to plan the task in another way, perhaps one more suited for the robot's abilities or situation.

Chapter 7

Conclusion

As stated in the introduction (chapter 1), the primary contributions of this work have been in the application of specific theories of human movement to a platform suitable for robotic control. Expressly, the research presented in this thesis has demonstrated an implementation of the minimum variance model[52] suitable for controlling a robot arm.[112]

This implementation has been shown to effectively capture several characteristics of human movement, among which are smooth, straight hand paths, bell-shaped velocity profiles and a speed-accuracy trade-off. This properties are achieved due to the intrinsic nature of the model, and apply even for a robotic plant model.

The model has also been successfully shown to match the characteristics of grasping. Specifically, the grip aperture profiles associated with digit trajectories follow the same pattern for variations in object size as those observed in human subjects.

Further validation of the human-like qualities of the movement model were obtained through the use of an action perception scheme to predict and recognise grasps produced by a human demonstrator. The system was able to successfully distinguish between normal grasps and two patterns of abnormal grasp, in the process producing prediction confidence profiles that were qualitatively similar to neural activation recordings from human subjects observing the same stimuli.

The background presented in chapter 2 described several important features that characterise human movement. Despite the complexities of the human motor system and its inherent neural, musculo-skeletal and kinematic redundancies, upper limb movements show stereotypical features both between trials and between individuals. Any theory that attempts to explain how the motor system plans such movements and generates the commands to execute them must explain and reproduce these characteristics.

With the goal of reproducing these features on a robot arm, the remainder of the background discussed models from computational neuroscience that have attempted to match these features, focusing on the class of models that involve the optimisation of some movement relevant criteria. Models discussed include the well-studied minimum jerk and minimum torque-change models, offering a good representation of this class of models. The degree to which they capture the features given earlier in the chapter, as well as their general suitability for implementation, was used as a basic measure for whether they could be used to achieve the goal. The lack of an accuracy constraint or the inclusion of any form of disturbance in the majority of these models lead to the introduction of the minimum variance model in the following chapter.

This implementation of the minimum variance model presented in chapter 3 is based on the previous work of Todorov and Jordan[117]. The structure of the scheme lends itself well to pre-computing and storing predicted costs for given movements. These are effectively primitives,[95] which can be called and executed, switched and superimposed, as required. They are also used in the form of inverse models in the action perception system described in chapter 5.

It has additionally been shown that this implementation can be readily extended to the task of grasping an object, by extending the arm model to include a gripping mechanism and treating prehension as pointing with the digits of the gripper, in line with a recent theory of grasping.[113] In their work, Smeets and Brenner[113] used the minimum jerk model to derive digit trajectories that matched grip aperture profiles from a wide range of literature.

Here, trajectories with the same characteristics were produced by the minimum variance model applied to the arm-gripper plant model. Via-points were added to the digit trajectories, with the aim of producing a perpendicular approach of the digits to the object. The exact position of these via-points (spatially and temporally) was chosen so as to give the maximum accuracy for the digits when arriving at the target positions on the object, without considering how this would effect the trajectory. With the via-point positions established, the grip aperture profiles were then examined for a range of variables, including object size. The results of these experiments showed that the grip aperture profiles, as measured by maximum grip aperture and the relative time at which it occurred, were well within the limits derived by Smeets and Brenner[113] from the literature.

The nature of the grasp model is such that it is possible to examine separately the contributions of the movement components to the variability of the digit end-points. The effects of different parameters on the variability of the reach and grasp parts of the prehension movement were analysed by looking at the average variance profiles for a large number of repeated movements for each parameter value. This aspect of the model allowed comparison with previous work on the nature of the variability of human movements, especially that of Kudoh et al.[77].

This use of the minimum variance model for grasping was then been combined with a high-level system for perceiving and recognising the actions of a human demonstrator.[26] When presented with grasping trajectories, some of which contained deviations from a natural grasping pattern, this system produced confidence profiles that followed a similar pattern to neural activation levels recorded from human subjects[45] observing comparable movements. This not only contributes further validation that the model successfully captures human-like features of movement in the form presented here, but it also provides the basis for a robotic system that can learn from human demonstration.

In summary, this thesis has shown a novel implementation of a biologically plausible model for human movement that captures many of the features of both reaching and grasping. The work on prehension is an extension to previous work on this model, and offers a middle road between two theories of grasping; the separation of planning for reach and grasp components, and the theory that grasping can be explained as pointing with the digits to targets on the object surface. This system for grasping lends itself well to a hierarchical implementation, and can be used in conjunction with an existing system for action perception to recognise and imitate observed movements.

Appendix

A: Spatial and Temporal Generalisation

The use of via-points to produce complex trajectories and meaningful patterns has been described in chapter 3. Here, it is shown how the representation of a movement as a series of via-points can be used to generalise that movement both spatially and temporally.

A.1 Via-point locations

The information needed to perform the generalisation is the coordinates of the start and end points, and the coordinates and temporal locations of the via-points. For an arbitrary movement, observed externally or performed by the motor system, it is not clear exactly where the via-points should be placed to adequately replicate or generalise that movement. Previous work has placed them according to what are considered recognisable features of the movement, including zero crossings (maxima and minima) of velocity or acceleration.

Although not looking directly at via-points, it is appropriate to include the work of Rao et al.[100], as they define movements in terms of dynamic instants where the forces acting on the hand change significantly. As forces cannot be measured from external observation, they use maxima of the movements spatio-temporal curvature (equation A.1), capturing velocity and acceleration information, to segment it into dynamic instants. As an added advantage, spatio-temporal curvature is view invariant.

Spatio-temporal curvature is calculated by projecting a three-dimensional position vector $\mathbf{r}_t = \begin{bmatrix} x_t & y_t & z_t \end{bmatrix}$ on to a two-dimensional surface to produce a spatio-temporal trajectory defined by $\mathbf{r}_t^{st} = \begin{bmatrix} x_t & y_t & t \end{bmatrix}$. Spatio-temporal velocity and acceleration can also be defined: $\mathbf{v}_t^{st} = \begin{bmatrix} x_t' & y_t' & 1 \end{bmatrix}$, $\mathbf{a}_t^{st} = \begin{bmatrix} x_t'' & y_t'' & 0 \end{bmatrix}$. The curvature of the spatio-temporal trajectory can then be defined in the standard way:

$$\kappa = \frac{\|\mathbf{r}_t^{st\prime} \times \mathbf{r}_t^{st\prime\prime}\|}{\|\mathbf{r}_t^{st\prime}\|^3}$$

Expanding this out using the spatio-temporal vectors defined above gives:

$$\kappa = \frac{\left\| \begin{bmatrix} x_t' & y_t' & 1 \end{bmatrix} \times \begin{bmatrix} x_t'' & y_t'' & 0 \end{bmatrix} \right\|}{\left\| \begin{bmatrix} x_t' & y_t' & 1 \end{bmatrix} \right\|^3} = \frac{\left\| \begin{bmatrix} y_t'' & x_t'' & x_t'y_t'' - y_t'x_t'' \end{bmatrix} \right\|}{\left\| \begin{bmatrix} x_t' & y_t' & 1 \end{bmatrix} \right\|^3}$$

which in turn can be re-written as:

$$\kappa = \frac{\sqrt{\ddot{x}_t^2 + \ddot{y}_t^2 + \left(\dot{x}_t\ddot{y}_t - \ddot{x}_t\dot{y}_t\right)^2}}{\left(\sqrt{\dot{x}_t^2 + \dot{y}_t^2 + 1}\right)^3} \tag{A.1}$$

Despite only showing the second-derivative of position, the first two terms of the top line of equation A.1 in fact have units of m^2s^{-3}, due to the vector cross product in the previous equation.

The requirement for identifying via-points in this work is that the selection criteria results in the best reproduction of the observed movement (as measured by the mean square distance between observed and replicated movements) for the lowest number of via-points. Requiring that the number of via-points be as low as possible prevents the strategy of placing a via-point at every time step of the observed trajectory; this would quickly scale to unfeasible levels for long movements.

As such, via-points were selected for a given curved trajectory as the maxima and minima of three criteria: velocity, acceleration, and curvature. The trajectory was then replicated using the selected via-points and the mean-square difference (MSD) between the replicated and original trajectories was plotted against the number of via-points.

The MSD was calculated using equation A.2 and the combined-segmentation method of Pomplun and Matarić[98]. This metric works in joint space to compensate for differences in arm length between observer and imitator, and is flexible enough to be used to compare single movements (with or without via-points) and combinations of movements performed in a sequence.

$$d(\alpha, \beta) = \sum_{n=0}^{\min\left(T_\alpha, T_\beta\right)} \sum_{j=1}^{J} \left(\alpha_n^{(j)} - \beta_n^{(j)}\right)^2 \tag{A.2}$$

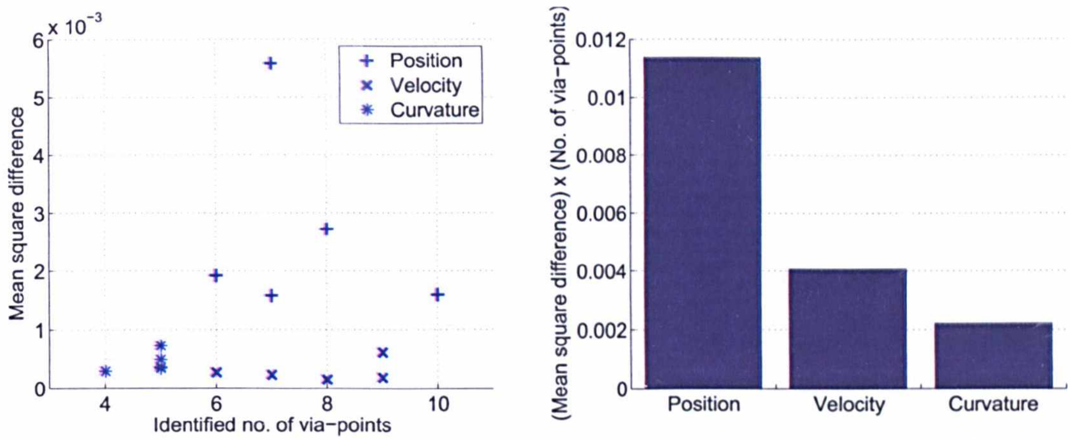

(a) (b)

Figure A.1: Via-point identification from zero-crossings of the derivatives of position, velocity and curvature. Trajectories were produced using the found via-points, and compared to the original trajectory: (a) Shows mean square difference between the original and new trajectories against the number of identified via-points; (b) Combining both measures confirms that via-points at maxima and minima of curvature give the best balance between similarity and no. of via-points.

Figure A.1(a) is the plot of number of points against MSD, for several repeated trials for each criterion. From this plot is can be seen that maxima and minima of acceleration captures the original trajectory well, but generally maxima and minima of curvature results in the best replicated trajectory for the least number of points. This is confirmed in the bar chart of Figure A.1(b) which shows MSD multiplied by number of points for each criterion.

Figure (a) shows the trajectory for which the via-points were selected, including the via-points found using the the curvature. Figure (b) shows both the spatio-temporal curvature and the change in the hands position on the x-axis, marking the maxima and minima of the curvature and showing how these relate to actual features of the x-axis trajectory.

A.2 Movement representation

Having identified the start and end points, and the via-points, the movement can now be put into a form suitable for generalisation.

For temporal generalisation the movement time is normalised, with the start at time

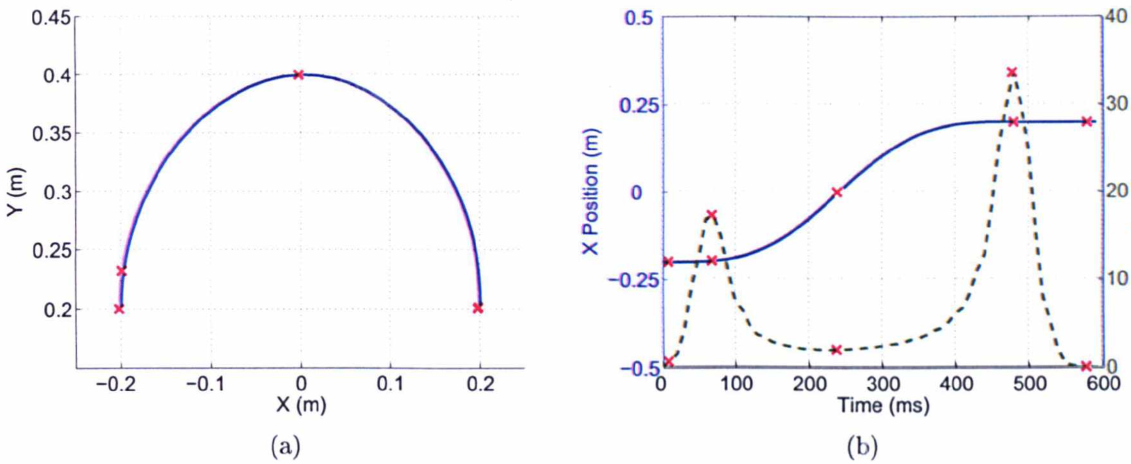

Figure A.2: The trajectory used to test the selection criteria for via-points. (a) The hand path, showing the positions of via-points corresponding to maxima and minima of spatio-temporal curvature; (b) The x-axis component of the hand path and the curvature (dotted line). The identified points occur at the start of the movement, the point where movement speed initially increases, the point of maximum velocity (when deceleration begins), the start of the post-movement period, and at the completion of the movement.

$t = 0$ and the end at time $t = 1$. The via-point temporal locations are also normalised to give their relative position within the time-scale of the movement. After this normalisation, the movement can be performed over any given time by multiplying the temporal positions by the required movement time. This can be summarised by equation A.3.

$$V_{t,new}^{(i)} = \left(\frac{V_{t,old}^{(i)}}{T_{old}} \right) \times T_{new} \tag{A.3}$$

Here, $V_t^{(i)}$ is the temporal position of the ith via-point and T is the movement time. The terms "old" and "new" denote the originally observed movement and the movement with the new required time. Obvious the start of the movement is still at time $t = 0$ while the end time becomes T_{new}. An example of this temporal generalisation is shown in Figure A.3(a), where a movement originally performed at one speed is performed again with a much shorter movement time. The basic shape of the original movement is still clear, as the relative temporal relationship between via-points has remained the same.

Spatial generalisation is performed in a similar way. The spatial relationship between the points of the movement is determined by the start position. The movement can be

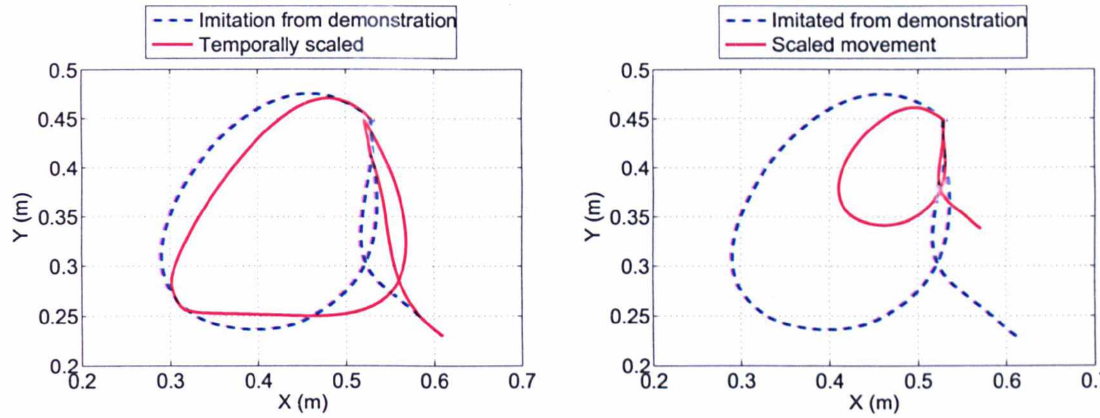

(a) (b)

Figure A.3: Plots showing the effects of temporal and spatial generalisation on a via-point trajectory: (a) A trajectory that draws the letter 'a', similar to the one shown in Figure 3.8, is shown performed at one speed (dotted line) and at a much faster speed (solid line). The faster movement appears cruder than the slower one as there is less time to move between via-points, but the basic same is retained; (b) The same trajectory (dotted line) with a repeated movement scaled by a factor of $\frac{1}{2}$ (solid line).

executed in a different part of the arm's workspace if the via-points and target point are adjusted for the new start point (equations A.4 and A.5). The movement can be scaled as well using this method, by applying a scaling factor to the general representation before adjusting for the new target position, as given by the term α in equations A.4 and A.5. Figure A.3(b) shows a movement scaled by a factor of a $\frac{1}{2}$, but performed from the same starting position and with the same movement time.

$$G_{new} = \alpha \left(G_{old} - S_{old}\right) + S_{new} \tag{A.4}$$

$$V_{p,new}^{(i)} = \alpha \left(V_{p,old}^{(i)} - S_{old}\right) + S_{new} \tag{A.5}$$

In these equations, G is the target goal of the movement, S is the start position of the movement and $V_p^{(i)}$ is the Cartesian position of the ith via-point. As noted above, the term α is the scaling factor and the terms "old" and "new" denote the observed movement and the movement with the new required starting position or scaling factor.

References

[1] J. Accot and S. Zhai. Beyond Fitts' law: Models for trajectory-based HCI tasks. In *Proceedings of CHI '97*, pages 295–302. 1997.

[2] R. M. Alexander. A minimum energy cost hypothesis for human arm trajectories. *Biological Cybernetics*, 76:97–105, 1997.

[3] A. Alissandrakis, C. L. Nehaniv, and K. Dautenhahn. Imitating with ALICE: Learning to imitate corresponding actions across dissimilar embodiments. *IEEE Transactions on Systems, Man, and Cybernetics, Part A: Systems and Humans*, 32(4): 482–496, 2002.

[4] C. G. Atkeson, J. G. Hale, F. E. Pollick, M. Riley, S. Kotosaka, S. Schaal, T. Shibata, G. Tevatia, A. Ude, S. Vijayakumar, and M. Kawato. Using humanoid robots to study human behaviour. *IEEE Intelligent Systems*, 15(4):46–56, 2000.

[5] M. Biegstraaten, J. B. J. Smeets, and E. Brenner. The influence of obstacles on the speed of grasping. *Experimental Brain Research*, 149:530–534, 2003.

[6] A. Billard. Learning motor skills by imitation: A biologically inspired robotic model. *Cybernetics and Systems*, 32:155–193, 2000.

[7] A. Billard. Imitation (a review). In M. A. Arbib, editor, *The Handbook of Brain Theory and Neural Networks*, pages 566–569. MIT Press, 2002.

[8] E. Bizzi, F. A. Mussa-Ivaldi, and S. F. Giszter. Computations underlying the execution of movement: A biological perspective. *Science*, 253:287–291, July 1991.

[9] E. Bizzi, N. Hogan, F. A. Mussa-Ivaldi, and S. F. Giszter. Does the nervous system use equilibrium-point control to guide single and multiple joint movements? *Behavioral and Brain Sciences*, 15:603–613, 1992.

[10] S.-J. Blakemore and J. Decety. From the perception of action to the understanding of intention. *Nature Reviews Neuroscience*, 2:561–567, August 2001.

[11] S.-J. Blakemore and C. Frith. Self-awareness and action. *Current Opinion in Neurobiology*, 13:219–224, 2003.

[12] C. Breazeal and B. Scassellati. Robots that imitate humans. *Trends in Cognitive Sciences*, 6(11):481–487, November 2002.

[13] R. Brooks, C. Breazeal, M. Marjanovic, B. Scassellati, and M. Williamson. The Cog project: Building a humanoid robot. In C. L. Nehaniv, editor, *Computation for Metaphors, Analogy and Agents*, volume 1562 of *Springer Lecture Notes in Artificial Intelligence*. Springer-Verlag, 1998.

[14] E. Burdet and T. E. Milner. Quantization of human motions and learning of accurate movements. *Biological Cybernetics*, 78(4):307–318, April 1998.

[15] E. Burdet, K. P. Tee, I. Mareels, T. E. Milner, C. M. Chew, D. W. Franklin, R. Osu, and M. Kawato. Stability and motor adaptation in human arm movements. *Biological Cybernetics*, 94(1):20–32, January 2006.

[16] E. Chinellato, A. Morales, R. B. Fisher, and A. P. del Pobil. Visual features for characterizing robot grasp quality. *IEEE Transactions on Systems, Man and Cybernetics (Part C)*, 35(1):35–41, February 2005.

[17] H. Cruse, E. Wischmeyer, M. Brüwer, P. Brockfield, and A. Dress. On the cost functions for the control of the human arm movement. *Biological Cybernetics*, 62: 519–528, 1990.

[18] R. H. Cuijpers, J. B. J. Smeets, and E. Brenner. On the relation between object shape and grasping kinematics. *Journal of Neurophysiology*, 91:2598–2606, January 2004.

[19] A. F. de C. Hamilton and D. M. Wolpert. Controlling the statistics of action: Obstacle avoidance. *Journal of Neurophysiology*, 87:2434–2440, 2002.

[20] A. Dearden and Y. Demiris. Learning forward models for robotics. In *Proceedings of IJCAI-2005*, pages 1440–1445. July 2005.

[21] J. Decety, J. Grezes, N. Costes, D. Perani, M. Jeannerod, E. Procyk, F. Grassi, and F. Fazio. Brain activity during observation of actions. *Brain*, 120:1763–1777, 1997.

[22] J. Demiris. *Movement imitation mechanisms in robots and humans*. PhD thesis, 1999.

[23] Y. Demiris. Robots as modelling tools for studying imitation. In D. Mareschal, S. Sirois, and G. Westermann, editors, *Neuroconstructivism*. Oxford University Press, 2005. (to appear).

[24] Y. Demiris. Imitation, mirror neurons, and the learning of movement sequences. In *Proceedings of the International Conference on Neural Information Processing (ICONIP-2002)*, pages 111–115. November 2002.

[25] Y. Demiris and A. Dearden. From motor babbling to hierarchical learning by imitation: A robot developmental pathway. In *Proceedings of the EPIROB-2005*, pages 31–37. July 2005.

[26] Y. Demiris and G. M. Hayes. Imitation as a dual-route process featuring predictive and learning components: A biologically-plausible computational model. In K. Dautenhahn and C. L. Nehaniv, editors, *Imitation in Animals and Artifacts*, chapter 13. MIT Press, 2002.

[27] Y. Demiris and M. Johnson. Distributed, predictive perception of actions: A biologically inspired robotics architecture for imitation and learning. *Connection Science Journal*, 15(4):231–243, December 2003.

[28] Y. Demiris and M. Johnson. Simulation theory for understanding others: A robotics perspective. In K. Dautenhahn and C. Nehaniv, editors, *Imitation and Social Learning in Robots, Humans and Animals: Behavioural Social and Communicative Dimensions*. Cambridge University Press, 2005.

[29] Y. Demiris and B. Khadhouri. Hierarchical Attentive Multiple Models for Execution and Recognition HAMMER. In *Proceedings of the ICRA-2005 Workshop on Robot Programming by Demonstration*. 2005. to appear.

[30] Y. Demiris and B. Khadhouri. Hierarchical, attentive multiple models for execution and recognition. *Robotics and Autonomous Systems*, to appear, 2006.

[31] Y. Demiris and G. Simmons. Perceiving the unusual: Temporal properties of hierarchical motor representation for action perception. *Neural Networks*, 2006. (to appear).

[32] A. H. Fagg, L. Zelevinsky, A. G. Barto, and J. C. Houk. Using crude corrective movements to learn accurate motor programs for reaching. In *Extended Abstracts of NIPS '97 Workshop: Can Artificial Cerebellar Models Compete to Control Robots?*, chapter 6, pages 20–24. 1997. URL `citeseer.ist.psu.edu/fagg97using.html`.

[33] A. H. Fagg, A. G. Barto, and J. C. Houk. Learning to reach via corrective movements. In *Proceedings of the Tenth Yale Workshop on Adaptive and Learning Systems*, pages 179–185. 1998. URL `http://citeseer.ist.psu.edu/fagg98learning.html`.

[34] C. Farrer, N. Franck, J. Paillard, and M. Jeannerod. The role of proprioception in action recognition. *Consciousness and Cognition*, 12:609–619, 2003.

[35] J. Feng, K. Zhang, and G. Wei. Towards a mathematical foundation of minimum-variance theory. *Journal of Physics A: Mathematical and General*, 35:7287–7304, 2002.

[36] J. Feng, K. Zhang, and Y. Luo. A study on an optimal movement model. *Journal of Physics A: Mathematical and General*, 36:7469–7484, 2003.

[37] P. M. Fitts. The information capacity of the human motor system in controlling the amplitude of movement. *Journal of Experimental Psychology*, 47(6):381–391, 1954.

[38] J. R. Flanagan and R. S. Johansson. Action plans used in action observation. *Nature*, 424:769–771, August 2003.

[39] J. R. Flanagan and D. M. Wolpert. Prediction precedes control in motor learning. *Current Biology*, 13:146–150, 2003.

[40] T. Flash. The control of hand equilibrium trajectories in multi-joint arm movements. *Biological Cybernetics*, 57:257–274, 1987.

[41] T. Flash and N. Hogan. The coordination of arm movements: An experimentally confirmed mathematical model. *Journal of Neuroscience*, 5(7):1688–1703, July 1985.

[42] T. Flash and T. J. Sejnowski. Computational approaches to motor control. *Current Opinion in Neurobiology*, 11:655–662, 2001.

[43] J. M. Fuster. Upper processing stages of the perception-action cycle. *Trends in Cognitive Sciences*, 8(4):143–145, 2004.

[44] M. Gangitano, F. M. Mottaghy, and A. Pascual-Leone. Phase-specific modulation of cortical motor output during movement observation. *Cognitive Neuroscience and Neuropsychology*, 12(7):1489–1492, May 2001.

[45] M. Gangitano, F. M. Mottaghy, and A. Pascual-Leone. Modulation of premotor mirror neuron activity during observation of unpredictable grasping movements. *European Journal of Neuroscience*, 20:2193–2202, 2004.

[46] A. P. Georgopoulos. Cognitive motor control: Spatial and temporal aspects. *Current Opinion in Neurobiology*, 12:678–683, 2002.

[47] M. Girgenrath, O. Bock, and S. Jüngling. Validity of the speed-accuracy tradeoff for prehension movements. *Experimental Brain Research*, 158:415–420, 2004.

[48] S. F. Giszter, K. A. Moxon, I. Rybak, and J. K. Chapin. A neurobiological persepctive on humanoid robot design. *IEEE Intelligent Systems*, pages 64–69, July/August 2000.

[49] H. Gomi and M. Kawato. Equilibrium-point control hypothesis examined by measured arm stiffness during multijoint movement. *Science*, 272:117–120, April 1996.

[50] J. Grezes, J. L. Armony, J. Rowe, and R. E. Passingham. Activations related to mirror and canonical neurones in the human brain: An fMRI study. *NeuroImage*, 18:928–937, 2003.

[51] J. G. Hale and F. E. Pollick. Biomimetic motion synthesis for the upper limb based on human motor production. In *7th International Conference on Simulation of Adaptive Behaviour*. August 2002.

[52] C. M. Harris and D. M. Wolpert. Signal-dependent noise determines motor planning. *Nature*, 394:780–784, August 1998.

[53] G. Hesslow. Conscious thought as simulation of behaviour and perception. *Trends in Cognitive Sciences*, 6(6):242–247, June 2002.

[54] M. R. Hinder and T. E. Milner. The case for an internal dynamics model versus equilibrium point control in human movement. *Journal of Physiology*, 549(3):953–963, 2003.

[55] B. Hoff. A model of duration in normal and perturbed reaching movement. *Biological Cybernetics*, 71:481–488, 1994.

[56] B. Hoff and M. A. Arbib. Models of trajectory formation and temporal interaction of reach and grasp. *Journal of Motor Behavior*, 25:175–192, 1993.

[57] J. M. Hollerbach and C. G. Atkeson. Deducing planning variables from experimental arm trajectories: Pitfalls and possibilities. *Biological Cybernetics*, 56:279–292, 1987.

[58] N. Iguchi, Y. Sakaguchi, and F. Ishida. The minimum end-point variance trajectory depends on the profile of the signal-dependent noise. *Biological Cybernetics*, 92: 219–228, 2005.

[59] M. Jeannerod. Intersegmental coordination during reaching at natural visual objects. In J. Long and A. Baddeley, editors, *Attention and performance IX*, pages 153–169. 1981.

[60] M. Jeannerod. The timing of natural prehension movements. *Journal of Motor Behavior*, 16:235–254, 1984.

[61] M. Jeannerod and V. Frak. Mental imaging of motor activity in humans. *Current Opinion in Neurobiology*, 9:735–739, 1999.

[62] M. Jeannerod, M. A. Arbib, G. Rizzolatti, and H. Sakata. Grasping objects: The cortical mechanisms of visuomotor transformation. *Trends in Neurosciences*, 18(7): 314–320, 1995.

[63] M. Johnson and Y. Demiris. Hierarchies of coupled inverse and forward models for abstraction in robot action planning, recognition and imitation. In *Proceedings of the AISB 2005 Symposium on Imitation in Animals and Artifacts*. 2005. (to appear).

[64] M. Johnson and Y. Demiris. Perspective taking through simulation. In *Proceedings of TAROS-2005*. September 2005. (to appear).

[65] D. G. Kamper, E. G. Cruz, and M. P. Siegel. Stereotypical fingertip trajectories during grasp. *Journal of Neurophysiology*, 90:3702–3710, 2003.

[66] Y. Kaneko, E. Nakano, R. Osu, Y. Wada, and M. Kawato. Trajectory formation based on the minimum commanded torque change model using the Euler-Poisson equation. *Systems and Computers in Japan*, 36(2):92–103, 2005.

[67] A. Karniel. Three creatures named forward model. *Neural Networks*, 15:305–307, 2002.

[68] A. Karniel and G. F. Inbar. Human motor control: Learning to control a time-varying, nonlinear, many-to-one system. *IEEE Transactions on Systems, Man, and Cybernetics - Part C: Applications and Reviews*, 30(1):1–11, February 2000.

[69] M. Kawato. Trajectory formation in arm movements: Minimization principles and procedures. In H. N. Zelaznik, editor, *Advances in Motor Learning and Control*, pages 225–259. Human Kinetics Publishers, 1996.

[70] M. Kawato. Internal models for motor control and trajectory planning. *Current Opinion in Neurobiology*, 9:718–727, 1999.

[71] C. Keysers, E. Kohler, M. A. Umilta, L. Nanetti, L. Fogassi, and V. Gallese. Audiovisual mirror neurons and action recognition. *Experimental Brain Research*, 153: 628–636, 2003.

[72] D. C. Knill and A. Pouget. The Bayesian brain: The role of uncertainty in neural coding and computation. *Trends in Neurosciences*, 27(12):712–719, December 2004.

[73] G. Knoblich. Self-recognition: Body and action. *Trends in Cognitive Sciences*, 6 (11):447–449, November 2002.

[74] E. Koechlin, C. Ody, and F. Kouneiher. The architecture of cognitive control in the human prefrontal cortex. *Science*, 302:1181–1185, November 2003.

[75] E. Kohler, C. Keysers, M. A. Umilta, L. Fogassi, V. Gallese, and G. Rizzolatti. Hearing sounds, understanding actions: Action representation in mirror neurons. *Science*, 297:846–848, August 2002.

[76] K. P. Körding and D. M. Wolpert. Bayesian integration in sensorimotor learning. *Nature*, 427:244–247, 2004.

[77] N. Kudoh, M. Hattori, N. Numata, and K. Maruyama. An analysis of spatiotemporal variability during prehension movements: Effects of object size and distance. *Experimental Brain Research*, 117:457–464, 1997.

[78] F. Lacquaniti, C. A. Terzuola, and P. Viviani. The law relating kinematic and figural aspects of drawing movements. *Acta Psychologica*, 54:115–130, 1983.

[79] G. E. Loeb, W. Levine, and J. He. Understanding sensorimotor feedback through optimal control. *Cold Spring Harbour Symposium on Quantative Biology*, 55:791–803, 1990.

[80] Z. Luo, M. Svinin, K. Ohta, T. Odashima, and S. Hosoe. On optimality of human arm movements. In *Proceedings of the IEEE International Conference on Robotics and Biomimetics 2004*, pages 447–452. August 2004.

[81] S. Ma and G. I. Zahalak. A distribution-moment model of energetics in skeletal muscle. *Journal of Biomechanics*, 24:21–35, 1991.

[82] I. S. MacKenzie. Movement time prediction in human-computer interfaces. In R. M. Baecker, W. A. S. Buxton, J. Grudin, and S. Greenberg, editors, *Readings in human-computer interaction (2nd Edition)*, pages 483–493. 1995.

[83] A. Matsui and Y. Wada. Examination of human trajectory planning criterion based on signal-dependent noise. *Systems and Computers in Japan*, 36(14):32–43, 2005.

[84] P. B. Matthews. Relationship of firing intervals of human motor units to the trajectory of post-spike after-hyperpolarization and synaptic noise. *The Journal of Physiology*, 492(2):597–628, April 1996.

[85] R. G. J. Meulenbroek, D. A. Rosenbaum, C. Jansen, J. Vaughan, and S. Vogt. Multijoint grasping movements - simulated and observed effects of object location, object size, and initial aperture. *Experimental Brain Research*, 138:219–234, 2001.

[86] H. Miyamoto, D. M. Wolpert, and M. Kawato. Computing the optimal trajectory of arm movement: The TOPS (Task Optimization in the Presence of Signal-dependent noise) model. In R. J. Dura, J. Santos, and M. Grana, editors, *Biologically Inspired Robot Behaviour Engineering*, volume 109 of *Studies In Fuzziness And Soft Computing*, chapter 14, pages 395–416. Springer-Verlag, 2003. ISBN 3-7908-1513-6.

[87] H. Miyamoto, J. Morimoto, K. Doya, and M. Kawato. Reinforcement learning with via-point representation. *Neural Networks*, 17:299–305, 2004.

[88] H. Miyamoto, E. Nakano, D. M. Wolpert, and M. Kawato. TOPS (Task Optimization in the Presence of Signal-dependent noise) model. *Systems and Computers in Japan*, 35(11):48–58, 2004.

[89] M. Mon-Williams, J. R. Tresilian, V. L. Coppard, and R. G. Carson. The effect of obstacle position on reach-to-grasp movements. *Experimental Brain Research*, 137: 497–501, 2001.

[90] A. Morales, E. Chinellato, A. H. Fagg, and A. P. del Pobil. Using experience for assessing grasp reliability. *International Journal of Humanoid Robotics*, 1(4):671–691, December 2004.

[91] P. Morasso. Spatial control of arm movements. *Experimental Brain Research*, 42: 223–227, 1981.

[92] F. A. Mussa-Ivaldi. Motor primitives, force-fields and the equilibrium point theory. In N. Gantchev and G. N. Gantchev, editors, *From Basic Motor Control to Functional Recovery*, pages 392–398. 1999.

[93] E. Nakano, H. Imamizu, R. Osu, Y. Uno, H. Gomi, T. Yoshioka, and M. Kawato. Quantitative examinations of internal representations for arm trajectory planning: Minimum commanded torque change model. *Journal of Neurophysiology*, 81(5): 2140–2155, 1999.

[94] K. S. Narendra and J. Balakrishnan. Adaptive control using multiple models. *IEEE Transactions on Automatic Control*, 42(2):171–187, February 1997.

[95] F. Nori and R. Frezza. A control theory approach to the anlysis and synthesis of the experimentally observed motion primitives. *Biological Cybernetics*, 93:323–342, 2005.

[96] E. Oztop and M. A. Arbib. Schema design and implementation of the grasp-related mirror neuron system. *Biological Cybernetics*, 87:116–140, 2002.

[97] E. Oztop and M. A. Arbib. A biologically inspired learning to grasp system. In *Proceedings of the 23rd Annual EMBS International Conference*, pages 857–860. IEEE, 2001.

[98] M. Pomplun and M. Matarić. Evaluation metrics and results of human arm movement imitation. In *Proceedings of the 1st IEEE-RAS International Conference on Humanoid Robotics*. 2000.

[99] N. Ramnani and R. C. Miall. A system in the human brain for predicting the actions of others. *Nature Neuroscience*, 7(1):85–90, January 2004.

[100] C. Rao, A. Yilmaz, and M. Shah. View-invariant representation and recognition of actions. *International Journal of Computer Vision*, 50(2):203–226, 2002.

[101] M. J. E. Richardson and T. Flash. Comparing smooth arm movements with the two-thirds power law and the related segmented-control hypothesis. *The Journal of Neuroscience*, 22(18):8201–8211, September 2002.

[102] G. Rizzolatti, L. Fadiga, V. Gallese, and L. Fogassi. Premotor cortex and the recognition of motor actions. *Cognitive Brain Research*, 3:131–141, 1996.

[103] G. Rizzolatti, L. Fogassi, and V. Gallese. Neurophysiological mechanisms underlying the understanding and imitation of action. *Nature Reviews Neuroscience*, 2(9):661–670, September 2001.

[104] G. Rizzolatti, L. Craighero, and L. Fadiga. The mirror system in humans. In M. I. Stamenov and V. Gallese, editors, *Mirror Neurons and the Evolution of Brain and Language*, volume 42 of *Advances in Consciousness Research*. John Benjamins Publishing Company, 2002.

[105] J. Rowe, K. Friston, R. Frackowiak, and R. Passingham. Attention to action: Specific modulation of corticocortical interactions in humans. *NeuroImage*, 17:988–998, 2002.

[106] P. N. Sabes. The planning and control of reaching movements. *Current Opinion in Neurobiology*, 10:740–746, 2000.

[107] S. Schaal. Is imitation learning the route to humanoid robots? *Trends in Cognitive Science*, 3(6):233–242, June 1999.

[108] L. F. Schettino, S. V. Adamovich, and H. Poizner. Effects of object shape and visual feedback on hand configuration during grasping. *Experimental Brain Research*, 151: 158–166, 2003.

[109] R. A. Schmidt. Principles of motor control and movement accuracy. In *Motor Learning and Performance: From Principles to Practice*, chapter 5, pages 101–126. Human Kinetics Publishers, 1991.

[110] G. Simmons and Y. Demiris. Object grasping using the minimum variance model. *Biological Cybernetics*, 2006. (to appear).

[111] G. Simmons and Y. Demiris. Imitation of human demonstration using a biologically inspired modular optimal control scheme. In *Proceedings of the 2004 4th IEEE-RAS/RSJ International Conference on Humanoid Robots*, volume 1, pages 215–234. November 2004.

[112] G. Simmons and Y. Demiris. Optimal robot arm control using the minimum variance model. *Journal of Robotic Systems*, 22(11):677–690, November 2005.

[113] J. B. J. Smeets and E. Brenner. A new view on grasping. *Motor Control*, 3:237–271, 1999.

[114] H. Tanaka, M. Tai, and N. Qian. Different predictions by the minimum variance and minimum torque-change models on the skewness of movement velocity profiles. *Neural Computation*, 16:2021–2040, 2004.

[115] D. Timmann, G. E. Stelmach, and J. R. Bloedel. Grasping component alterations and limb transport. *Experimental Brain Research*, 108:486–492, 1996.

[116] E. Todorov. Optimality principles in sensorimotor control. *Nature Neuroscience*, 7 (9):907–915, September 2004.

[117] E. Todorov and M. I. Jordan. Optimal feedback control as a theory of motor coordination. *Nature Neuroscience*, 5(11):1226–1235, November 2002.

[118] M. A. Umilta, E. Kohler, V. Gallese, L. Fogassi, L. Fadiga, C. Keysers, and G. Rizzolatti. I know what are you doing: A neurophysiological study. *Neuron*, 31(1): 155–165, 2001.

[119] Y. Uno, M. Kawato, and R. Suzuki. Formation and control of optimal trajectory in human multijoint arm movement: Minimum torque-change model. *Biological Cybernetics*, 61:89–101, 1989.

[120] P. Viviani and R. Schneider. A developmental study of the relationship between geometry and kinematics in drawing movements. *Journal of Experimental Psychology: Human Parception and Performance*, 17:198–218, 1991.

[121] Y. Wada and M. Kawato. A via-point time optimization algorithm for complex sequential trajectory formation. *Neural Networks*, 17:353–364, 2004.

[122] B. Webb. Can robots make good models of biological systems? *Behavioural and Brain Sciences*, 24(6), 2001.

[123] M. M. Williamson. Postural primitives: Interactive behaviour for a humanoid robot arm. In P. Maes, M. Matari'c, J.-A. Meyer, J. Pollack, and S. Wilson, editors, *Fourth International Conference on Simulation of Adaptive Behaviour*, pages 124–131. MIT Press, 1996.

[124] A. Wohlschlager, M. Gattis, and H. Bekkering. Action generation and action perception in imitation: An instance of the ideomotor principle. *Philosophical Transactions of the Royal Society London B*, 358:501–515, 2003.

[125] D. M. Wolpert. Computational approaches to motor control. *Trends in Cognitive Sciences*, 1(6):209–216, September 1997.

[126] D. M. Wolpert and M. Kawato. Multiple paired forward and inverse models for motor control. *Neural Networks*, 11:1317–1329, April 1998.

[127] D. M. Wolpert, R. C. Miall, and M. Kawato. Internal models in the cerebellum. *Trends in Cognitive Sciences*, 2(9):338–347, September 1998.

[128] D. M. Wolpert, Z. Ghahramani, and J. R. Flanagan. Perspectives and problems in motor learning. *Trends in Cognitive Sciences*, 5(11):487–494, November 2001.